US Army Corps of Engineers

TECHNICAL REPORT ITL-90-7

(2)

METHODS OF EVALUATING THE STABILITY AND SAFETY OF GRAVITY EARTH-RETAINING STRUCTURES FOUNDED ON ROCK

Phase 2 Study

by

R. M. Ebeling

Information Technology Laboratory

DEPARTMENT OF THE ARMY
Waterways Experiment Station, Corps of Engineers
3909 Halls Ferry Road, Vicksburg, Mississippi 39180-6199

and

J. M. Duncan, G. W. Clough

Virginia Polytechnic Institute
and State University
Blacksburg, Virginia 24061

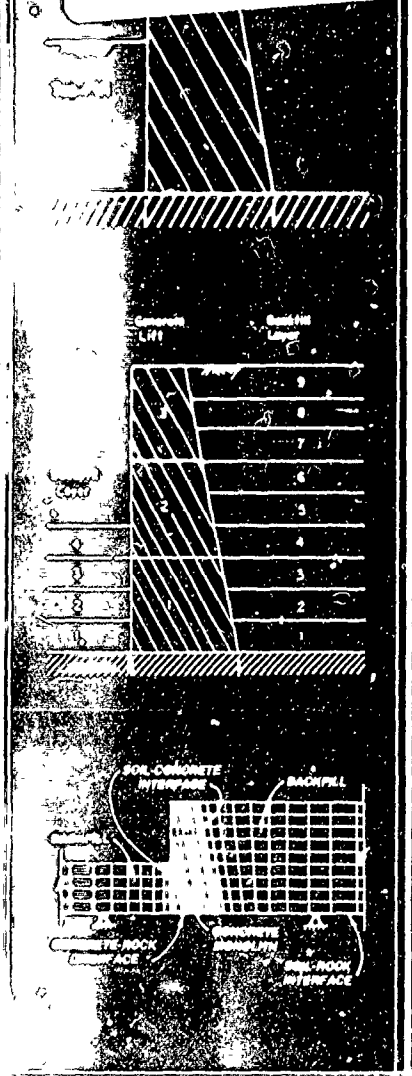

October 1990
Final Report

Approved For Public Release; Distribution Unlimited

Prepared for DEPARTMENT OF THE ARMY
US Army Corps of Engineers
Washington, DC 20314-1000

Under Civil Works Research and Development
Work Unit 31713

Destroy this report when no longer needed. Do not return it to the originator.

The findings in this report are not to be construed as an official Department of the Army position unless so designated by other authorized documents.

The contents of this report are not to be used for advertising, publication, or promotional purposes. Citation of trade names does not constitute an official endorsement or approval of the use of such commercial products.

Unclassified

SECURITY CLASSIFICATION OF THIS PAGE

REPORT DOCUMENTATION PAGE

Form Approved OMB No. 0704-0188

1a. REPORT SECURITY CLASSIFICATION Unclassified	1b RESTRICTIVE MARKINGS
2a. SECURITY CLASSIFICATION AUTHORITY	3 DISTRIBUTION/AVAILABILITY OF REPORT Approved for public release; distribution unlimited.
2b. DECLASSIFICATION/DOWNGRADING SCHEDULE	
4. PERFORMING ORGANIZATION REPORT NUMBER(S) Technical Report ITL-90 7	5. MONITORING ORGANIZATION REPORT NUMBER(S)
6a. NAME OF PERFORMING ORGANIZATION See reverse. / 6b. OFFICE SYMBOL (If applicable)	7a. NAME OF MONITORING ORGANIZATION
6c. ADDRESS (City, State, and ZIP Code) See reverse.	7b. ADDRESS (City, State, and ZIP Code)
8a. NAME OF FUNDING/SPONSORING ORGANIZATION US Army Corps of Engineers / 8b. OFFICE SYMBOL (If applicable)	9. PROCUREMENT INSTRUMENT IDENTIFICATION NUMBER
8c. ADDRESS (City, State, and ZIP Code) Washington, DC 20314-1000	10 SOURCE OF FUNDING NUMBERS See reverse. PROGRAM ELEMENT NO. / PROJECT NO. / TASK NO. / WORK UNIT ACCESSION NO.

11. TITLE (Include Security Classification)
Methods of Evaluating the Stability and Safety of Gravity Earth-Retaining Structures Founded on Rock, Phase 2 Study

12. PERSONAL AUTHOR(S)
Ebeling, R. M.; Duncan, J. M.; Clough, G. W.

13a. TYPE OF REPORT	13b. TIME COVERED	14. DATE OF REPORT (Year, Month, Day)	15. PAGE COUNT
Final report	FROM 1985 TO 1988	October 1990	125

16. SUPPLEMENTARY NOTATION
Available from National Technical Information Service, 5285 Port Royal Road, Springfield, VA 22161.

17. COSATI CODES		
FIELD	GROUP	SUB-GROUP

18. SUBJECT TERMS (Continue on reverse if necessary and identify by block number)
Earth pressures; Retaining walls; Soil-structure interaction; Finite element analysis; Rock foundations; Stability

19. ABSTRACT (Continue on reverse if necessary and identify by block number)

The objective of this study was to investigate the accuracy of the procedures employed in the conventional equilibrium method of analysis of gravity earth-retaining structures founded on rock, using the finite element method of analysis. This study was initiated when a number of existing large retaining structures at various navigation lock sites in the United States that showed no signs of instability or substandard performance failed to meet the criteria currently used for design of new structures.

The results of the following load analyses show that when the loss of contact along the base of a wall is modeled in the finite element analysis, the calculated values of effective base contact area and maximum contact pressure are somewhat larger than those calculated using conventional equilibrium analyses. The values of the mobilized base friction angle calculated by both methods are in precise agreement.

(Continued)

20. DISTRIBUTION/AVAILABILITY OF ABSTRACT ☐ UNCLASSIFIED/UNLIMITED ☐ SAME AS RPT ☐ DTIC USERS	21 ABSTRACT SECURITY CLASSIFICATION Unclassified
22a. NAME OF RESPONSIBLE INDIVIDUAL	22b TELEPHONE (Include Area Code) / 22c. OFFICE SYMBOL

DD Form 1473, JUN 86 *Previous editions are obsolete.* SECURITY CLASSIFICATION OF THIS PAGE

Unclassified

A

6a and c. NAME OF PERFORMING ORGANIZATION (Continued).

USAEWES
Information Technology Laboratory
3909 Halls Ferry Road
Vicksburg, MS 39180-6199

Department of Civil Engineering
Virginia Polytechnic Institute
and State University
Blacksburg, VA 24061

10. SOURCE OF FUNDING NUMBERS (Continued).

Contract No. DACW39-86-K-0007, under Civil Works Research and Development Work Unit 31713.

19. ABSTRACT (Continued).

Comparisons between the results of backfill placement analyses using the finite element method and the conventional equilibrium analyses indicate that conventional analyses are very conservative. The finite element analyses indicate that the backfill exerts downward shear loads on the backs of retaining walls. These shear forces have a very important stabilizing effect on the walls. Expressed in terms of a vertical shear stress coefficient ($K_v = \tau_{xy}/\sigma_v$), this shear loading ranged in value from 0.09 to 0.21, depending on the geometrical features and the values of the material parameters involved in the problem.

Another important factor not considered in the conventional equilibrium method is that the displacements of the wall have a significant influence on the distribution of both the stabilizing and destabilizing forces exerted on the wall. In general, as the wall moves away from the backfill, the lateral forces exerted on the wall by the backfill decrease, and the lateral forces exerted on the front of the wall by the toe-fill increase.

Keywords: Soil structure interaction; Soils/pressure; Loads forces; Walls/deformation/displacement; Foundations structures/rock; Soil stabilization; Backfills/stiffness; Shear stresses; Earth fills.

(MM)

PREFACE

The work described in this report was sponsored by Headquarters, US Army Corps of Engineers, as part of the Civil Works Research and Development program on Structural Engineering (CWR&D). The work was performed under CWR&D Work Unit 31713, "Soil-Structure Interaction Studies of Walls," for which Mr. Reed L. Mosher, Computer-Aided Engineering Division (CAED), Information Technology Laboratory (ITL), US Army Engineer Waterways Experiment Station (WES), is Principal Investigator.

This report covers the work performed by Virginia Polytechnic Institute and State University (VPI&SU), under Contract No. DACW39-86-K-0007, and work performed by Dr. R. M. Ebeling, CAED, WES. The work was under the direct supervision of Mr. Mosher and under general supervision of Drs. Edward Middleton, Chief, CAED, and N. Radhakrishnan, Chief, ITL, WES.

This is the second of two studies on VPI&SU's research activities on the stability of gravity walls founded on rock. The first report is REMR-CS-29 (Ebeling et al. in preparation).

Commander and Director of WES was COL Larry B. Fulton, EN. Technical Director was Dr. Robert W. Whalin.

CONTENTS

LIST OF TABLES

LIST OF FIGURES

CONVERSION FACTORS, NON-SI TO SI (METRIC) UNITS OF MEASUREMENT

Non-SI units of measurement used in this report can be converted to SI (metric) units as follows:

Multiply	By	To Obtain
degrees (angle)	0.01745329	radians
feet	0.3048	metres
inches	25.4	millimetres
kips (force)	4.448222	kilonewtons
pounds (force) per square foot	47.88026	pascals
pounds (force) per square inch	0.006894757	megapascals
pounds (mass) per cubic foot	16.01846	kilograms per cubic metre
pounds (mass) per cubic inch	27.6799	grams per cubic centimetre
tons (force) per square foot	95.76052	kilopascals

METHODS OF EVALUATING THE STABILITY AND SAFETY OF GRAVITY EARTH-RETAINING STRUCTURES FOUNDED ON ROCK

Phase 2 Study

PART I: INTRODUCTION

1. This report describes the continued research investigation of the behavior of earth-retaining structures founded on rock. This program of research was initiated after a number of existing structures, e.g. navigation lock walls under the jurisdiction of the US Army Corps of Engineers, that showed no signs of instability or substandard performance failed to meet the criteria used for the design of new structures. The traditional analysis procedure for these structures uses conventional equilibrium methods, the type used widely for analysis of earth-retaining structures. Because the conditions of equilibrium are insufficient for a complete analysis of all aspects of soil-structure interaction, these conventional equilibrium methods necessarily involve assumptions regarding the loading and resisting forces that act on the structures. The finite element method of analysis was used to compare the results of the finite element analysis with the conventional equilibrium analysis as a means of determining whether current criteria and methods are more conservative than necessary. The study of behavior of earth-retaining structures founded on rock was divided into two phases. The first phase (Ebeling et al. in preparation) defined the analytical requirements for this category of structure and developed new finite element procedures. The analytical procedures, described in Part IV of the first phase of study, can be used for analysis of walls that are loaded so heavily that gaps develop between the base and the foundation, i.e. structures deemed to be in a condition of incipient instability. In this report, the second phase of the study, finite element analyses and equilibrium methods utilizing the results of finite element analyses were performed to determine the effects of various geometrical and material parameters.

2. In the finite element "backfill" analyses, the loadings on the wall are generated automatically by simulating placement of the backfill behind the wall. The magnitude of the forces acting on the wall is dependent upon the relative movement of the soil and the monolith. These backfill placement

analyses are believed to be the most realistic that can be performed using the finite element method.

3. The finite element method differs from the conventional method of analysis in several ways. Two of the principal differences are: (a) the deformations of the wall are considered in the analysis, and (b) no assumptions with regard to the applied earth loads are required.

4. Several observations were made in the early studies described by Ebeling et al. (in preparation). Among these were:

a. The simulated placement of backfill against the wall using the finite element method resulted in the development of stabilizing shear forces acting on the back of the wall.

b. For very small values of wall displacement, i.e. less than 1 in.* for a 40-ft-high wall, the resulting lateral earth pressures were appreciably less than the at-rest pressures.

c. The lateral translation of the wall away from the backfill, displacing the toe-fill, resulted in earth pressures greater than the at-rest pressures on the front of the wall.

d. As a result of these factors, comparisons between the results of backfill placement analyses and conventional equilibrium analyses of retaining structures indicated that the conventional analysis is very conservative.

5. The initial finite element studies (Ebeling et al. in preparation) showed that the shear force acting on the back of the wall was a near constant value for variations in the unit weight and Poisson's ratio of the backfill and variations in the shear stiffness assigned to the concrete-to-rock interface along the base of the wall. Additional analyses have been performed to assess the influences on the shear load of variations in these factors: (a) the stiffness of the backfill, (b) the concrete-to-soil interface shear stiffness, and (c) the geometry of the wall. In addition, analyses were also conducted to study the effects of submerged backfill and water pressures on the wall.

6. Differences in the earth loads calculated in finite element analyses (FEA) and those assumed in conventional equilibrium analyses (CEA) reflect the mobilization of different levels of resistance within the backfill and different orientations of the principal stress axes. Methods for including shear loads in equilibrium analyses and for evaluating the safety of retaining walls

---

* A table of factors for converting non-SI units of measurement to SI (metric) units is presented on page 5.

were investigated, as described in subsequent sections of this report.

7. The interdependence between wall deformations and the forces acting on the wall were examined in a series of equilibrium analyses. In these analyses, the deformation of the wall during backfilling was sufficient to break the cohesive bond between the wall and the rock foundation, resulting in a situation where resistance to sliding is provided only by friction. Using the results of finite element analyses, relationships between the height of backfill, the earth loads, and the deformation of the wall were developed.

8. This report is divided into four parts and two appendixes. Part II discusses the results of the advanced backfill placement analyses. These analyses were performed to investigate the effects of additional variations in material parameters, additional wall configurations, and the presence of water behind and in front of the wall.

9. Part III describes an assessment of the methods used for inclusion of the factor of safety in conventional design analyses of earth-retaining structures.

10. The findings of the studies discussed herein are summarized in Part IV, together with recommendations of topics for further study.

11. In Appendix A, two methods for the interpretation of the finite element results of the simulated backfill placement analyses are described.

12. Appendix B contains a user's guide for the modified version of the finite element program SOILSTRUCT described in Part IV of the first phase of study (Ebeling et al. in preparation).

PART II: ADVANCED BACKFILL PLACEMENT ANALYSES OF RETAINING STRUCTURES USING THE ALPHA METHOD

13. A series of advanced backfill placement analyses of gravity-retaining structures founded on rock and performed using the finite element method are described in this part. In a backfill placement analysis, both the wall and the soil backfill are represented in the finite element mesh. The loadings exerted by the backfill on the wall are generated automatically during placement of the backfill behind the wall. This soil-structure interaction method of analysis is believed to afford the most realistic model of the backfill procedure for a wall that can be performed using the finite element method.

14. The backfill placement analyses described in Part II consider additional variations in material parameters beyond those discussed by Ebeling et al. (in preparation) in the first phase of this study. They also include additional wall configurations and water behind and in front of the wall. The finite element program SOILSTRUCT, with the alpha method incorporated in it, was used in the analyses. The alpha method allows accurate analysis of step-by-step separation of the base of the wall from its foundation during backfilling, as discussed in the first phase of the study. For those analyses with water, uplift pressures were applied when a crack developed along the base of the wall.

Structures Analyzed

15. The four hypothetical structures discussed in this part are shown in Figures 1-5. All of the monoliths retain 40 ft of backfill (H = 40 ft), are 16 ft wide at the base (B = 16 ft), and are buttressed by 17.8 ft of toe-fill. The four structures differ in the widths at the top of the wall and the slopes along the back of the wall. Their features are representative of the existing walls discussed in Part III of the initial study (Ebeling et al. in preparation).

16. Figure 1 shows the base case structure used exclusively in the backfill placement analyses described in the first phase report. The width at the top of wall is 8 ft, one-half the width of the base. No water table was present in this analysis.

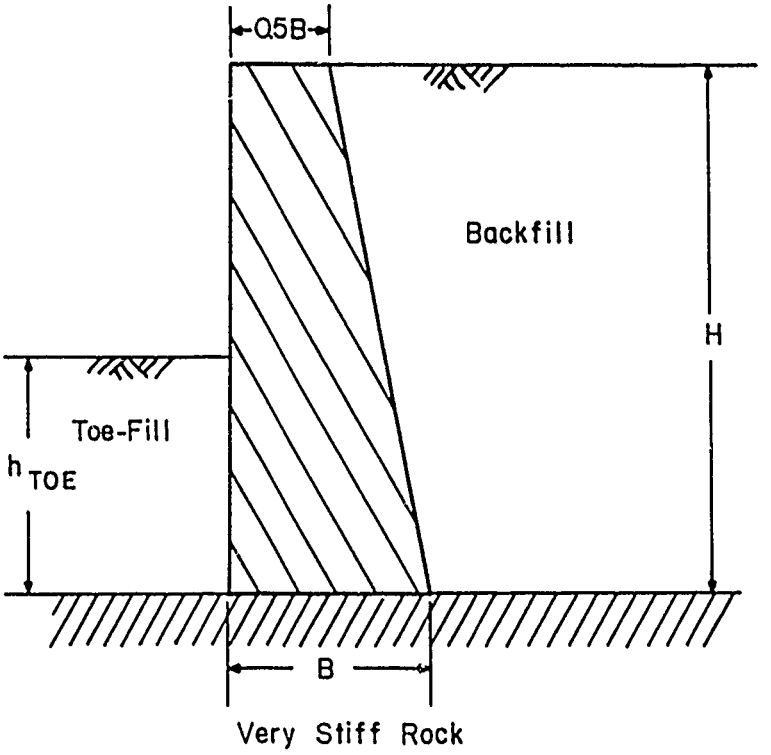

Figure 1. Base case hypothetical structure used in the backfill placement analyses

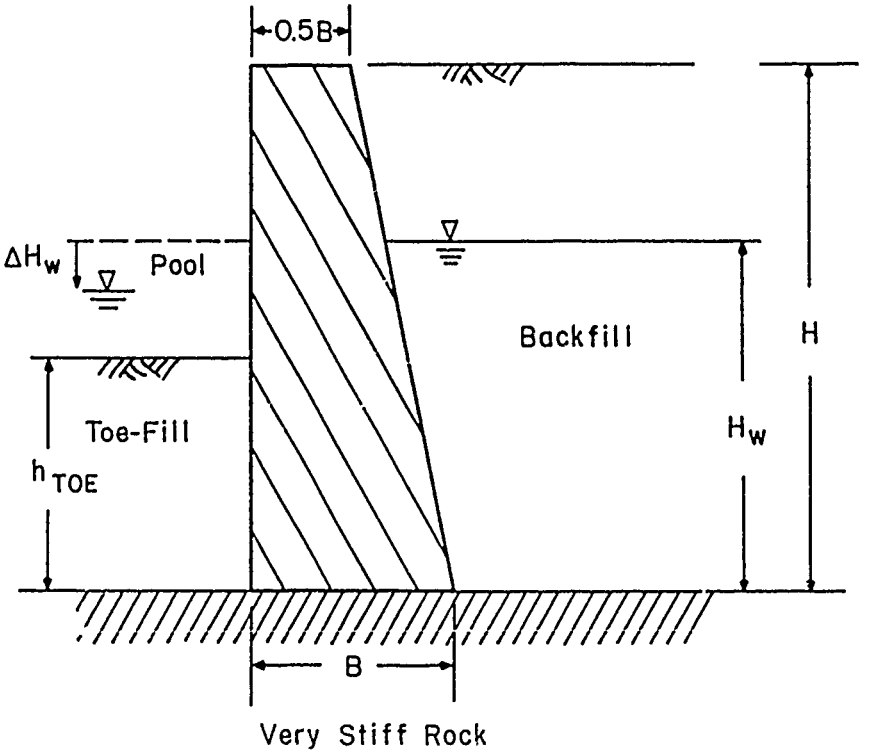

Figure 2. Hypothetical structure used in the backfill placement analysis with partially submerged soil behind the wall and a pool in front

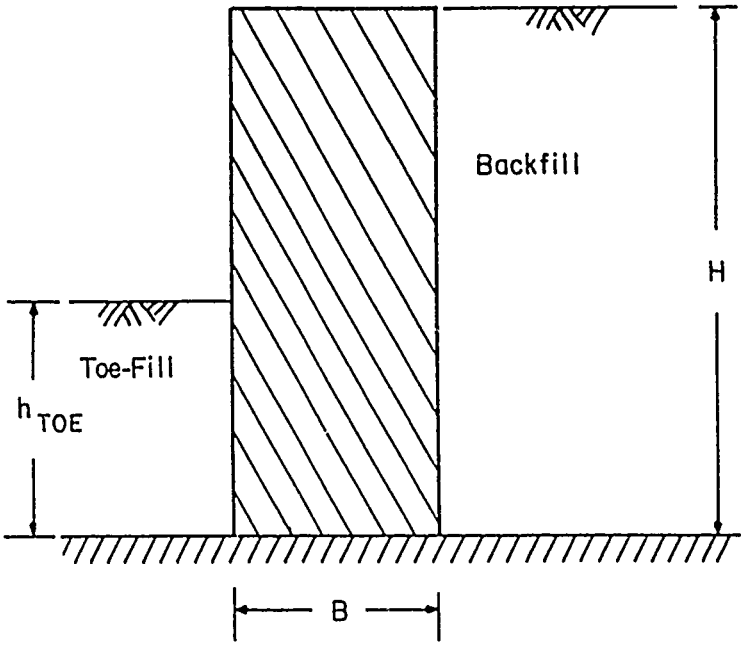

Figure 3. Rectangular hypothetical structure used in the backfill placement analysis

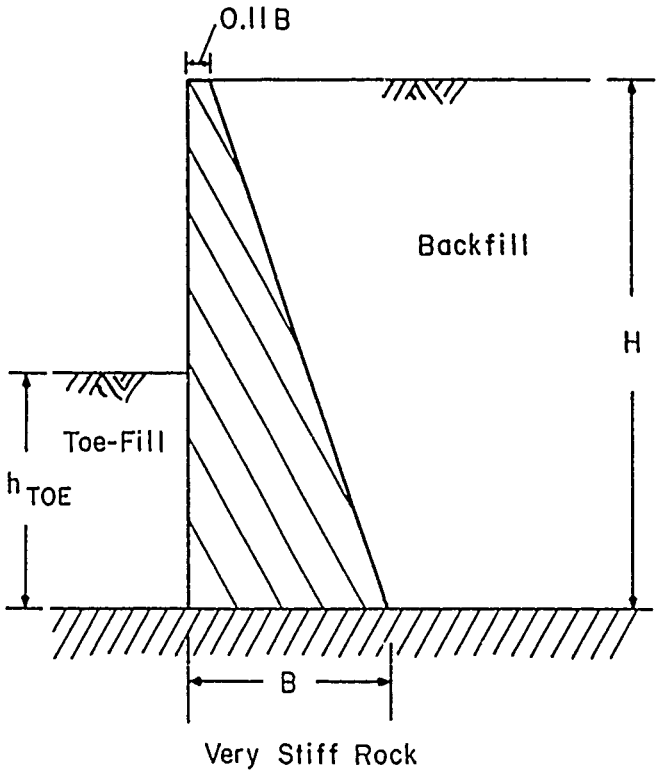

Figure 4. Sloping face hypothetical structure used in the backfill placement analysis

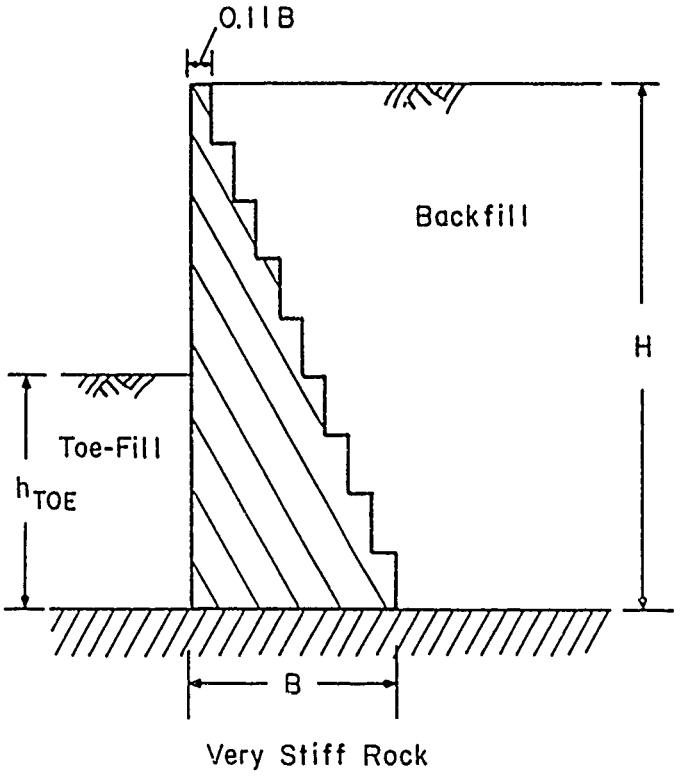

Figure 5. Stepped face hypothetical structure used in the backfill placement analysis

17. The same structure is shown in Figure 2 retaining a partially submerged soil backfill and buttressed by a submerged toe-fill and a pool of water. After completion of backfilling, both the water table within the backfill and the pool of water in front of the wall were at a height equal to 26.7 ft (0.67H). In subsequent analyses, the elevation of the pool was lowered in two 4.45-ft increments to the elevation of the top of the toe-fill.

18. A rectangular earth-retaining wall is shown in Figure 3. Figure 4 shows a sloping face wall with a crest width equal to 1.78 ft, or 0.11B. A stepped face wall with the same top width is shown in Figure 5. There was no water behind or in front of the wall shown in Figures 3-5.

Analyses Performed

19. A series of backfill placement analyses were performed to study the influence of five geometrical, material, and loading parameters. The ranges of values considered for the variables are shown in Table 1. The purpose of these analyses was to supplement the backfill placement analyses in the first

Table 1

Values of Parameters Used in Backfill Placement Analyses

a. Description of Parameters Used in Base Case Analysis.

Constant Parameters	Constant Soil Backfill Parameters
H = height of wall = 40 ft	$\gamma_{backfill}$ = unit weight of backfill = 135 pcf
B = width of base of wall = 16 ft	$\nu_{backfill}$ = Poisson's ratio of backfill = 0.15
B/H = 0.4	ϕ = friction angle of backfill = 39 deg
h_{toe} = height of soil backfill beyond toe = 17.8 ft	n = backfill stiffness parameter exponent = 0.4
h_{toe}/H = 0.45	R_f = backfill failure ratio parameter = 0.7
γ_c = unit weight of concrete = 150 pcf	δ = wall-to-soil interface friction
E_C = modulus of elasticity of concrete = 3×10^6 psi	δ/ϕ = 0.8**
K_n = normal stiffness of interface* = 3×10^6 pci	
K_s = shear stiffness of interface* = 1×10^4 pci	
Poisson's ratio of concrete = 0.2	

Variable Parameters	Variable Soil Backfill Parameters
K_s = shear stiffness of interface** = 15 to 400 pci	K = backfill stiffness parameter constant
H_w = height of water behind wall	
ΔH_w = change in pool elevation	
T = Width at top of wall	

Equations for Soil Stress-Strain Model

E_t = tangent modulus = $[1 - R_f SL]^2 K P_a (\sigma_3/P_a)^n$

SL = stress level = $(\sigma_1 - \sigma_3)/(\sigma_1 - \sigma_3)_f$

$(\sigma_1 - \sigma_3)_f = (2c \cos \phi + 2\sigma_3 \sin \phi)/(1 - \sin \phi)$

P_a = atmospheric pressure

(Continued)

* Concrete-to-rock.
** Concrete-to-soil.

Table 1 (Concluded)

b. Parameters Changed from Values Used in the Base Case Analysis.

Case†	T ft	T/B	H_w ft	ΔH_w ft	Backfill Stiffness Parameter K	Comments††
17a	8	0.5	--	--	450	Base case, AM
20a	8	0.5	--	--	[200]	AM
21a	8	0.5	--	--	[1,200]	AM
22a	8	0.5	--	--	[2,500]	AM
23a	8	0.5	--	--	[4,000]	AM
24a	8	0.5	--	--	[6,000]	AM
25a	8	0.5	--	--	450	[$(K_s{**})_{min}$], AM
26a	8	0.5	--	--	450	[$(K_s{**})_{max}$], AM
27b	8	0.5	[26.7]	[0]	450	AM
28b	8	0.5	[26.7]	[4.45]	450	AM
29b	8	0.5	[26.7]	[8.9]	450	AM
30a	[16]	1.0	--	--	450	AM
31a	[1.8]	0.11	--	--	450	AM
32a	[1.8]	0.11	--	--	450	[stepped wall], AM

Note: -- indicates no data. Parameters in brackets are those changed from the values for the base case.

** Concrete-to-soil.

† a = no hydrostatic uplift pressure applied to area of separation along the base. b = full hydrostatic uplift pressure applied to area of separation along the base.

†† AM = alpha method.

phase of study (Ebeling et al. in preparation) by investigating the influence of the following parameters on the calculated results:

a. The stiffness assigned to the backfill.

b. The interface stiffnesses.

c. The presence of water in front of and behind the wall.

d. Variations in wall geometry.

20. As in previous backfill placement analyses, a number of factors that affect the stability of the wall were studied. These include:

a. The distribution of stresses along the base of the wall, the front and back of the wall, and along several planes through the backfill.

b. The magnitudes of the resultant forces on these planes, and the positions of their points of action.

c. The magnitudes of the mobilized angles of friction on these planes.

d. The magnitudes of the earth pressure coefficients that characterize the magnitudes of the earth pressures on vertical planes within the backfill.

e. The percent of effective contact between the base of the wall and the foundation (B_e/B).

f. The lateral displacement of the monolith.

g. The magnitude of the maximum compressive stress developed at the toe of the wall.

Effect of the Stiffness of the Backfill

21. Six analyses were performed to investigate the influence of backfill stiffness. The base case structure shown in Figure 1 was used. The stiffness of the backfill was varied to cover a range of values characteristic of typical backfill soils.

Loading scheme

22. In backfill placement analyses, the loadings exerted on the wall by the backfill are dependent upon the magnitude and direction of wall movement. These loads are not predetermined, but depend on soil-structure interaction.

23. Prior to backfilling, the construction of the wall was simulated in three lifts, each 13.33 ft high. The simulation is idealized in Figure 6 for the base case structure. Construction of the wall was followed by placement of 40 ft of backfill in nine layers, each 4.44 ft thick. The first four

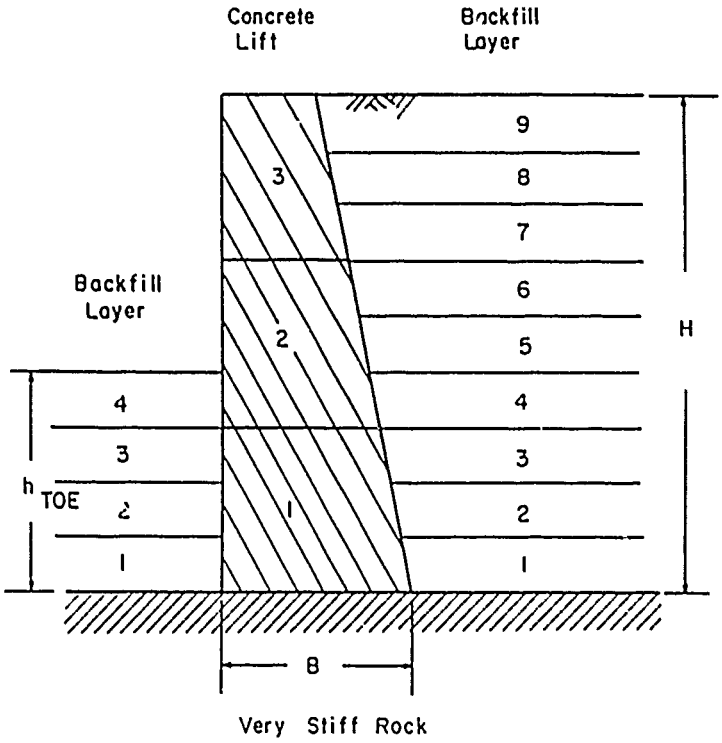

Figure 6. Idealization of the base case structure for backfill placement analysis--no water

layers were placed simultaneously in front of and behind the wall to a height of 17.8 ft. No water pressures were represented in this analysis.

Finite element mesh

24. The finite element mesh used for the backfill placement analysis of the base case structure is shown in Figure 7. This mesh and the other meshes used in these analyses were designed to model gravity walls founded on very stiff rock. The nodes along the base were fixed, and thus simulated a rigid boundary at the top of rock. Interface elements were included in four regions: (a) between the wall and the backfill, (b) between the wall and the foundation, (c) between the backfill and the rock, and (d) between the toe-fill and the rock.

25. There are 258 two-dimensional and interface elements in the mesh shown in Figure 7; 57 elements model the wall, 117 elements model the backfill, and 40 elements model the toe-fill. The remaining elements model the interfaces.

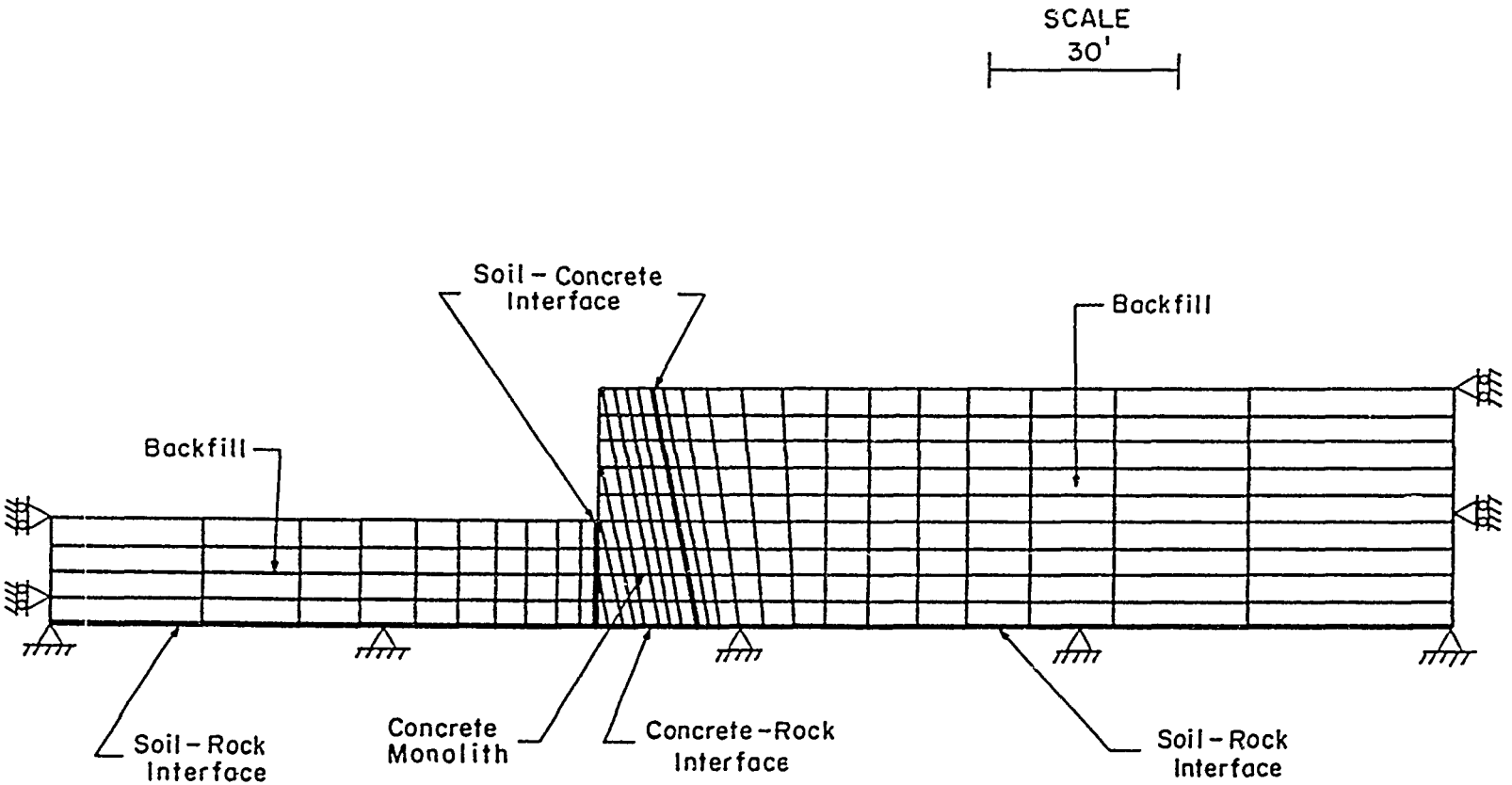

Figure 7. Finite element mesh used to model a base case hypothetical structure with additional backfill beyond the toe

Material properties

26. As in the backfill placement analyses discussed in Part VI of the first phase of this study (Ebeling et al. in preparation), the wall was modeled as a linear elastic material and the soil as a hyperbolic, nonlinear, stress-dependent material. The values of the parameters used in these analyses are listed in Table 1 along with some of the key equations of the hyperbolic stress-strain relationships.

27. The features of the interfaces were discussed in Part VI of the initial phase of this study by Ebeling et al. (in preparation). A very useful feature of the interface along the base of the wall is its ability to model the development of a crack during backfilling, using the alpha method (AM) of analysis described in Part IV of the Ebeling et al. (in preparation) study.

28. The properties of the concrete and the interface between the wall and its foundation used in these analyses are the same as those used in the backfill placement analyses discussed in the first phase of study. The modulus of the concrete was 3,000,000 psi, and the Poisson's ratio of the concrete was 0.15. The normal stiffness of the interface between the wall and the foundation was 3,000,000 pci, and the shear stiffness was 10,000 pci.

29. In the backfill analyses discussed initially (Ebeling et al. in preparation), the properties assigned to the backfill and the interfaces were characteristic of a clean granular backfill with a relative density of about 75 percent. The unit weight was 135 pcf, and the angle of internal friction was 39 deg. The magnitudes of the parameters used to model the hyperbolic stress-strain behavior were: the modulus number, $K = 450$; the modulus exponent, $n = 0.4$; and the failure ratio, $R_f = 0.7$. The typical range in values of K for clean granular backfill is from 200 to 1,200. In this series of six analyses, the value of K was varied from a minimum value of $K = 200$ to a maximum value of $K = 6,000$, with intermediate values of $K = 450$ (base case analysis), 1,200, 2,500, and 4,000. Values of K greater than 1,200 were used in the analyses so that the trends in the results for extreme values of K could be established.

30. The shear stiffness values assigned to the interfaces between the soil and the concrete and between the soil and the rock ranged from 20 to 300 pci, depending on the confining pressure. The normal stiffness assigned to all of the interfaces was 3,000,000 pci. The friction angle of the wall/soil interface was 31 deg, about 80 percent of the angle of internal friction for the soil.

Results of the
backfill placement analyses

31. The results of the analyses (Cases 17a, 20a, 21a, 22a, 23a, and 24a) are summarized in Table 2. The resultants of the stress distributions computed using the program SOILSTRUCT were computed manually. Their magnitudes and points of action were determined for each of the several planes shown in Figure 8. The Sections labeled A-A and C-C pass through the heel of the monolith. Section A-A extends vertically within the backfill, and Section C-C passes along the soil-to-wall interface. Section E-E is a vertical plane at the toe of the monolith. Vertical Sections B-B and H-H are located far behind and far in front of the wall. The resultant forces acting on these planes were used to determine the at-rest earth pressure coefficients, which characterize the lateral loads on an unyielding wall.

Forces on Section B-B

32. Due to its distance from the monolith, the stresses which developed on the vertical Section B-B were not influenced by soil-structure interaction. The stresses on this plane, therefore, reflect only the influence of the material parameters assigned to the soil.

33. The magnitude of the resultant lateral force acting on Section B-B F_h was found to be nearly exactly the same for all values of the modulus number K. For example, with K equal to 450 (base case), F_h was computed to be 55,329 lb, and with K equal to the maximum value of 6,000, F_h was found to be 55,137 lb, a difference of only 192 lb, or less than 1 percent.

34. The lateral earth pressure coefficient K_h for Section B-B is equal to the at-rest earth pressure coefficient K_o. Values of $K_h = K_o$ were calculated from the finite element results using the expression

$$K_h = \frac{F'_h}{\int_0^H \bar{\sigma}_v \, dh} \tag{1}$$

where

F'_h = resultant lateral effective force

H = height of soil above the base of the wall

$\bar{\sigma}_v$ = the vertical effective stress at height h

Table 2

Summary of Results for Backfill Placement Analyses of the Base Case Structure

Case	Backfill Stiffness Parameter K	Section B-B*, Vertical Section Beyond Heel				Monolith							
						Base							Crest
		F_h lb	K_o	h_{Fh} ft	h_{Fh}/H	T lb	N lb	x_n ft	x_n^* ft	B_e/B	q_{max} psf	δ_{mb} deg	u_x/H
17a	450	55,329	0.51	14.2	0.36	37,299	110,671	2.808	2.886	0.50	33,474	18.6	0.000050
20a	200	55,338	0.51	14.2	0.36	37,487	112,242	2.869	2.914	0.56	32,106	18.5	0.000049
21a	1,200	55,318	0.51	14.2	0.36	37,375	107,183	2.594	2.672	0.50	34,367	19.2	0.000055
22a	2,500	55,282	0.51	14.2	0.36	37 081	102,451	2.135	2.264	0.38	38,371	19.9	0.000064
23a	4,000	55,217	0.51	14.2	0.36	36,596	98,991	1.858	1.985	0.38	41,077	20.3	0.000074
24a	6,000	55,137	0.51	14.2	0.36	35,734	96,062	1.684	1.811	0.34	42,204	20.4	0.000080
25a	450	55,329	0.51	14.2	0.36	39,993	105,513	2.157	2.234	0.44	37,978	20.8	0.000063
26a	450	55,329	0.51	14.2	0.36	37,121	110,847	2.859	2.904	0.56	31,711	18.5	0.000049

* Locations of sections are shown in Figure 8.

(Continued)

Table 2 (Continued)

Case	Section C-C, Soil-to-Concrete Interface, Heel					Backfill Wedge			Section A-A, Vertical Section Through Heel						
	F_s lb	F_n lb	ℓ ft	ℓ/L	δ_m deg	W_s lb	W_s/area pcf	x_{W_s} ft	F_v lb	F_h lb	K_v	K_h	h_{Fh} ft	h_{Fh}/H	δ_m deg
17a	25,031	54,986	14.2	0.37	24.5	20,480	128	2.84	14,795	49,008	0.14	0.45	14.7	0.37	16.8
20a	25,833	54,681	14.2	0.35	25.3	20,620	129	2.99	15,435	48,558	0.14	0.45	14.7	0.37	17.6
21a	22,739	55,688	14.1	0.35	22.2	20,502	128	2.84	12,718	50,145	0.12	0.46	14.5	0.36	14.2
22a	18,858	55,906	14.2	0.35	18.6	20,523	128	2.83	8,932	51,117	0.08	0.47	14.5	0.36	9.9
23a	15,865	55,777	14.3	0.35	15.9	20,603	129	2.84	5,892	51,573	0.06	0.48	14.3	0.36	6.5
24a	13,291	55,344	14.3	0.35	13.5	20,635	129	2.83	3,252	51,657	0.03	0.48	14.2	0.36	3.6
25a	20,198	57,240	13.9	0.34	19.4	20,846	130	2.85	10,185	52,166	0.09	0.48	14.2	0.35	11.1
26a	25,312	54,813	14.2	0.35	24.8	20,585	129	2.92	14,986	48,784	0.14	0.45	14.7	0.37	17.1

(Continued)

Table 2 (Concluded)

Case	Section A-A		Section H-H, Vertical Section Beyond Toe				Section E-E, Soil-to-Concrete Interface, Toe							
	$\frac{K_h A\text{-}A}{K_o B\text{-}B}$	EPI	F_h lb	K_o	h_{Fh} ft	h_{Fh}/h_{toe}	F_v lb	F_h lb	K_v	K_h	h_{Fh} ft	h_{Fh}/h_{toe}	δ_m deg	$\frac{K_h E\text{-}E}{K_o H\text{-}H}$
17a	0.88	0.21	12,714	0.6	6.6	0.37	3,342	11,711	0.16	0.55	6.62	0.37	15.9	0.92
20a	0.88	0.22	12,719	0.6	6.6	0.37	4,187	11,066	0.20	0.52	6.66	0.37	20.7	0.87
21a	0.91	0.17	12,720	0.6	6.6	0.37	1,963	12,772	0.09	0.60	6.73	0.38	8.7	0.99
22a	0.92	0.14	12,732	0.6	6.6	0.37	996	14,041	0.05	0.66	6.98	0.39	4.1	1.10
23a	0.94	0.11	12,760	0.6	6.6	0.37	496	14,986	0.02	0.70	7.36	0.41	1.9	1.17
24a	0.94	0.11	12,822	0.6	6.6	0.37	175	15,929	0.01	0.75	7.81	0.44	0.6	1.24
25a	0.94	0.10	12,714	0.6	6.6	0.37	2,482	12,174	0.12	0.57	6.62	0.37	11.5	0.96
26a	0.88	0.21	12,714	0.6	6.6	0.37	3,276	11,663	0.15	0.55	6.65	0.37	15.7	0.92

(Sheet 3 of 3)

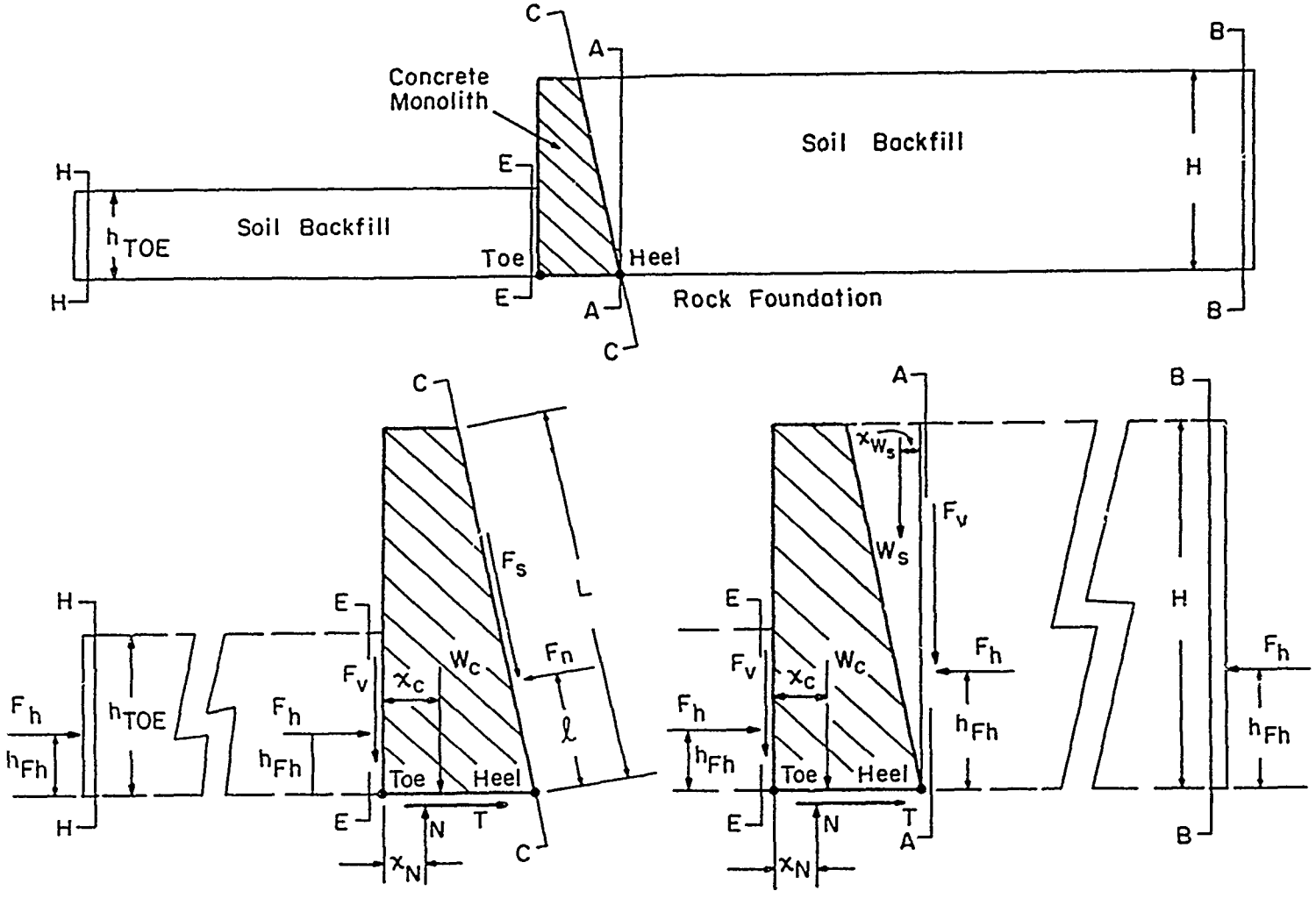

Figure 8. Planes along surfaces of the monolith and within the backfill on which resultant forces are computed--no water

With no water in the backfill, Equation 1 simplifies to the relationship

$$K_h = \frac{F'_h}{0.5 \cdot \gamma_{backfill} \cdot H^2} \tag{2}$$

For the six analyses summarized in Table 2, K_o is equal to 0.51 using Equation 2. The value of K_o serves as a convenient index to the magnitude of loading this wall would be subjected to if it did not move.

35. It may be seen that the resultant lateral force acts at 0.36H above the base in all six analyses. This is slightly higher than the value of 0.33H corresponding to an exactly triangular at-rest pressure distribution.

36. The values of K_v shown in Table 2 were calculated using the equation:

$$K_v = \frac{F_v}{\int_0^H \bar{\sigma}_v \, dh} \tag{3}$$

The resulting vertical shear force on Section B-B (F_v) is zero for all analyses as a result of the fact that there are no differential settlements from one side of Section B-B to the other. The vertical shear stress coefficient (K_v) at this section is, thus, zero, since F_v is zero. For the analyses where no water table is present, Equation 3 becomes

$$K_v = \frac{F_v}{0.5 \cdot \gamma_{backfill} \cdot H^2} \tag{4}$$

37. The values of δ_m shown in Table 2 were calculated using the equation:

$$\tan(\delta_m) = \frac{F_v}{F'_h} \tag{5}$$

The mobilized angle of friction (δ_m) is also zero at Section B-B.

Forces on the wall

38. The values of the resultant forces on the monolith are summarized in Table 2. The magnitude of the shear force acting on the base of the monolith (T) decreased with increasing values of the modulus number K . However, for values of K within the range for typical backfill soils and values of K between 200 and 1,200, T was nearly constant with a value of 37,400 lb.

39. The resultant normal force on the base of the wall (N) decreased slightly as the value of K increased. An increase in the value of K from 200 to 1,200 resulted in a 4.5 percent decrease in the value of N . It may be seen that distance between the resultant force and the toe of the wall (x_n) decreased as the value of K increased. This reflects the decrease in the magnitude of the shear stress applied to the wall by the backfill as the stiffness of the backfill increased.

40. The values of x_n^* shown in Table 2 are the distances from the toe to the resultants of the normal force for the elements remaining in compression. It may be seen that there is good agreement between the values of x_n and x_n^* , indicating that the numerical accuracies of the results are very good.

41. The magnitude of the normalized effective base contact area (B_e/B) decreased with increasing backfill stiffness. Fifty-six percent of the base remained in compression for a value of K equal to 200, while the effective base contact area was reduced to 50 percent for a value of K equal to 1,200.

42. As the stiffness of the backfill increased, the maximum compressive stress at the toe of the monolith (q_{max}) increased. As the value of K was increased within the range of values representative of backfill soils, q_{max} increased from 32,106 to 34,367 psf, an increase of less than 1 percent.

43. The mobilized angle of internal friction along the base (δ_{mb}) increased with increasing backfill stiffness. As the backfill modulus number K increased from 200 to 6,000, the value of δ_{mb} increased from 18.5 to 20.4 deg. The change results from the decrease in the magnitude of the normal force on the base, since the shear force is nearly constant.

44. The lateral movement of the monolith also increased with increasing values of K . The normalized lateral deformation at the crest of the monolith (u_x/H) increased from 0.000049 for $K = 200$ to 0.000080 for $K = 6,000$. These values of wall deformation are extremely small compared to the values which Terzaghi (1934) found were needed for the development of active pressures in his full scale tests on dense sand ($u_x/H \approx 0.0014$).

Forces on Section C-C

45. Section C-C is the interface between the wall and the backfill. The forces acting on this plane are affected by the value of K_o for the backfill, the settlement of the backfill as it is placed, and the effects of the movements of the wall during backfilling.

46. The magnitude of the resultant shear force (F_s) decreased with increasing stiffness of the backfill. For $K = 200$, the value of F_s was 25,833 lb, and for $K = 1,200$, the value of F_s was 22,739 lb, a decrease of 3,094 lb (12.0 percent). This is due to a reduction in the amount of settlement of the backfill as the soil stiffness increased.

47. The normal force on Section C-C (F_n) remained nearly constant, varying only from 54,681 to 55,906 lb as K was varied. For all six analyses, the resultant normal force acted at a distance of 14 ft above the heel, as measured along the face. This length corresponds to 35 percent of the interface length (L).

48. The mobilized angle of friction for the interface (δ_m) decreased from 25.3 deg for $K = 200$ to 24.5 deg for $K = 450$, and to 22.2 deg for $K = 1,200$. The decrease in δ_m with increasing values of K results from a decrease in the settlement of the backfill and the magnitude of F_s.

Forces on Section A-A

49. Section A-A is a vertical plane, within the backfill, passing through the heel of the wall. Like Section C-C, the forces acting on this plane are affected by the soil-structure interaction.

50. The magnitude of the vertical shear force (F_v) acting on Section A-A decreased with increasing soil stiffness. F_v was equal to 15,435 lb for $K = 200$, decreasing to 14,795 lb for the base case value of $K = 450$, and to 12,718 lb for $K = 1,200$. Figure 9 shows this trend. The value of K_v would be expected to approach zero as the stiffness of the backfill approaches the stiffness of concrete. For the typical range in stiffnesses of good quality backfill materials, K_v ranges in value from about 0.12 to about 0.15. The downdrag force, F_v, provides a stabilizing influence on the wall.

51. The magnitude of the resultant lateral force on Section A-A (F_h) increased with increasing values of K. The lateral earth pressure coefficient (K_h) was equal to 0.45 for $K = 200$, increasing to 0.47 for $K = 6,000$. For the typical range in K values for good quality backfill, the value of the lateral earth pressure coefficient for Section A-A (K_h) divided by K_o range from 0.88 to 0.91.

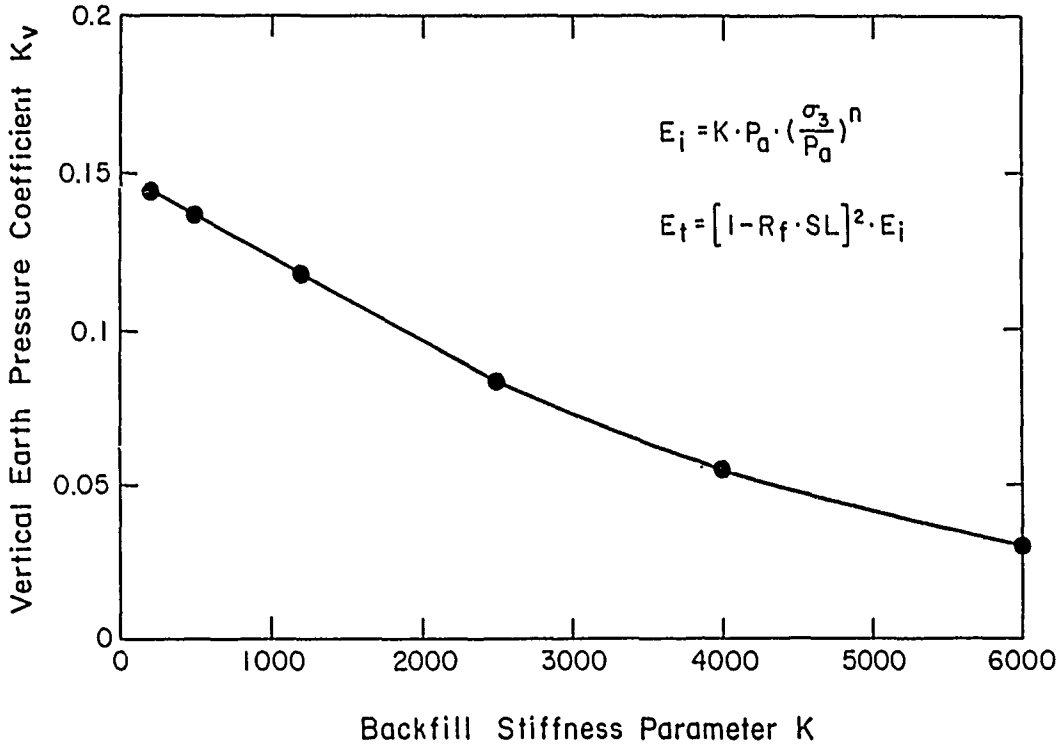

Figure 9. Variation of vertical earth pressure coefficient with backfill stiffness parameter

52. The earth pressure index (EPI) reflects the magnitude of K_h for Section A-A, compared to K_o and K_a. The EPI is given by

$$EPI = \frac{K_o - K_h}{K_o - K_a} \tag{6}$$

A value of EPI = 0 represents a condition of no wall movement and no soil-structure interaction. Complete soil-structure interaction occurs when a value of EPI = 1.0 is reached. This represents a condition where the wall movements have reached their maximum effect, and the minimum magnitude force is exerted by the backfill on the wall ($K_h = K_a$). For the value of K between 200 and 1,200, the EPI was found to vary from 0.17 to 0.22.

53. The mobilized angle of internal friction for Section A-A (δ_m) was found to decrease with increasing values of backfill stiffness. It may be seen that δ_m decreased from 17.6 deg for K = 200, to 16.8 deg for K = 450, and to 14.2 deg for K = 1,200. This variation reflects the

simultaneous decrease in F_v and increase in F_h, which occur with increasing values of backfill stiffness.

Forces on Section H-H

54. Like Section B-B, the stresses developed on Section H-H are not affected by soil-structure interaction and reflect only the parameters of the fill. The lateral earth pressure coefficient (K_h) at this section corresponds to at-rest pressure and is equal to 0.6 for all six analyses. Since the height and the number of lifts used to simulate the toe-fill are not the same as those used for the backfill, the lateral earth pressure coefficients for these two sections are not equal. This is due to the incremental computational procedure used in the analyses, as discussed in Part VI of the first phase of this study by Ebeling at al. (in preparation).

Forces on Section E-E

55. Section E-E is a vertical plane passing through the toe of the monolith. It was observed that as the stiffness of the soil increased, the magnitude of the vertical earth pressure coefficient (K_v) decreased and the magnitude of the lateral earth pressure coefficient (K_h) increased. The value of K_v decreased from 0.20 for $K = 200$ to a value of 0.09 for $K = 1,200$, while K_h increased from 0.52 to 0.60. The change in the resultant forces on Section E-E are the combined results of the changes in the magnitude of the settlement of the toe-fill, and movement of the wall toward the toe-fill.

Conclusions on the effect of stiffness of the backfill

56. In the hyperbolic soil model, two parameters control the stress-strain behavior of the backfill: (a) modulus number, and (b) Poisson's ratio. It was observed in the parametric studies described by Ebeling et al. (in preparation) that variations in the value of Poisson's ratio assigned to the backfill resulted in variations in the magnitude of the lateral force acting on the wall. In this series of parametric studies, changes in the stiffness assigned to the backfill influenced the magnitude of both the shear and lateral forces acting on the wall. As the stiffness of the backfill increased, the magnitude of the shear stress acting on the back of the wall decreased slightly, while the magnitude of lateral force exerted on the wall increased slightly. The downdrag force exerted by the backfill provides a stabilizing influence on the wall, and a decrease in its magnitude results in a lower margin of safety against overturning about the toe of the wall.

Effect of the Interface Shear Stiffness

57. Two analyses were performed to determine the influence of changing the shear stiffness (K_s) of the interfaces between the concrete and soil and between the rock and soil. The mesh shown in Figure 7 was used in these analyses. In Case 25a, the values of K_s used in the analyses ranged from 17 to 45 pci, depending on the normal stress in the elements. In Case 26a, the values of K_s ranged from 23 to 405 pci. The values of all of the other parameters were the same as in the base case analysis (17a).

Forces on Section B-B

58. The magnitude of the resultant lateral force (F_h) and shear force (F_v) acting on Section B-B was the same for both analyses, as seen in Table 2. This is in agreement with the observation that the magnitude of the stresses developed within this region of the mesh are dependent solely on the properties assigned to the backfill. As in the base case analysis, K_h was equal to 0.51, and K_v and δ_m were equal to zero.

Forces on the wall

59. The magnitude of the resultant shear force acting along the base of the wall (T) decreased from 39,993 to 37,121 psf with increasing concrete-to-soil and rock-to-soil interface stiffnesses. The reduction in the shear force on the base of the wall is due to the fact that when the interface between the soil and the underlying rock foundation is stiffer, movement of the backfill toward the wall is inhibited, and the earth load on the wall is reduced.

60. When K_s was increased, the magnitude of the normal force on the base of the wall (N) increased and its point of action (x_n) moved nearer to the heel of the wall. This reflects an increase in the magnitude of downdrag force and a decrease in lateral force acting on the back of the wall.

61. The normalized effective base contact area (B_e/B) increased from 0.44 for the minimum values of K_s to 0.50 for the standard values, and ultimately to 0.56 for the maximum values of K_s used in the analyses. As the effective base contact area increased, the maximum compressive stress at the toe of the wall decreased from 37,978 to 31,711 psf.

62. The mobilized angle of friction along the base (δ_{mb}) decreased from 20.8 to 18.5 deg as the interface stiffnesses increased.

63. The normalized lateral deformation at the crest of the monolith (u_x/H) decreased from 0.000063 to 0.000049 as a result of the decrease in the magnitude of the lateral force applied to the wall.

Forces on Section C-C

64. An increase in the shear stiffness of the interface between the back of the wall and the backfill resulted in an increase in the magnitude of the shear force acting along Section C-C. The normal force decreased slightly as a result of the increase in stiffness of the interface between the backfill and the underlying rock. The elevation of the resultant normal force remained at the same point along the interface in the three analyses. The mobilized friction angle increased from 19.4 to 24.8 deg as the interface stiffnesses were increased.

Forces on Section A-A

65. The shear force on vertical Section A-A increased and the lateral force decreased as the magnitude of K_s increased. The corresponding values of K_v ranged in value from 0.09 to 0.14 and the values of K_h from 0.48 to 0.45. The points of action of the resultant normal forces in the three analyses differ by less than 1 ft. The value of δ_m increased from 11.1 to 17.1 deg as K_s was increased. The value of the EPI increased from 0.10 to 0.21, indicating a greater level of soil-structure interaction with larger K_s values.

Forces on Section H-H

66. As was the case for Section B-B, the resultant forces acting on vertical Section H-H are the same for all three analyses. This is due to the lack of soil-structure interaction at large distances from the wall. The lateral earth pressure coefficient (K_h) at this section corresponds to K_o and is equal to 0.6. With F_v equal to zero, K_v and δ_m are also equal to zero for Section H-H.

Forces on Section E-E

67. The resultant shear force on vertical Section E-E is the net effect of two different modes of displacement, the initial settlement of the toe-fill during backfilling followed by the upward movement of the fill near the toe as the wall displaces toward the toe-fill. An increase in the shear stiffness results in an increase in the magnitude of the shear forces resulting from both of these displacements. It was observed that the wall movements were quite small, and thus the settlement of the toe-fill during backfilling controlled the development of the resulting interface forces.

68. The values of the lateral force were nearly constant for the three analyses. Expressed in terms of K_h, their values varied from 0.55 to 0.57

for the three analyses. The interface shear stresses, expressed in terms of K_v, increased from 0.12 to 0.16 as the interface shear stiffnesses were increased.

Conclusions on the effect of interface shear stiffness

69. Increases in the values of the shear stiffness of the concrete-to-soil interfaces result in a more stable wall because it results in larger shear stresses along the front and back faces of the wall. Also, changes in the value of K_s between the backfill and the underlying rock result in reduced earth loads on the wall, and thus a more stable wall.

Effect of Water in Front of and Behind the Wall

70. Three analyses were performed to determine the influence of a partially submerged backfill, submerged toe-fill, and a pool of water in front of the wall. The base case retaining structure, shown in Figure 2, was used in the evaluation. The results for Case 27b represent the completion of the backfill placement analysis with the elevation of the water outside the wall the same as that of the water table within the backfill (26.7 ft). The pool of water in front of the wall was subsequently lowered in two 4.45-ft increments to the elevation of the top of the toe-fill, 17.8 ft above the base of the wall (Cases 28b and 29b). The analyses were performed using the finite element mesh for the base case structure shown in Figure 7. All the parameters were the same as the base case (17a) except that the buoyant unit weight was assigned to the submerged backfill.

Loading scheme

71. Figure 10 shows the method used for incorporating water pressures in the backfill placement analyses. For this analysis the water table was assumed to rise as the backfill was placed. The simultaneous placement of backfill layer 6 and the rise in water table from the top of layer 5 to the top of layer 6 is shown in Figure 10. This procedure models the behavior of a free-draining backfill. By assigning buoyant unit weights to submerged backfill layer 6 during the analysis, the computed effective stresses within the backfill were consistent with fully drained conditions in the backfill.

72. Water pressures were applied normal to the front and back of the wall simulating the simultaneous rise in water table on either side of the wall. The incremental change in hydrostatic pressures shown in Figure 10

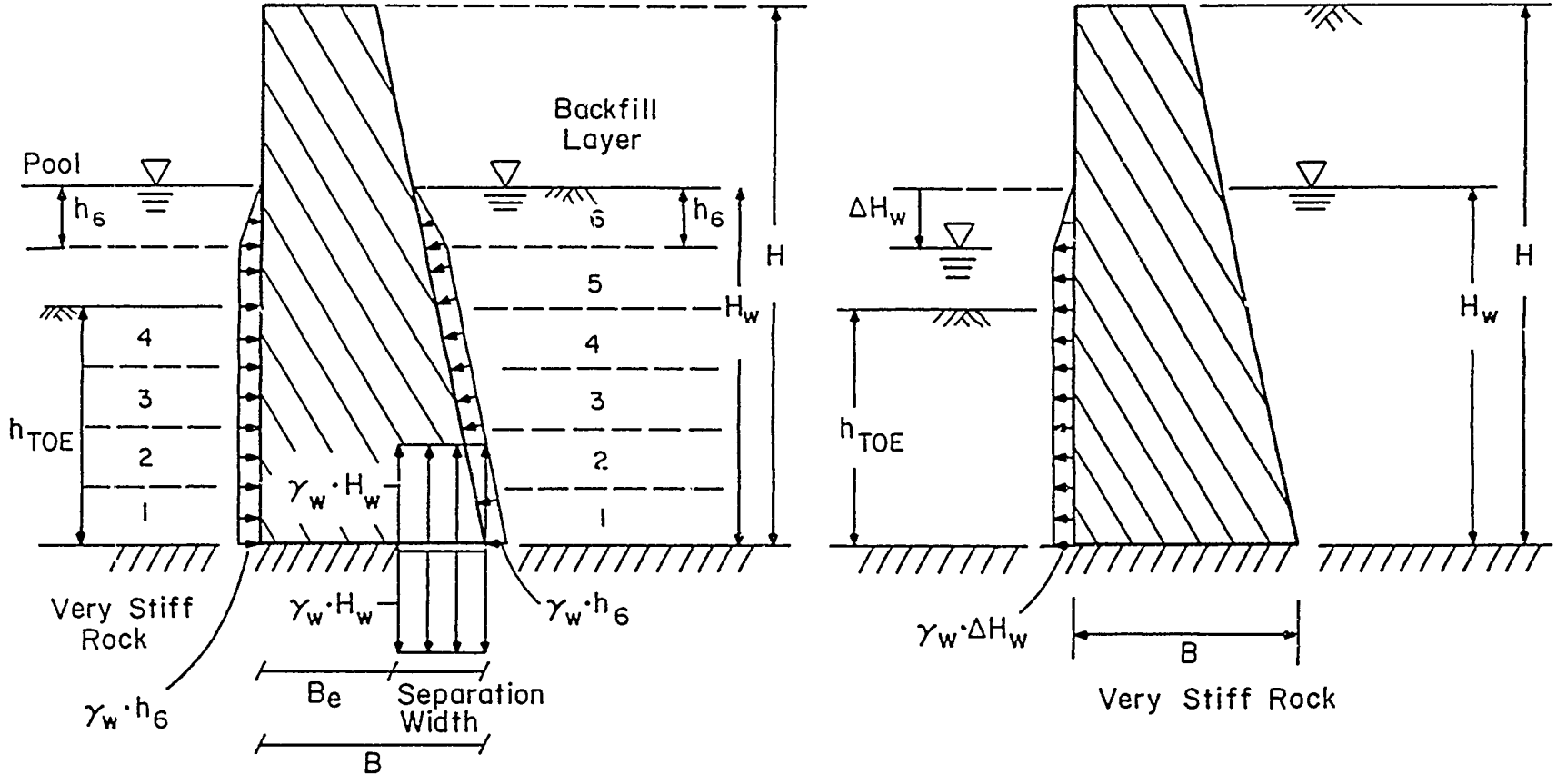

Figure 10. Idealization of a structure during placement of a submerged soil lift and during lowering of the pool elevation

correspond to the change in water table from the top of layer 5 to the top of layer 6. In this manner, the full hydrostatic water pressures acting on the wall were applied incrementally during all stages of backfilling.

73. Also depicted in Figure 10 is the possible separation of a portion of the base of the wall from its foundation. Due to the development of such a crack along the base, water would fill the void and exert a pressure equal to the hydrostatic pressure in the backfill. This water pressure acts on both the wall and the rock foundation within the cracked region of the interface.

74. The method used to model the lowering of the pool in front of the wall is shown at the right side of Figure 10. For each of the two changes in the pool elevation (ΔH_w = 4.45 ft), a pressure distribution equal to the change in hydrostatic pressure was applied normal to the face, directed away from the front of the wall.

Results of the
backfill placement analyses

75. The results of the three analyses (27b, 28b, and 29b) are summarized in Table 3. The difference in the three cases is the value of h_u, the elevation of this resultant water pressure force in front of the wall. The values of h_u are 8.9 ft for Case 27b, 7.4 ft for Case 28b, and 5.9 ft for Case 29b. The analyses were summarized using resultant effective forces and the forces due to water pressures acting on the planes shown in Figure 11, the same planes used in previous discussions.

Forces on Section B-B

76. With the same material parameters and the same water table elevation in the backfill in the three analyses, the magnitude of the resultant lateral effective force (F_h') acting on Section B-B was nearly a constant value of 44,100 lb/ft. The resultant water pressure force (U) was a constant 22,242 lb/ft. The point of action of F_h' and U were at 14.1 and 8.9 ft above the base of the wall. The value of K_h was equal to 0.51, in accordance with Equation 1. With no differential settlements at Section B-B, the resultant shear force (F_v) was equal to zero, as were K_v (Equation 3) and δ_m.

Forces on the wall

77. The toe-fill and the pool of water in front of the wall both have a stabilizing influence, because the base is not required to provide the entire resistance to the forces acting on the back of the wall. As shown in Figure 12, the magnitude of the shear force along the base (T) increased as the

Table 3

Summary of Results for Backfill Placement Analyses of the Base Case Structure--Partially Submerged Soil and Pool

Case	Backfill Stiffness Parameter K	Section B-B, Vertical Section Beyond Heel							Monolith				
									Base				
		F'_h lb	K_o	U lb	h_{Fh} ft	h_{Fh}/H	h_u ft	h_u/H	T lb	N' lb	U lb	x_n ft	x^*_n ft
27b	450	44,120	0.51	22,242	14.1	0.35	8.9	0.22	32,268	89,417	16,661	1.688	1.843
28b	450	44,075	0.51	22,242	14.1	0.35	8.9	0.22	38,278	86,374	19,993	0.780	1.049
29b	450	44,053	0.51	22,242	14.1	0.35	8.9	0.22	42,336	83,297	23,325	0.247	0.682

Case	Monolith					Section C-C, Soil-to-Concrete Interface, Heel							
	Base				Crest								
	x_u ft	B_e/B	q_{max} psi	δ_{mb} deg	u_x/H	F_s lb	F'_n lb	U lb	ℓ ft	ℓ/L	ℓ_u ft	ℓ_u/L	δ_m deg
27b	11.0	0.34	38,482	19.8	0.000064	19,989	43,612	22,681	15.4	0.38	9.1	0.22	24.6
28b	10.0	0.22	56,893	23.9	0.000109	20,445	43,180	22,681	15.4	0.38	9.1	0.22	25.3
29b	9.0	0.13	81,436	26.9	0.000161	20,962	42,321	22,681	15.4	0.38	9.1	0.22	26.4

(Continued)

Table 3 (Continued)

Case	Backfill Wedge			Section A-A, Vertical Section Through Heel											
	W_s ft	W_s/area pcf	x_{W_s} ft	F_v lb	F'_h lb	U lb	K_v	K_h	h_{Fh} ft	h_{Fh}/H	h_u ft	h_u/H	δ_m deg	$\frac{K_h A\text{-}A}{K_o B\text{-}B}$	EPI
27b	20,862	130	2.85	11,742	38,843	22,242	0.137	0.453	16.0	0.40	8.9	0.22	16.8	0.88	0.21
28b	20,930	131	2.82	12,036	38,332	22,242	0.140	0.447	16.0	0.40	8.9	0.22	17.4	0.87	0.23
29b	20,936	131	3.36	12,369	37,393	22,242	0.144	0.436	15.8	0.40	8.9	0.22	18.3	0.85	0.27

Case	Section H-H, Vertical Section Beyond Toe						
	F'_h lb	U lb	K_o	h_{Fh} ft	h_{Fh}/h_{toe}	h_u ft	h_u/h_{toe}
27b	6,969	22,242	0.61	6.6	0.37	8.9	0.50
28b	6,969	15,446	0.61	6.6	0.37	7.4	0.42
29b	6,973	9,885	0.61	6.6	0.37	5.9	0.33

(Continued)

(Sheet 2 of 3)

Table 3 (Concluded)

Case	Section E-E, Soil-to-Concrete Interface, Toe										
	F_v lb	F'_h lb	U lb	K_v	K_h	h_{Fh} ft	h_{Fh}/h_{toe}	h_u ft	h_u/h_{toe}	δ_m deg	$\frac{K_h E\text{-}E}{K_o H\text{-}H}$
27b	1,474	6,576	22,242	0.13	0.60	6.7	0.38	8.9	0.50	12.6	0.98
28b	1,401	6,850	15,446	0.62	0.62	6.7	0.38	7.4	0.42	11.6	1.02
29b	1,317	7,412	9,885	0.67	0.67	6.7	0.38	5.9	0.33	10.1	1.11

(Sheet 3 of 3)

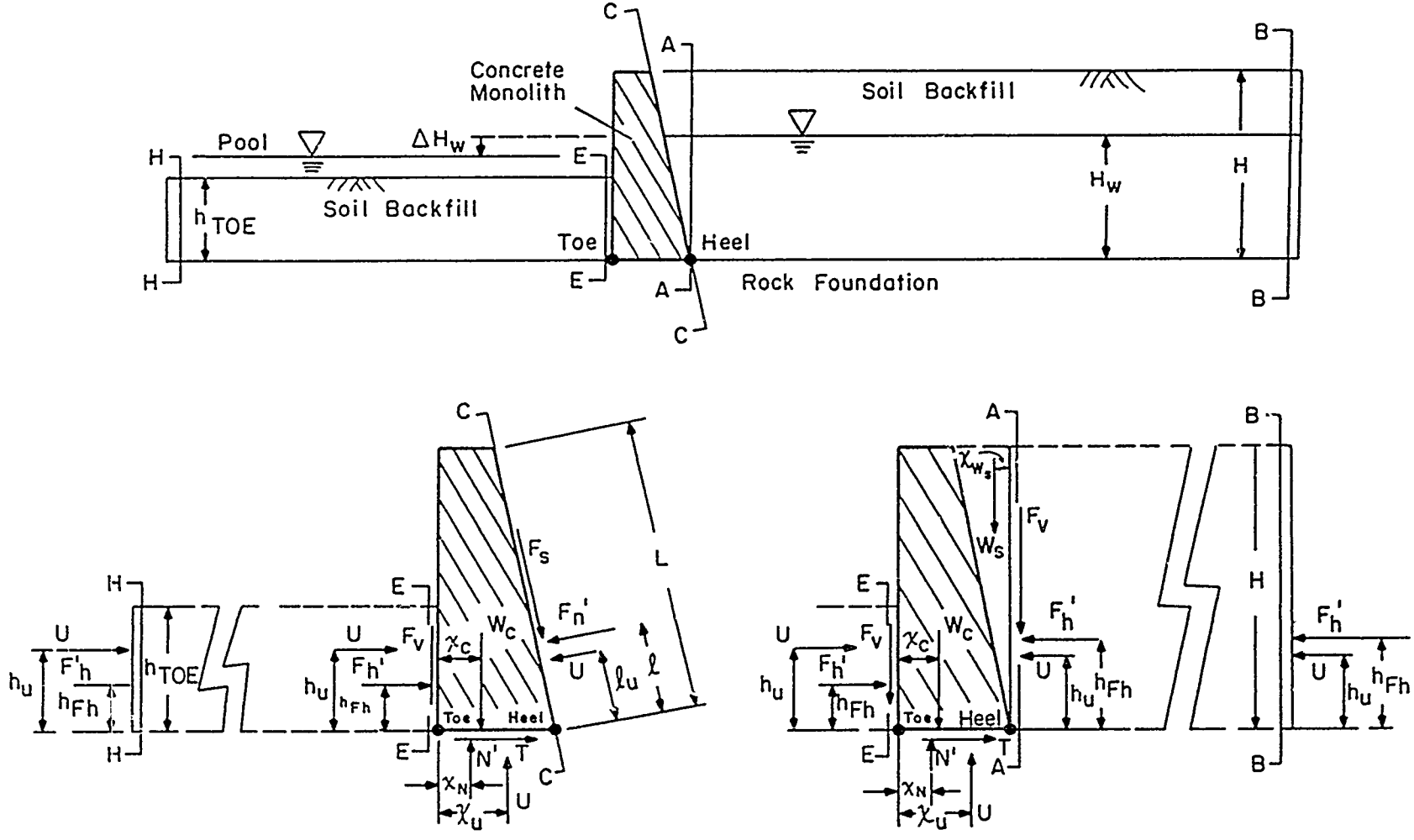

Figure 11. Planes along surfaces of the monolith and within the backfill, on which resultant forces are computed, water table

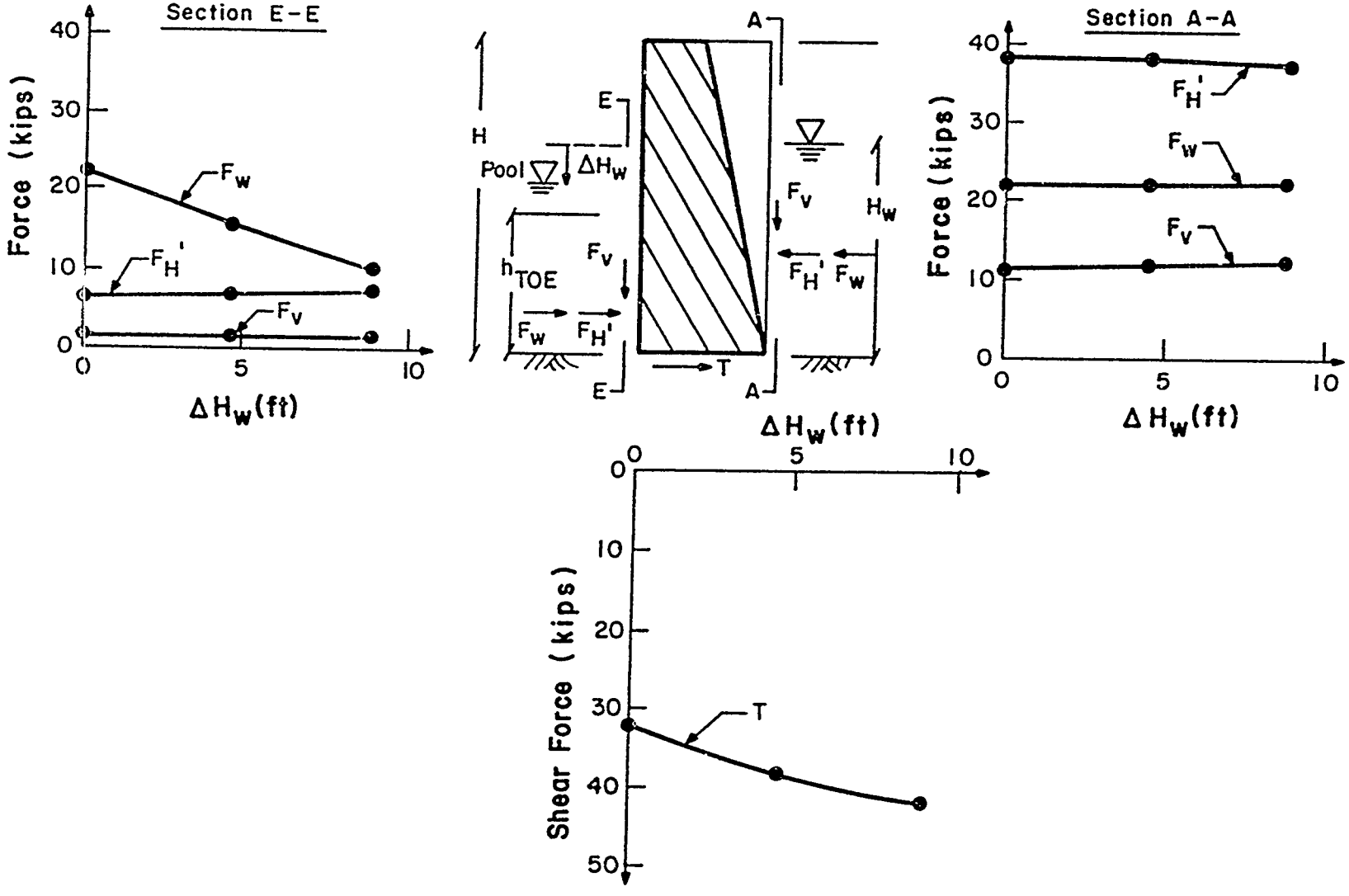

Figure 12. Forces acting on the wall versus change in pool level in front of the wall

pool elevation was lowered. Initially, T provided 53 percent of the total lateral resistance. The contribution of T increased to 71 percent when the elevation of the pool was lowered 8.9 ft.

78. The magnitude of the effective normal force (N') decreased with decreasing elevation of the water in front of the wall, as a result of a decrease in effective base contact area and corresponding increase in uplift pressures. When the pool was lowered 8.9 ft, the value of N' decreased from 89,417 to 83,297 lb, a decrease of 6,120 lb. At the same time, the uplift pressure increased by 6,664 lb. The vertical shear forces acting on the front and back of the wall accounted for the difference of 544 lb.

79. When the water level in front of the wall was lowered by 8.9 ft, the normalized effective base contact area (B_e/B) decreased by 62 percent from a value equal to 0.34 to a value of 0.13. The mobilized angle of internal friction along the base (δ_{mb}) increased from 19.8 to 26.9 deg. The normalized lateral deformation of the crest of the wall (u_x/H) increased by a factor of two and one-half when the pool was lowered, from 0.000064 to 0.000161.

Forces on Section C-C

80. An 8.9-ft decrease in pool elevation in front of the wall resulted in a 5-percent increase in the magnitude of the shear force (F_s) and a 3 percent decrease in the magnitude of the normal effective force (F'_n) acting on the back of the wall. The change in the magnitudes of F_s and F'_n were attributed to increased lateral deformations of the wall away from the backfill. The effective normal force acts at the same location along the interface in all three cases. The mobilized friction angle for Section C-C increased from $\delta_m = 24.6$ deg for Case 27b to $\delta_m = 26.4$ deg for Case 29b. The pore water pressure acting on Section C-C remained unchanged since the elevation of the water table within the backfill was the same.

Forces on Section A-A

81. The changes in the vertical and lateral effective forces on Section A-A were very nearly the same as for Section C-C: F_v increased by 5 percent and F'_h decreased by 4 percent; the mobilized angle of friction increased from 16.8 to 18.3 deg; the value of the EPI increased from 0.21 for Case 27b to 0.27 for Case 29b, indicating a slightly larger level of soil-structure interaction.

Forces on Section H-H

82. As for Section B-B, the stresses developed on vertical Section H-H are independent of the lateral movement of the wall. The at-rest earth

pressure coefficient (K_o) is equal to 0.61 for the three cases. F_v is equal to zero, resulting in values of K_v and δ_m equal to zero.

Forces on Section E-E

83. The variation in the forces acting on the vertical section through the toe of the wall (Section E-E) with pool elevation are shown in Figure 12. The decrease in the pool elevation is accompanied by a decrease in the hydrostatic water force F_w acting on Section E-E. As F_w decreases, the shear and lateral effective forces (F_v and F'_h) acting on the front of the wall change very little. This is due to the relatively small increase in wall movements. As the pool of water was lowered, K_h increased from 0.60 to 0.67, K_v decreased from 0.13 to 0.12, and δ_m decreased from 12.6 to 10.1 deg. However, the magnitude of the shear force (T) acting on the base of the wall increased considerably.

Conclusions on the effects of water in front of and behind the wall

84. The pool of water in front of the wall provides a stabilizing influence on the wall. A decrease in the margin of safety against wall instability occurs when the pool is lowered When the pool is lowered, a corresponding contribution to the resisting force is lost, which is then provided by increased shear resistance on the base of the wall and, to a small extent, by the toe-fill. The exact proportion of the redistribution of the resisting force between the base shear force and the toe-fill depends upon the movements of the wall. The larger the wall movements during the lowering of the pool, the larger the contribution of toe-fill. In this series of analyses most the redistributed resisting force was due to increased shear force on the base of the wall, because the wall movements were small.

Effect Of Wall Geometry

85. The effect of wall geometry was investigated using the results of two sets of backfill placement analyses; the first set of analyses dealing with the effect of wall shape and the second set of analyses dealing with the effect of having a stepped or a planar back on the wall. The influence of wall shape is determined from a comparison of the results of the backfill placement analyses of the three structures shown in Figure 4 (31a), Figure 1 (base case, 17a), and Figure 3 (30a). These walls differ by the width of their crest (T) varying from a minimum value corresponding to 0.11B, to 0.5B,

and 1.0B. In the second set of analyses, the results of the planar back wall shown in Figure 4 (31a) is compared to the results of the stepped back wall shown in Figure 5 (32a). No water table was simulated in the analyses, and the standard set of material parameters were used. The results are summarized in Table 4.

Finite element meshes

86. The finite element meshes used for the analyses are shown in Figure 7 (base case) and Figures 13-15. The features of the three meshes are identical, with the exceptions of the regions near the walls.

87. The mesh used to model the rectangular wall shown in Figure 13 has a total of 273 elements; 72 elements model the wall, 117 model the backfill, and 40 model the toe-fill. The remaining elements model the interfaces between the foundation and the overlying structure and the fills.

88. Figure 14 shows the 245-element mesh used to model the sloping face wall with $T/B = 0.11$; 44 elements model the wall, 117 model the backfill, 40 the toe-fill, and the remaining elements model the interface between the three different material regions.

89. A total of 274 elements were used to model the stepped face wall shown in Figure 15; 45 elements model the wall, 153 model the backfill, and 40 model the toe-fill. The remaining elements model all material interfaces. No interface elements were included along the back of the wall.

Forces on Section B-B

90. The magnitude of the resultant lateral forces acting on Section B-B (F_h) are equal for the three walls with planar backs and varying crest widths, due to the fact that the same soil properties were used in the three analyses. The lateral earth pressure coefficient (K_h) corresponds to K_o and equals 0.51.

Forces on the wall

91. Both the magnitudes of the normal forces (N) acting along the base and the values of x_n (the distance from the toe to N) increased with increasing crest width. N and x_n vary from minimum values of 104,000 lb and 1.7 ft for $T/B = 0.11$, to maximum values of 121,800 lb and 4.7 ft for $T/B = 1.0$. The increase in the values of N and x_n with increasing crest width reflects the increase in the mass of the wall, accompanied by a decrease in the magnitudes of the shear and normal forces acting on the back of the wall.

Table 4

Summary of Results for Backfill Placement Analyses--Additional Structures

Case	Backfill Stiffness Parameter K	Section B-B, Vertical Section Beyond Heel				Monolith							
						Base							Crest
		F_h lb	K_o	h_{Fh} ft	h_{Fh}/H	T lb	N lb	x_n ft	x_n^* ft	B_e/B	q_{max} psf	δ_{mb} deg	u_x/H
a. Wall Geometry													
31a	450	55,351	0.51	14.2	0.36	39,364	104,095	1,724	1,811	0.36	66,586	20.7	0.000100
17a	450	55,329	0.51	14.2	0.36	37,299	110,671	2,808	2,886	0.5	33,474	18.6	0.000050
30a	450	55,289	0.51	14.2	0.36	33,780	121,783	4,699	4,718	0.86	22,355	15.5	0.000029
b. Stepped and Planar Face Walls													
31a	450	55,351	0.51	14.2	0.36	39,364	104,095	1,724	1,811	0.36	66,586	20.7	0.000100
32a	450	55,351	0.51	14.2	0.36	37,980	113,441	3,047	3,065	0.62	30,466	18.5	0.000075

(Continued)

Table 4 (Continued)

Case	Section C-C, Soil-to-Concrete Interface, Heel					Backfill Wedge			Section A-A, Vertical Section Through Heel						
	F_s lb	F_n lb	ℓ ft	ℓ/L	δ_m deg	W_s lb	W_s/area pcf	x_{W_s} ft	F_v lb	F_h lb	K_v	K_h	h_{Fh} ft	h_{Fh}/H	δ_m deg
a. Wall Geometry															
31a	27,544	64,184	14.8	0.35	23.2	37,581	132	4.79	9,849	51,270	0.09	0.48	14.9	0.37	10.9
17a	25,030	54,986	14.2	0.37	24.5	20,480	128	2.84	14,795	49,008	0.14	0.45	14.7	0.37	16.8
30a	22,389	45,316	13.9	0.35	26.3	--	--	--	22,389	45,316	0.21	0.42	13.9	0.35	26.3
b. Stepped and Planar Face Walls															
31a	27,544	64,184	14.8	0.35	23.2	37,581	132	4.79	9,849	51,270	0.09	0.48	14.9	0.37	10.9
32a	19,550	58,844	15.5	0.36	19.6	44,112	155	4.88	12,622	48,053	0.12	0.45	15.1	0.38	14.7

(Continued)

Table 4 (Concluded)

Case	Section A-A		Section H-H, Vertical Section Beyond Toe				Section E-E, Soil-to-Concrete Interface, Toe							
	$\frac{K_h A\text{-}A}{K_o H\text{-}H}$	EPI	F_h lb	K_o	h_{Fh} ft	h_{Fh}/h_{toe}	F_v lb	F_h lb	K_v	K_h	h_{Fh} ft	h_{Fh}/h_{toe}	δ_m deg	$\frac{K_h E\text{-}E}{K_o H\text{-}H}$
a. Wall Geometry														
31a	0.93	0.13	12,683	0.59	6.6	0.37	3,265	11,906	0.15	0.56	6.6	0.37	15.3	0.94
17a	0.88	0.21	12,714	0.6	6.6	0.37	2,342	11,711	0.16	0.55	6.62	0.37	15.9	0.92
30a	0.82	0.32	12,714	0.6	6.6	0.37	3,394	22,535	0.16	0.54	6.6	0.37	16.4	0.91
b. Stepped and Planar Face Walls														
31a	0.93	0.13	12,683	0.59	6.6	0.37	3,265	11,906	0.15	0.56	6.6	0.37	15.3	0.94
32a	0.87	0.24	12,714	0.6	6.6	0.37	3,334	11,642	0.16	0.54	6.6	0.37	16.0	0.91

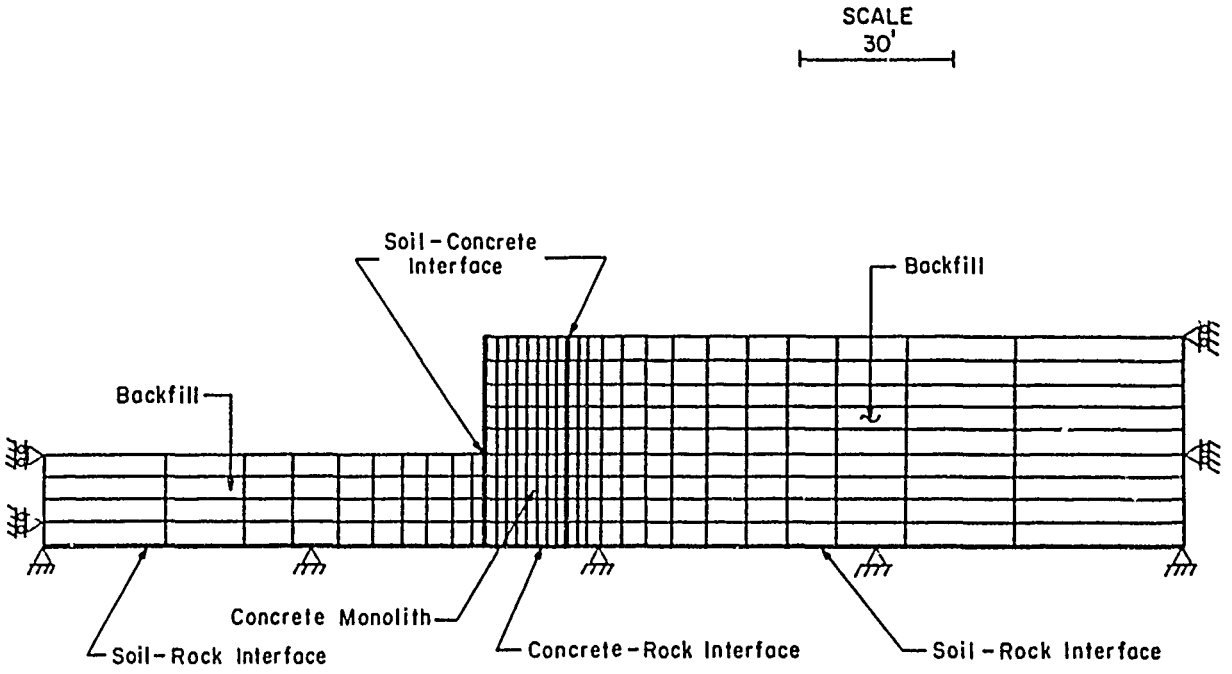

Figure 13. Finite element mesh used to model a rectangular hypothetical structure with additional backfill beyond the toe (Case 30a)

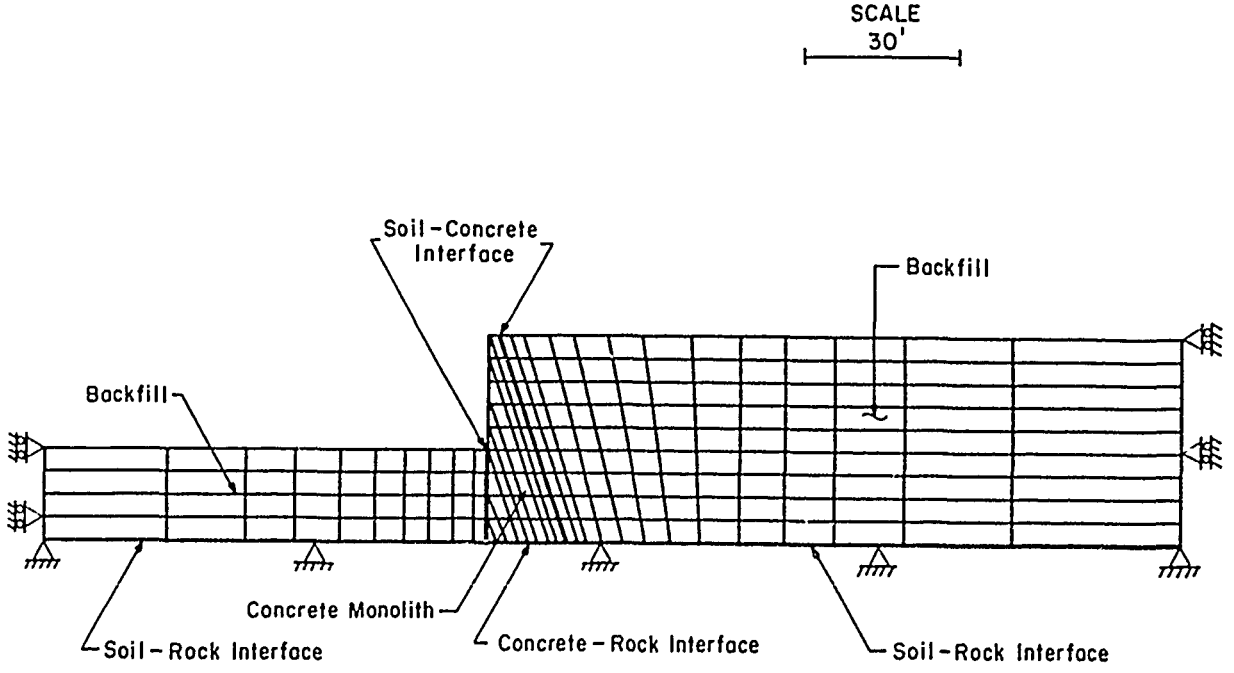

Figure 14. Finite element mesh used to model a sloping face hypothetical structure with additional backfill beyond the toe (Case 31a)

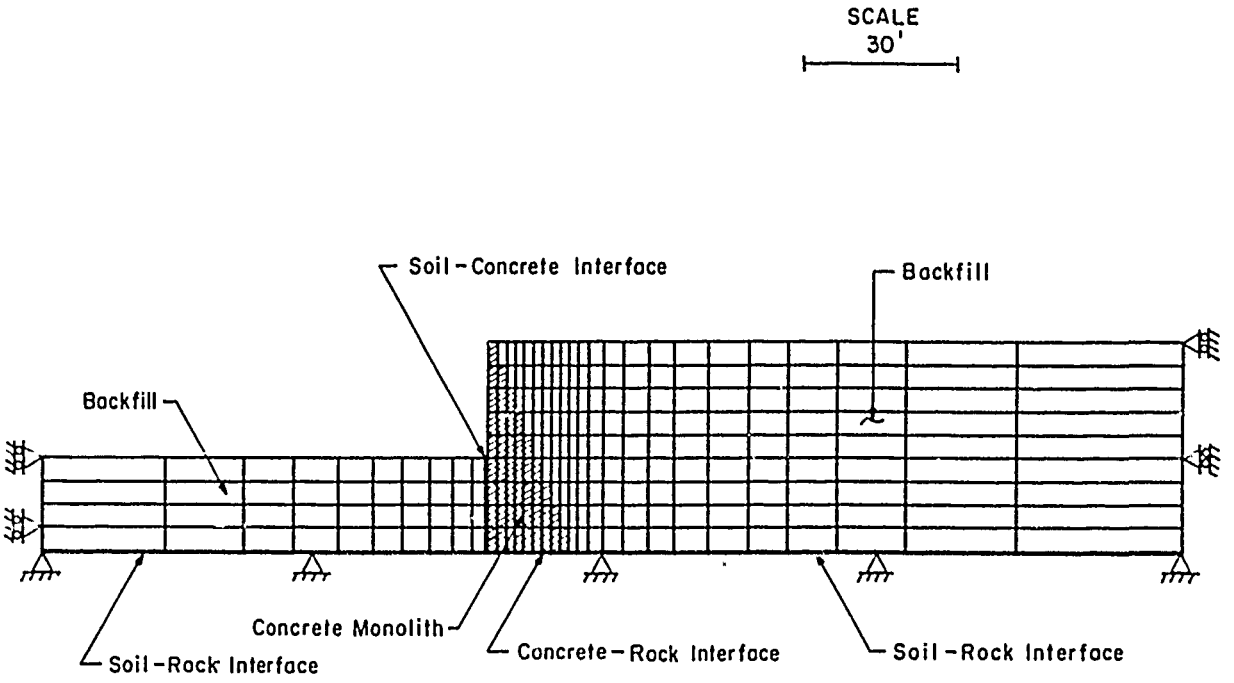

Figure 15. Finite element mesh used to model a stepped-face hypothetical structure with additional backfill beyond the toe (Case 32a)

92. The effective base contact area (B_e/B) increased from 0.36 to 0.86 as the crest width, or equivalently the mass of the wall, increased. The mobilized friction angle along the base (δ_{mb}) decreased from 20.7 to 15.5 deg. The lateral deformation at the crest of the wall decreased by a factor of almost 3-1/2 (u_x/H from 0.0001 to 0.000029). As expected, these results indicate that the margin of wall stability increases with increasing wall mass.

Forces on Section C-C

93. The magnitude of the resultant shear force on Section C-C (F_s) decreased by 19 percent and the resultant normal force (F_n) decreased by 29 percent as the back of the wall approaches vertical. The point of action of the normal force was constant at 14 ft above the heel. Figure 16 shows the increase in mobilized friction angle (δ_m) with increasing crest widths, T . δ_m increased from 23.2 to 26.3 deg (13 percent) as Section C-C approaches vertical.

Forces on Section A-A

94. The vertical resultant force on Section A-A (F_v) and the corresponding shear stress coefficient (K_v) increased by a factor of 2-1/3 as the back of the wall approaches vertical (Figure 16). The lateral earth pressure coefficient (K_h) decreased from $K_h = 0.48$ (Case 31a) to $K_h = 0.42$

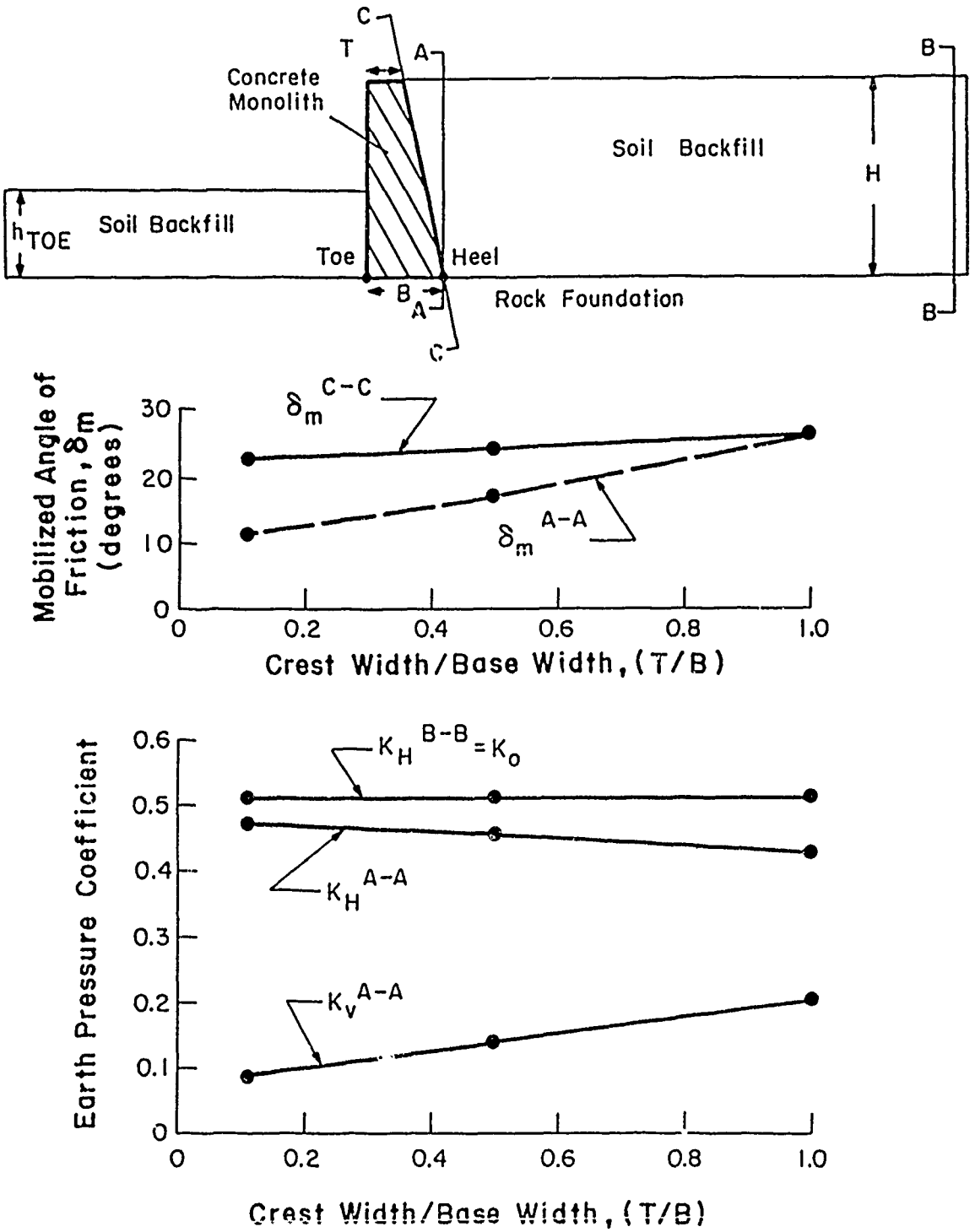

Figure 16. Variation of mobilized angle of friction and earth pressure coefficients on plane A-A and plane C-C with walls of different face slopes

(Case 30a), corresponding to a 12-percent decrease in the value of the resultant force F_h . The mobilized angle of friction for Section A-A increased from 10.9 to 26.3 deg.

95. The distributions of shear stresses along vertical planes within the backfill and corresponding values of K_v , decrease in magnitude with increasing distances from the heel of the wall, as shown in Figure 17 for the rectangular wall (Case 30a). At a distance of 40 ft the shear stresses are nearly equal to zero. An interesting observation is that the height of the wall is also equal to 40 ft.

96. Figure 18 shows the variation in the values of K_v with distance from the heel of the wall for the three walls. It is observed that the value of K_v becomes larger as the back of the wall approaches vertical. K_v increased from a value equal to 0.09 (T/B = 0.11), to $K_v = 0.14$ (T/B = 0.5), and ultimately $K_v = 0.21$ (T/B = 1.0). In addition, the distance between the heel of the wall and the vertical plane on which the shear stress is zero (equivalently $K_v = 0$) and increases as the width at the crest of the wall increases.

Forces on Sections H-H and E-E

97. The lateral earth pressure coefficient (K_h) for Section H-H is 0.6 and equal to K_o , since the base case material parameters were used in the three analyses.

98. The shear forces on Section E-E (F_v) are nearly a constant value of 3,300 lb, with a corresponding value of K_v equal to 0.16, for the three analyses. The lateral earth pressures showed a slight variation, with the values of K_h between 0.54 and 0.56, indicating that the lateral force (F_h) is more sensitive to wall displacements than F_v on Section E-E.

Conclusions on the
effect of wall shape

99. The margin of wall stability increased with increasing wall mass, as expected. The shear force on the vertical plane through the heel of the wall increased and the normal force decreased, both changes contributing to an increase in wall stability.

Effect of a stepped back on the wall

100. The results of the backfill placement analyses for the wall with a stepped back (Case 32a) are summarized in Table 4. These results may be compared to the results for Case 31a, in which the crest width was the same (1.8 ft), and the back of the wall was planar.

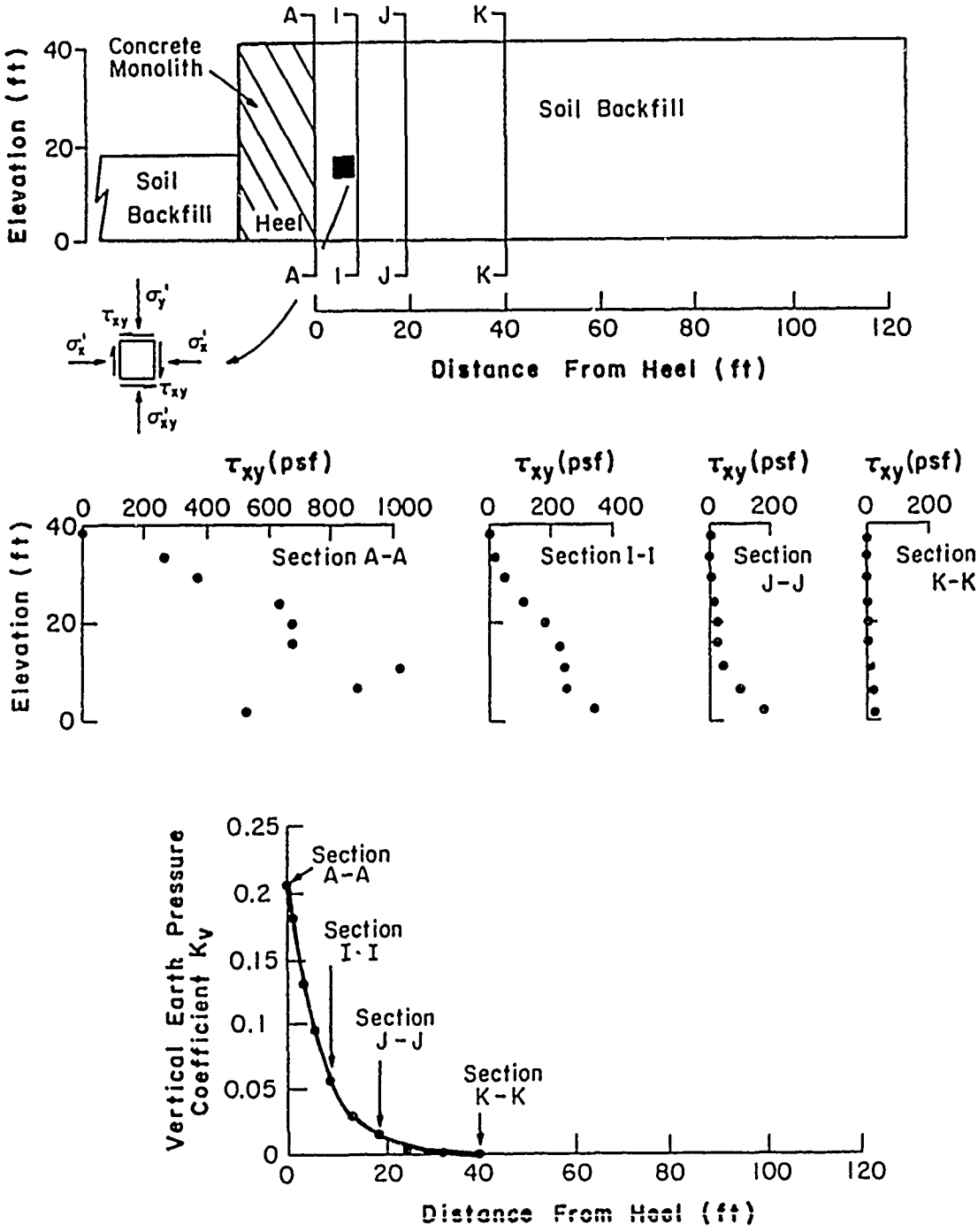

Figure 17. Variation of distribution of shear stress and vertical earth pressure coefficient with distance from the heel of the wall

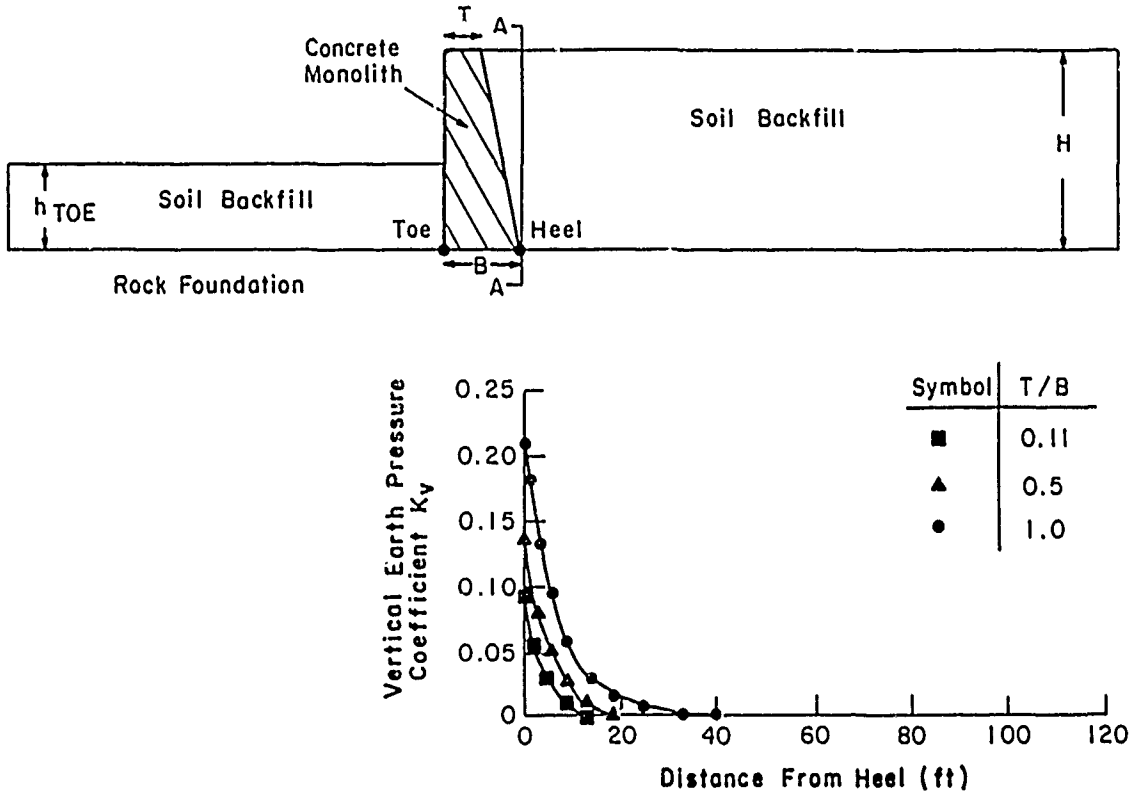

Figure 18. Variations of vertical earth pressure coefficient with distance from the heel of the wall for walls of different face slopes

101. Due to the fact that same soil properties were assigned to the backfill, the magnitude of the resultant lateral forces on Section B-B are the same for both analyses with a corresponding lateral earth pressure coefficient (K_o) equal to 0.51.

102. The effective base contact area increased by a factor of 2 and the maximum compressive stress decreased by a factor of 2 for the stepped back wall (32a) as compared to the results of the planar back wall (31a). The mobilized friction angle along the base decreased from 20.7 to 18.5 deg, reflecting both the decrease in the value of base shear and the increase in the value of base normal force. These observations indicate that the presence of an irregular back on the wall results in a more stable monolith.

103. The presence of a stepped back results in a decrease in the mobilized angle of friction acting on Section C-C from 23.2 to 19.6 deg, reflecting the decrease in the values of both the shear and normal forces.

104. The presence of a stepped back complicates the stress distributions within the backfill compared to that for a wall with a planar back.

This is believed to be not only an inherent feature introduced by the presence of irregular wall geometry adjacent to the backfill but also the result of the analytical boundary condition specified along the interface. The nodal points along the stepped interface were shared by both the wall and the backfill, introducing a kinematic constraint since the predominant orientation of backfill displacements are downward while those of the wall are lateral. This is in contrast to the planar back wall for which interface elements were placed along all faces of the wall, allowing for relative displacements along the interface between the backfill and the wall. For the stepped back wall (32a) K_v is within the range of values from 0.12 to 0.17 and $K_h = 0.45$ along Section A-A, while for the planar back wall (31a) $K_v = 0.09$ and $K_h = 0.48$. A more complete discussion of the details regarding the accuracy of the results is given in Appendix A.

105. The results of these analyses show that a wall with a stepped back has a larger margin of stability than a corresponding wall with a planar back. The presence of a stepped back results in larger values of K_v and smaller values of K_h along Section A-A.

Summary

106. In the backfill placement analyses discussed in the first phase study (Ebeling et al. in preparation), a downdrag force was observed on the back of the wall, resulting from the settlement of the fill under its own weight. The magnitude of the downdrag force was nearly the same for a range of values of Poisson's ratio, unit weight of the backfill, base interface shear stiffness, and depth of toe-fill. F_v is conveniently described in terms of a vertical shear stress coefficient (K_v); the value of K_v was observed to be within the narrow range from 0.13 to 0.14 for a number of cases in which the values of these parameters were varied.

107. In the backfill placement analyses discussed in paragraphs 13 through 69, variations in the magnitudes of the stiffness of the backfill or interface shear stiffness resulted in larger variations in the value of K_v, ranging from 0.09 to 0.15. In the evaluation of walls with different geometries, the magnitude of K_v varied with the inclination of the face of the wall, increasing in value from 0.09 to 0.21 as the back of the wall approached vertical. In addition, a stepped face wall had a larger value of K_v than a planar face wall.

108. An increase in the stiffness of the backfill, or a reduction in the values of the soil-to-concrete interface shear stiffnesses resulted in a

slight increase in the lateral earth pressures acting on the wall. As the back of the wall approached vertical, the lateral earth pressures decreased. As expected, the margin of wall stability increased with increasing wall mass.

109. A pool of water in front of the wall provides a stabilizing influence. A decrease in the pool elevation results in reduction of the resisting force and an increase in base shear and the force exerted by the toe-fill. The distribution of the resisting force between base shear and toe-fill resistance depends on the magnitude of the movements that result from lowering the water level in front of the wall.

PART III: EVALUATION OF THE STABILITY OF RETAINING STRUCTURES USING CONVENTIONAL EQUILIBRIUM METHODS

110. Part III describes evaluations of the stability of earth-retaining structures founded on rock using conventional equilibrium methods. In Part VI of the Ebeling et al. (in preparation) initial phase of study, a comparison between the results of CEA and FEA was made for the base case structure. The CEA and FEA results were extended, as described in these paragraphs, to include consideration of the behavior of the backfill and toe-fill. The interdependency between the mobilized shear resistances on the base of the wall and the earth pressures within the soil fills were investigated. The results were summarized using conventional concepts of the factor of safety against shear failure along the base of the wall (sliding) and within the backfill (referred to as shear factors), related to the magnitudes of the forces acting on the wall.

111. An additional set of analyses are described in which the deformations of a retaining structure during backfilling are sufficient to break the bond between the base of the wall and its rock foundation. The influence of the base shear properties on the base of the wall was examined.

Factor of Safety and Shear Factors

112. Earth-retaining structures of the type discussed in this report can be considered in three parts: the wall, the backfill, and the toe-fill. The backfill applies the driving force while the wall and the toe-fill provide the resisting forces. In a CEA, assumptions are made regarding the magnitude of the forces applied by the backfill, because the conditions of equilibrium are insufficient for determining the magnitude of the load without assumptions. The magnitude of these assumed earth loads correspond to some level of mobilized shear resistance within the backfill. The magnitude of the earth loads can be described using a shear factor (SF). For each fill region there exists an SF, defined as the ratio of the ultimate shear force along a potential slip plane divided by the shear force required for equilibrium.

113. When earth loads on a retaining wall are assumed and the factor of safety against sliding (FS_{base}) is computed, corresponding values of the SF's for the backfill and toe-fill can be inferred from the magnitude of the earth

loads. This interdependence between these factors has been examined using CEA procedures.

114. The base case structure without toe-fill is shown in Figure 19.

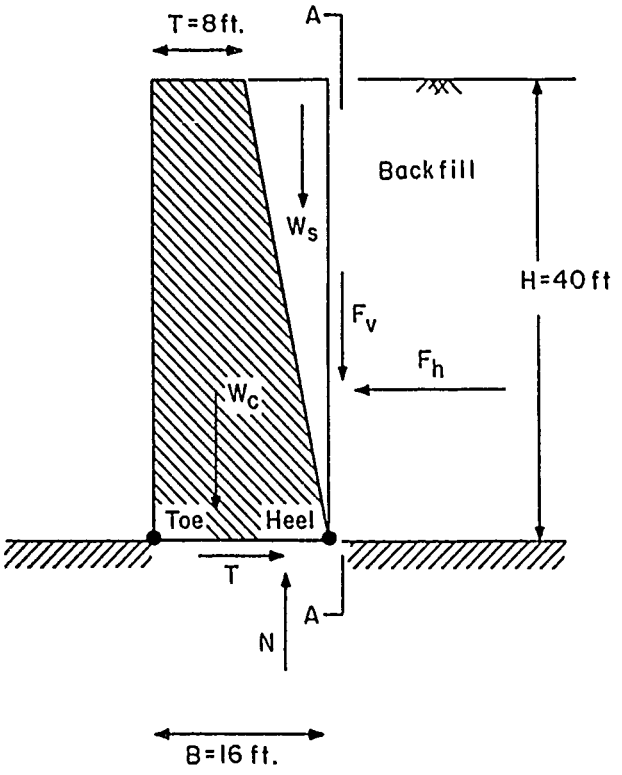

Figure 19. Base case hypothetical structure without toe-fill

The structure is 16 ft wide at the base, 8 ft wide at the crest, and retains 40-ft of backfill. In the Case 13a CEA, summarized in Table 7, Part VI of the Ebeling et al. (in preparation) first phase study, the at-rest earth pressure force, corresponding to $K_o = 0.51$, was applied to Section A-A, the vertical plane through the heel of the wall. Using the CEA forces on the base of the structure, the mobilized base friction angle was 30.5 deg, which is equal to the assumed angle of sliding resistance for the interface. That is, the factor of safety against sliding along the base (FS_{base}) was equal to 1.0.

115. The assumptions regarding the magnitude of the forces acting on Section A-A reflect a corresponding value of the mobilized shear resistance within the backfill, characterized by the SF ($SF_{backfill}$). For the cohesionless backfill of Case 13a, the SF is given by

$$SF_{backfill} = \frac{\tan \phi'}{\tan \phi'_m} \tag{7}$$

where

ϕ' = effective angle of internal friction

ϕ'_m = mobilized angle of internal friction

116. A limiting case occurs when the strength of the soil is fully mobilized ($SF_{backfill} = 1.0$), which coincides with the development of active earth pressures within the backfill.

117. The mobilized angle of friction (ϕ'_m) for this case, corresponding to $K_h = 0.51$ and $K_v = 0$, is equal to 19 deg. This value of ϕ'_m is determined using the Rankine relationship

$$K_h = \tan^2\left[45 - \left(\frac{\phi'_m}{2}\right)\right] \tag{8}$$

This relationship is only valid when K_v is equal to zero. In cases where K_v is not zero, another equilibrium relationship would be used. Coulomb's relationships for K_h and K_v, discussed by Kezdi (1975), can be used when K_v has a value greater than zero.

118. With ϕ' equal to 39 deg for the backfill, the $SF_{backfill}$, defined by Equation 7, is equal to 2.36. It can be observed that although the wall is on the verge of sliding with the assumed earth load, the backfill has a significant margin of safety against shear failure.

119. In the previously described CEA, the assumed set of forces acting on Section A-A ($K_h = 0.51$ and $K_v = 0$) corresponded to $SF_{backfill} = 2.36$ and $FS_{base} = 1.0$. Variations in the value assumed for K_h, between K_o (0.51) and K_a (0.23), results in the relationship between the values of $SF_{backfill}$ and FS_{base} shown in Figure 20. It can be observed that when the strength of the backfill is fully mobilized ($SF_{backfill} = 1.0$), and $K_h = K_a$, the wall has an ample margin of safety against sliding ($FS_{base} = 2.24$). The values of $SF_{backfill}$ and FS_{base} would be equal (1.47) if K_h was equal to 0.35.

120. When assumptions are made regarding the magnitude of the forces acting on a wall, a level of mobilized shear resistance within the backfill is implied, and this value may be characterized by a shear factor. This shear factor may be determined using conventional earth pressure theories. There is thus an interdependence between the computed factor of safety against failure in shear along the base of the wall and the shear factor for the backfill.

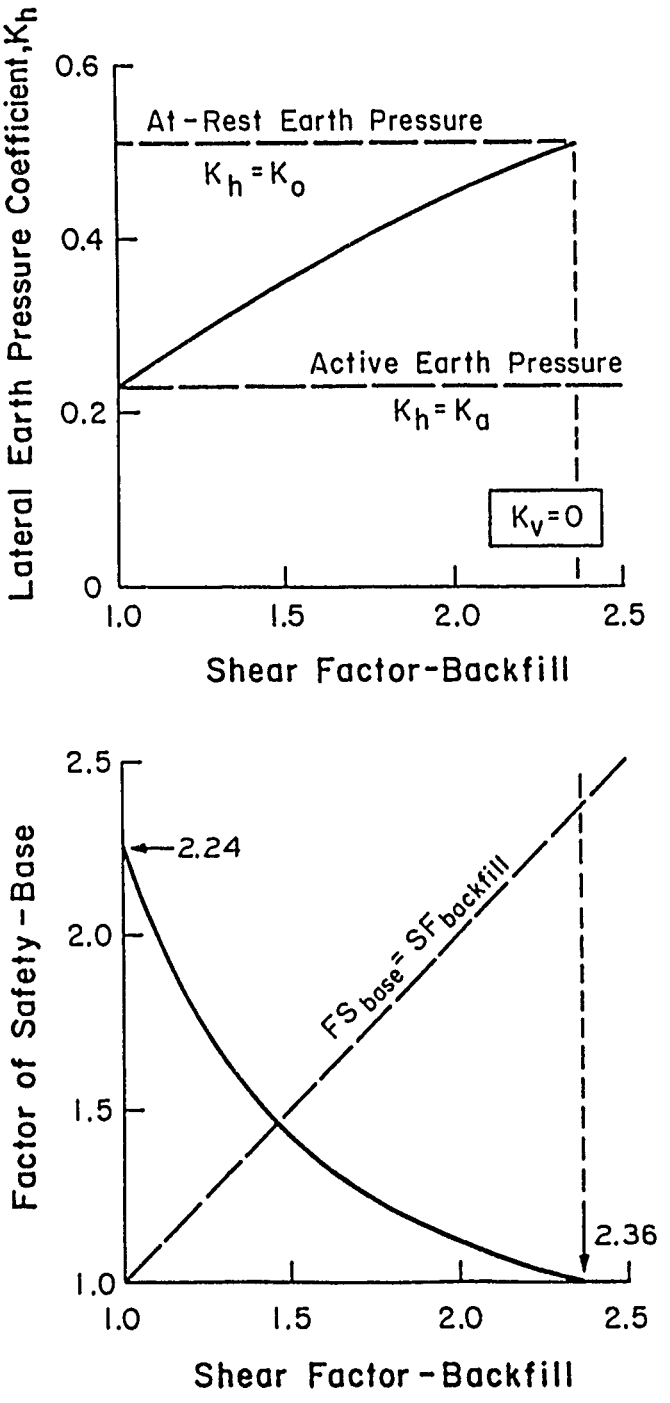

Figure 20. Variations of the lateral earth pressure coefficient and the factor of safety against base shear failure with shear factor of the backfill

Factor of Safety, Shear Factors, Load Factor, and Resistance Ratio

121. In FEA's, the loading exerted by the backfill on the wall is determined by the interaction between the wall and the backfill during placement of the backfill behind the wall. The finite element method of analysis differs from CEA in that it is not necessary to estimate or assume the magnitude of the loads imposed on the structure by the backfill.

122. The results from three backfill placement analyses of the base case structure were summarized in Table 7 of the first phase study (Ebeling et al. in preparation). No water pressures were represented in the analyses. The effect of soil fill at the toe of the wall was investigated using the results of Case 13a (without toe-fill) and Case 17a (with 17.8 ft of toe-fill). In Case 19a the shear stiffness assigned to the interface along the base of the wall was reduced from its standard value, resulting in increased wall movements, reduced backfill loads, and greater toe-fill resistance forces.

123. The effective force acting on Section A-A (called F^*) is the resultant of the forces F_v and F_h'. The resultant effective earth pressure coefficient (K^*) can be defined as

$$K^* = \frac{F^*}{\int_0^H \bar{\sigma}_v \, dh} \tag{9}$$

Using the relationships presented in Part II, K^* can be expressed as

$$K^* = \left(K_v^2 + K_h^2 \right)^{1/2} \tag{10}$$

Table 5 shows that the values of K^* for the backfill are nearly equal to K_h, due to the small contribution of the shear force acting on Section A-A. The mobilized angles of internal friction (ϕ_m') within the backfill were computed using Figure 6 of the Department of the Navy NAVFAC DM7.2 Manual (1982). Coulomb's relationships, discussed by Kezdi (1975), may also be used, and they result in the same values of ϕ_m'. Figure 21 shows the resulting variation of the shear factor with the mobilized angle of friction of the

Table 5

Shear Factor, Load Factor, and Resistance Ratio for Backfill and Toe-Fill

a. Shear and Load Factors for Backfill

Case	Section A-A				Backfill			
	K_v	K_h	K^*	δ_m deg	ϕ'_m deg	Shear Factor $SF_{backfill}$	K_a	Load Factor
13a	0.138	0.453	0.474	16.9	19	2.35	0.23	2.06
17a	0.137	0.454	0.474	16.8	19	2.35	0.23	2.06
19a	0.138	0.337	0.364	22.2	25	1.74	0.23	1.58

b. Shear Factor and Resistance Ratio for Toe-Fill

Case	Section E-E				Toe-Fill			
	K_v	K_h	K^*	δ_m deg	ϕ'_m deg	Shear Factor SF_{toe}	K_p	Resistance Ratio
13a	--	--	--	--	--	--	--	--
17a	0.156	0.548	0.569	15.9	14	3.25	14.24	0.04
19a	0.069	1.446	1.448	2.7	12	3.81	14.24	0.10

Note: Shear factor = $\tan \phi' / \tan \phi'_m$ where $\phi' = 39$ deg
Load factor = K^*/K_a
Resistance ratio = K^*/K_p
-- indicates not applicable

backfill. It is observed that as the mobilized angle of friction increases, the resultant force applied to the wall decreases; that is, the wall does less of the work resisting the applied force as more of the work is done by the backfill.

124. For Cases 13a and 17a, ϕ'_m was equal to 19 deg, and for Case 19a, ϕ'_m was equal to 25 deg as shown in Table 5a. Using Equation 7, with the effective angle of internal friction equal to 39 deg, the resulting

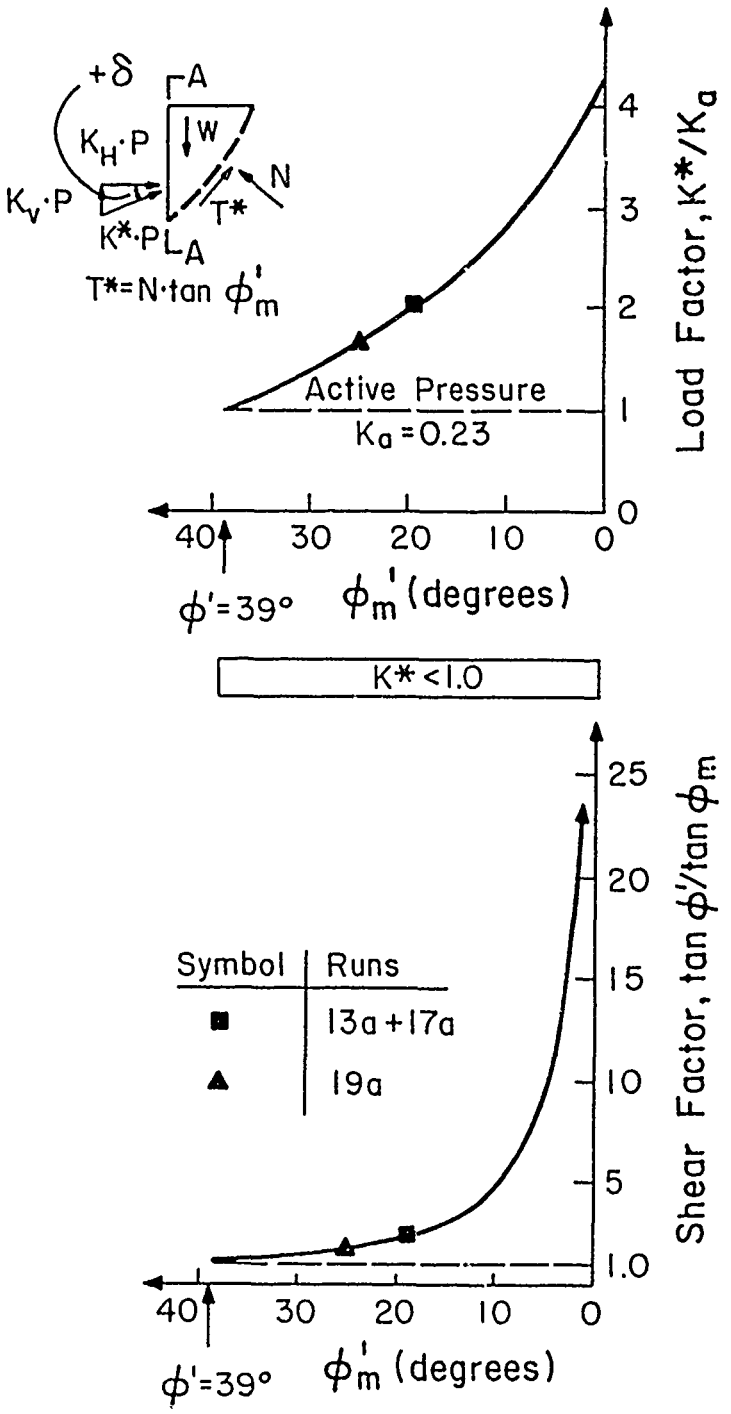

Figure 21. Variations of shear factor and load factor with mobilized angle of friction, backfill

shear factors for the backfills ($SF_{backfill}$) were found to be equal to 2.35 and 1.74 as shown in this table. From Table 7 (Ebeling et al. in preparation), $FS_{base} = 1.29$ for Case 13a, $FS_{base} = 1.75$ for Case 17a, and $FS_{base} = 11.6$ for Case 19a. For the base case analyses (13a and 17a), the margin of safety is greater for the backfill than the base, where the reverse is observed for Case 19a.

125. Another index that can be used to characterize the magnitude of the applied load is referred to as the load factor, defined as the ratio of the resultant earth pressure coefficient (K^*) divided by the active earth pressure coefficient ($K_a = 0.23$). The variation in the load factor with mobilized angle of friction for the backfill is shown in Figure 21. The larger the value of ϕ'_m, the smaller the load applied to the wall (K^*). The limiting value of load factor equal to unity corresponds to the full mobilization of the shear resistance within the backfill. In this condition, the earth pressures are equal to their active values. For Cases 13a and 17a, the load factor was equal to 2.06, and for Case 19a, the load factor was equal to 1.58.

126. The presence of 17.8 ft of toe-fill (Cases 17a and 19a) provides additional resistance to the loads applied by the backfill, and decreases the contribution required from the wall to the total resistance. The proportion of total resisting force provided by the toe-fill depends on the magnitude of the wall deformations; increased wall deformations result in larger contributions from the toe-fill.

127. Characterizing the magnitude of the force applied by toe-fill is more involved than was the case for the backfill. The value of ϕ'_m is dependent upon the orientation of the shear force developed along the slip plane (T*) as shown in Figure 22. When the shear force (T*) counteracts the effect of the gravity force, the relationship for the shear factor (SF_{toe}) to the left of $\phi'_m = 0$ is valid.

128. When T^* acts in the direction consistent with W, the relationship to the right of $\phi'_m = 0$ is valid. In this case, the value of K^* is greater than 1.0. The equilibrium relationship used is that associated with the development of passive pressures, which is sensitive to the value of the mobilized angle of friction on Section E-E (δ_m).

129. The reversal in the direction of T^* occurs when $K^* = 1.0$, for which $T^* = 0$ and $\phi'_m = 0$, resulting in an infinite value for the shear factor. Thus, the shear factor has two limitations as an index; it is

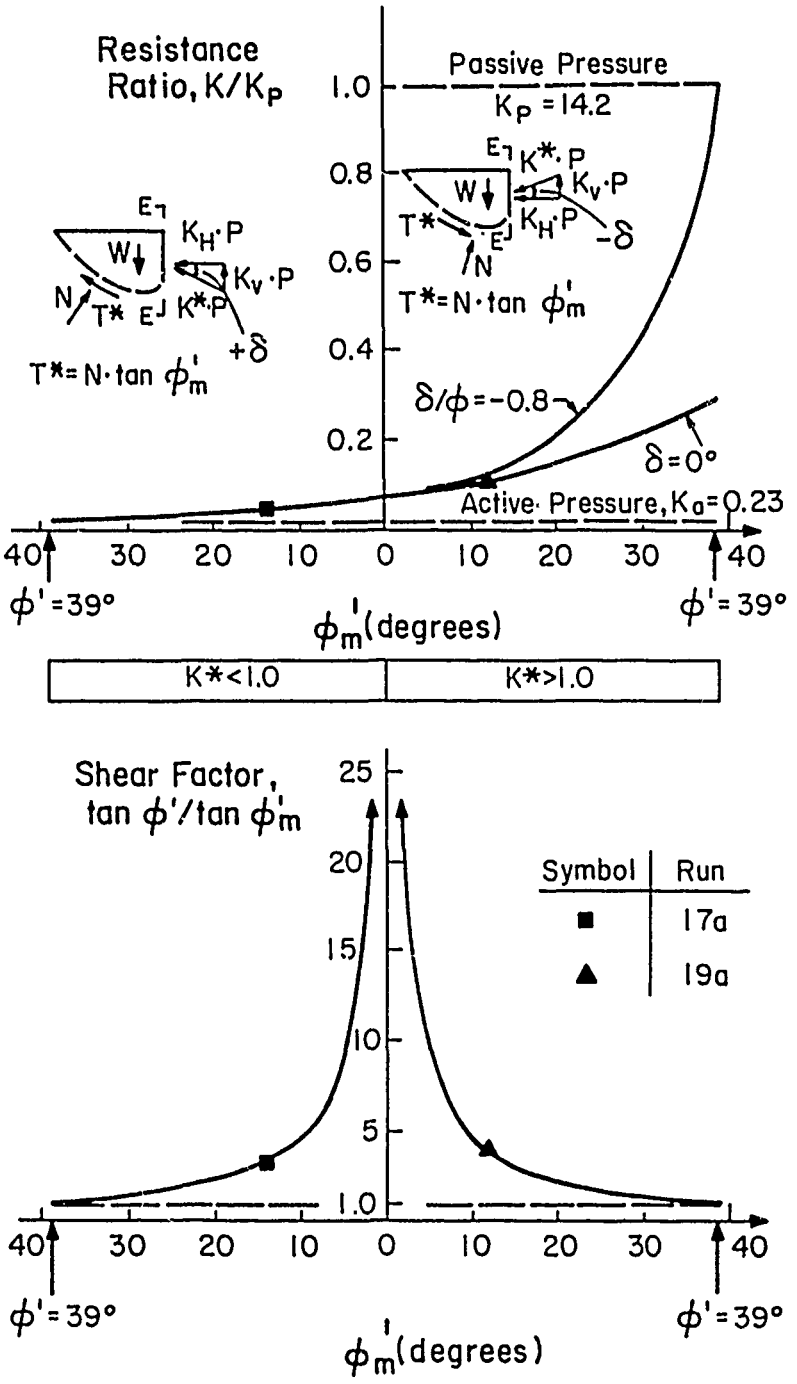

Figure 22. Variations of shear factor and resistance ratio with mobilized angle of friction, toe-fill

discontinuous, and each value represents two different levels of wall loads, corresponding to two different directions of the shear stress on a potential slip plane.

130. Another index that can be used for the toe-fill, which overcomes the limitations of the shear factor, is referred to as the resistance ratio. The resistance ratio is defined as the ratio of the resultant effective earth pressure coefficient (K^*) for Section E-E divided by the passive earth pressure coefficient ($K_p = 14.24$ for $\delta/\phi' = 0.8$). Figure 22 shows the variation in the resistance ratio with mobilized angle of friction for the toe-fill. It can be seen that, unlike the shear factor, the resistance ratio is continuous and single valued. The resistance ratio has a minimum value of $K_a/K_p = 0.02$, when the earth pressures are equal to their active value ($K^* = K_a$), and a maximum value of unity, when the earth pressures are equal to their passive value ($K^* = K_p$).

131. As noted previously, the active and passive states of stress both correspond to full mobilization of the shear resistance within the backfill but with T* acting in opposite directions. In Case 17a, the resistance ratio of the toe-fill is equal to 0.04. The resistance ratio increases to a value of 0.10 as a result of the increased wall deformations in Case 19a (Table 5). Although there was a two and one-half fold increase in the resistance ratio in Case 19a, 90 percent of the resisting force provided by toe-fill still has not been mobilized.

132. In the base case analysis (17a), the driving force of the backfill was characterized by $SF_{backfill} = 2.35$, with the load factor equal to 2.06, while the resisting forces of the base and the toe-fill were characterized by $FS_{base} = 1.75$ and the resistance ratio of the toe-fill was equal to 0.04. With the increased wall deformations for Case 19a, $SF_{backfill} = 1.74$ (26 percent decrease), the load factor was 1.58 (23 percent decrease), $FS_{base} = 11.6$, and the resistance ratio was 0.10. It may be observed that increased wall deformations resulted in an increase in the degree of soil-structure interaction, exemplified by:

a. Mobilization of a greater portion of the available shear resistance within the backfill, as evinced by the decrease in the value of $SF_{backfill}$.

b. A reduction in the magnitude of the load applied by the backfill to the wall, characterized by a decrease in the value of the load factor.

c. An increase in the resistance provided by the toe-fill, with a corresponding increase in the value of the resistance ratio.

d. The required contribution of shear on the wall to the total resisting force was reduced, as exemplified by the increase in the value of the FS_{base}.

Loss of Bond Between Wall and Foundation

133. This section describes a set of three equilibrium analyses considering a hypothetical case in which the deformations of a retaining structure during backfilling are sufficient to break the bond along the interface between the base of the wall and the rock foundation. The interdependence between the forces acting on the wall, the ultimate shear resistance along the base of the wall, and the resulting deformations were examined in the analyses.

134. The structure shown in Figure 23 retains backfill 20 ft in height,

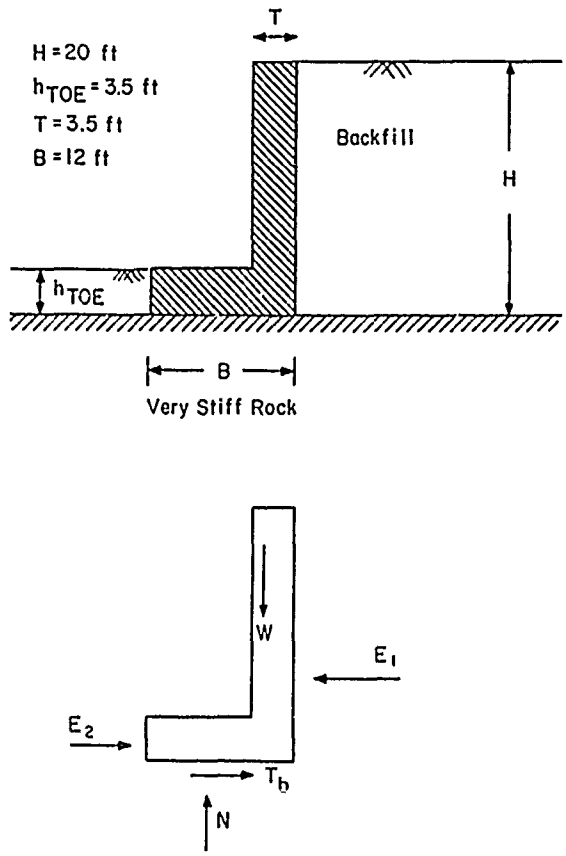

Figure 23. Hypothetical structure used in example of loss of bond along the base of the wall

is 3.5 ft thick, 12 ft wide at its base, and is buttressed by 3.5 ft of toe-fill. The forces acting on the structure are:

W = weight of the retaining structure
= 14,963 lb

E_1 = earth load resulting from the placement of backfill

E_2 = resisting force due to the presence of toe-fill

N = normal force along the base of the wall
= W

T_b = shear load along the base of the wall

135. The vertical shear forces acting on the back and the front of the wall were assumed to be equal to zero, which from previous equilibrium analyses (i.e. Part VI (Ebeling et al. in preparation)) is known to be a conservative assumption. No water pressures were considered in the analyses.

Material parameters

136. The standard set of material parameters were assigned to the clean granular backfill (D_r = 75 percent); the unit weight of the soil is equal to 135 pcf and the effective angle of internal friction is 39 deg. The strength of the concrete-to-rock interface was modeled using Mohr-Coulomb strength parameters. In a limited number of direct shear tests conducted by the US Army Corps of Engineers on the interfaces between concrete and competent rock, described by Benson et al. (1987), deformations on the order of 0.01 in. resulted in the loss of bond between the materials. Prior to loss of bond between the concrete and rock, the peak shear resistance of the interface between the base of the wall and the rock foundation (τ_p) was given by

$$\tau_p = C_a + \sigma_n \cdot \tan \delta_{bp} \tag{11}$$

where

C_a = bond, or adhesion, between the concrete and the rock
= 2,000 psf

σ_n = normal stress along the interface

δ_{bp} = peak angle of internal friction

137. The three analyses differed by the values of the angle of internal friction assigned to the interface; δ_{bp} = 30 deg for Case 1, δ_{bp} = 15 deg for Case 2, and δ_{bp} = 10 deg for Case 3.

138. For lateral wall deformations greater than 0.01 in., the loss of bond along the base of the wall was characterized by a value of C_a equal to zero and a residual shear strength (τ_r) given as

$$\tau_r = \sigma_n \cdot \tan \delta_{br} \tag{12}$$

where δ_{br} is the residual angle of internal friction. The values of δ_{br} were equal to the values of δ_{bp} for all three cases.

E_1 and E_2 for
complete backfill and toe-fill

139. The magnitude of the lateral forces E_1 and E_2, resulting from the placement of fill behind and in front of the wall, may be expressed using the lateral earth pressure coefficient K_h. The variation of the lateral earth pressure coefficient with wall movement is shown in Figure 24. The average yield of the soil is defined as the average lateral deformation of the backfill along the wall-to-soil interface ($(u_x)_{ave}$) divided by the height of the backfill (H*). This term was first introduced by Terzaghi (1936) to explain the consistency between the measured lateral load versus deformation behavior of the sand backfills in the 1934 tests (Terzaghi 1934) using translating and rotating walls. It is important to recognize that the relationship in Figure 24 models the variation of K_h with average yield based on the final fill height (H*).

140. When the average displacement along the soil-wall interface ($(u_x)_{ave}$) is equal to zero, the values of the at-rest earth pressure coefficients (K_o) are equal to 0.5 for the backfill and 0.6 for the toe-fill. As the wall displaces the toe-fill, idealized at the upper left in Figure 24, K_h increases from a value of $K_o = 0.6$, as shown in this chart at the bottom of this figure. When $(u_x)_{ave}$ was equal to 4.2 in. [$(u_x)_{ave}/H^* = 0.1$], the earth pressures attained their passive values ($K_p = 4.4$) in the toe-fill.

141. As the wall moved away from the backfill, shown at the upper right in Figure 24, K_h decreased from a value of $K_o = 0.5$, as shown by this chart at the bottom of the figure. When $(u_x)_{ave}$ was equal to 0.96 in. ($(u_x)_{ave}/H^* = 0.004$), the earth pressures were equal to their active values ($K_a = 0.23$) within the backfill. It can be seen that the values of average yield required to attain active pressures within the backfill are an order of magnitude smaller than those required to attain passive pressures.

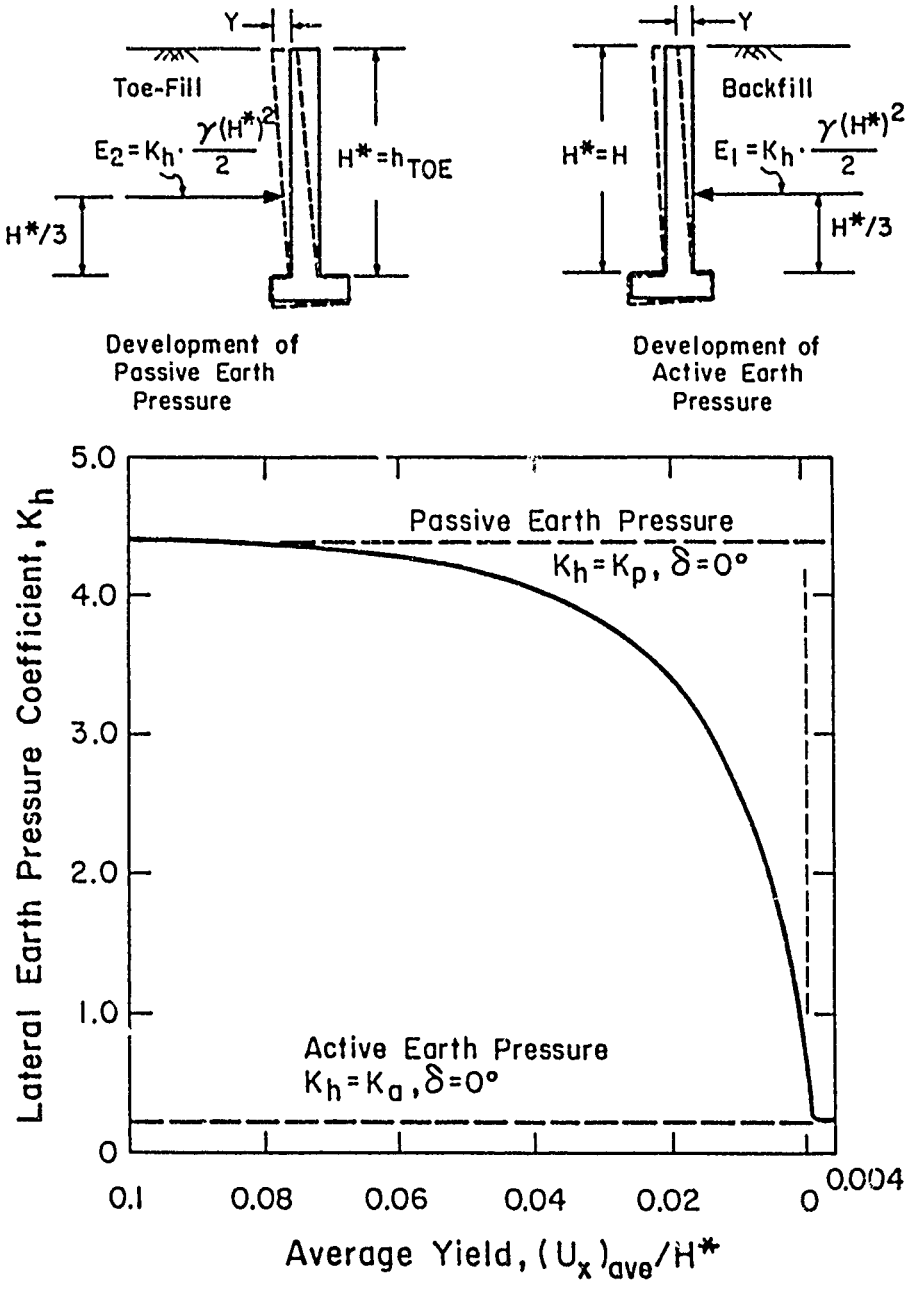

Figure 24. Variation of the lateral earth pressure coefficient with average yield

142. When the variation in K_h of Figure 24 is normalized by its extreme values, the development of the limiting states of pressures (K_p and K_a) may be compared with those measured in tests involving retaining walls (Terzaghi 1934, Johnson 1953) or computed in previous analytical studies (Clough and Duncan 1971), as shown in Figures 25 and 26.

143. In Figure 25 the reduction in K_h with average yield away from the backfill is shown. For the backfill, a normalized value of zero

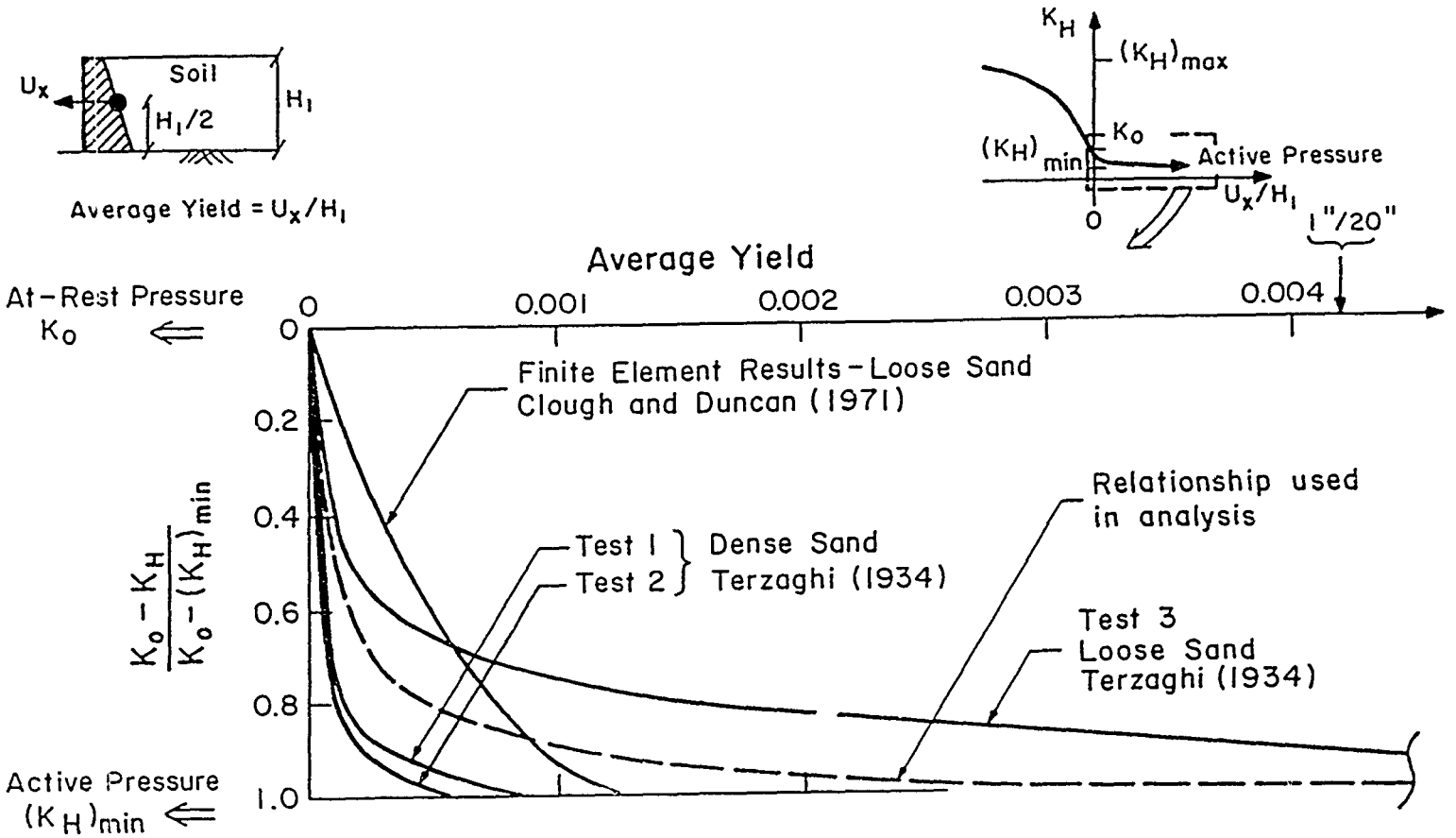

Figure 25. Variation of normalized lateral earth pressure coefficient with average yield of the wall away from the backfill

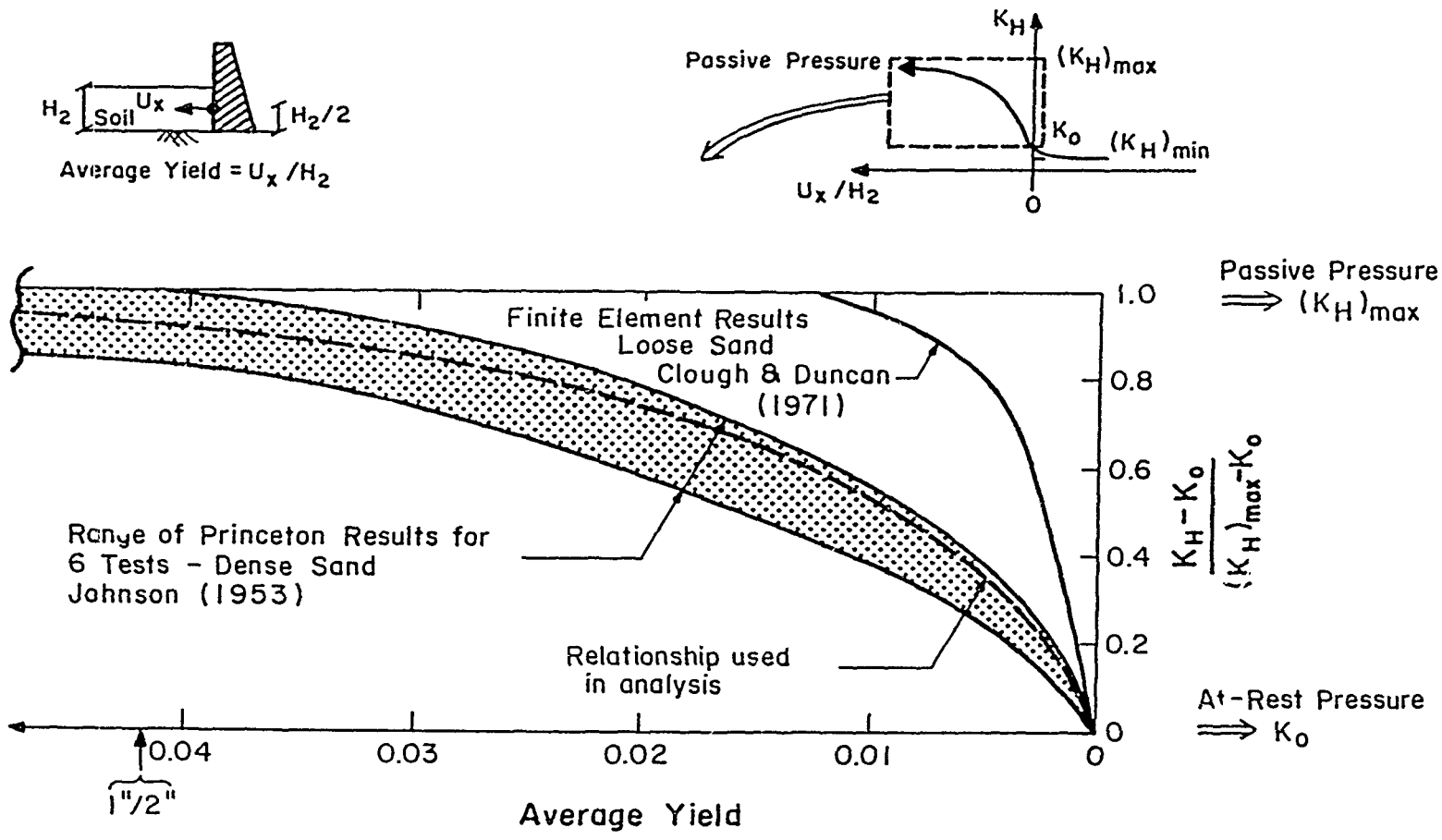

Figure 26. Variation of normalized lateral earth pressure coefficient with average yield of the wall displacing fill

corresponds to K_o (0.50) and a normalized value of unity corresponds to $(K_h)_{min} = K_a$ (0.23). It can be seen that the shape of the normalized curve in Figure 25 is nonlinear. A significant portion of the reduction in K_h occurred during the first stages of wall movement away from the backfill. The shape of the curve used in the analyses was consistent with the three tests conducted by Terzaghi (1934) using a wall retaining approximately 5 ft of loose or dense sand, and with the analytical studies of Clough and Duncan (1971), who used the finite element method to analyze a wall retaining 10 ft of loose sand.

144. In Figure 26, the increase in K_h with movement of the wall toward the toe-fill is shown. For the toe-fill, a normalized displacement value of zero corresponds to K_o (0.6) and a normalized displacement value of unity corresponds to $(K_h)_{max} = K_p = 4.4$. The shape of the normalized curve for the toe-fill was more nearly linear than was the case for the backfill. It can be observed that the relationship of Figure 24 is consistent with the shape of the curves for the six experimental tests conducted by Johnson (1953) using a wall retaining 2 ft of dense sand.

Values of E_1 and E_2 during placement of soil fill in the finite element analyses

145. This section describes the development of a relationship between the height of the fill, the applied forces, and the displacements for the wall. It is based on the results of the backfill placement analyses using the finite element method and therefore models the behavior of a wall when there is no loss of bond and no sliding of the wall along the concrete-to-rock interface.

146. Several backfill placement analyses of retaining walls were discussed in Part VI of the first phase study (Ebeling et al. in preparation) and in Part II of this report. The variations of earth pressure forces with wall movement are shown in Figure 27 for the 40-ft-high wall of Case 13a (no toe-fill) and Case 17a (17.8 ft of toe-fill). The nine points represent the results after placement of each of the 4.44-ft-thick soil lifts. It can be seen that the relationship between F_h and $(u_x)_{ave}$ (Figure 27) is nonlinear.

147. After completion of backfilling for Case 13a (no toe-fill), $F_h = 48{,}922$ lb ($K_h = 0.45$) and $(u_x)_{ave} = 14 \times 10^{-4}$ ft. The eight intermediate values of F_h and $(u_x)_{ave}$ were normalized by these final values, as shown in Figure 28.

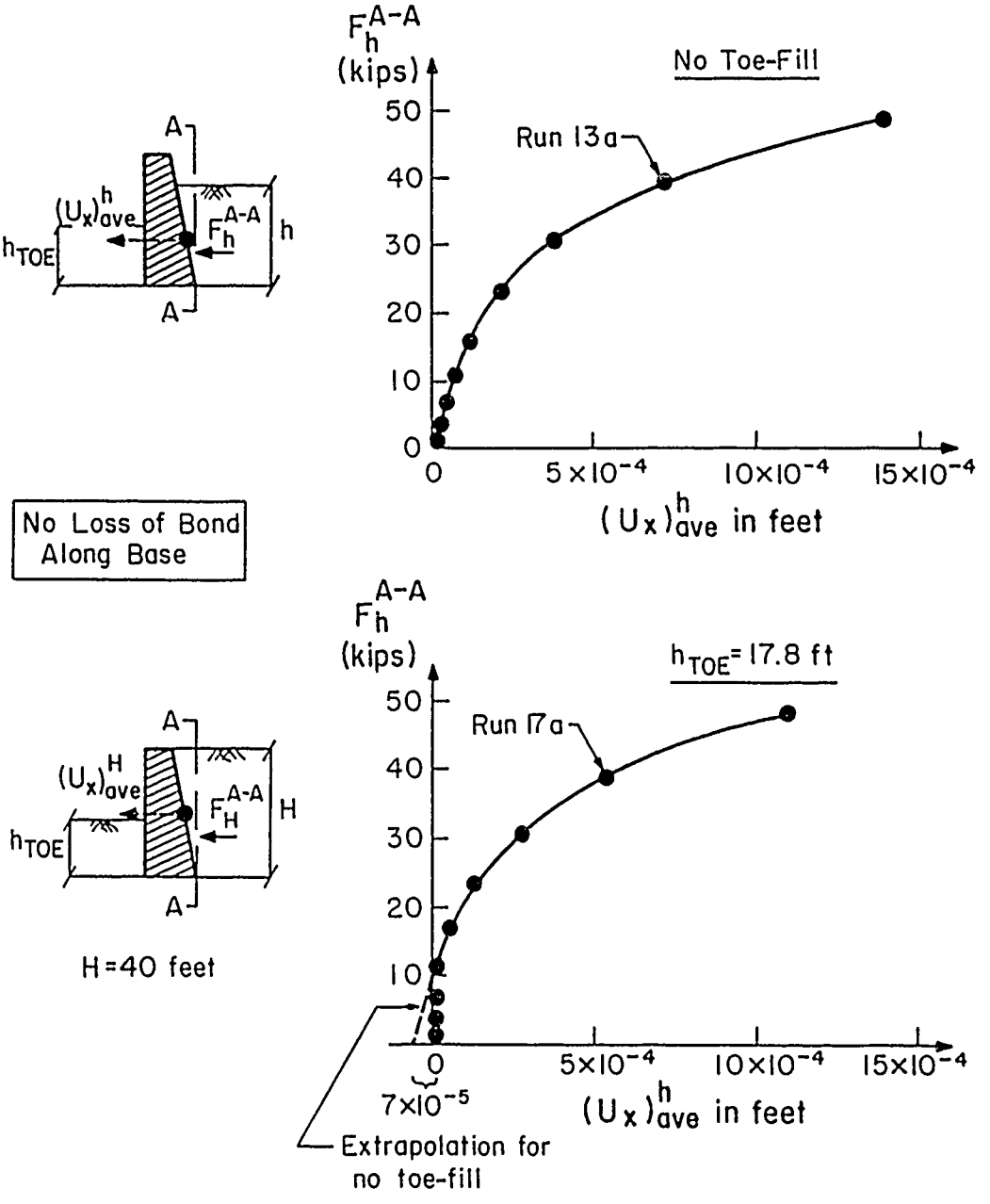

Figure 27. Variation of lateral force acting on plane A-A with wall displacement

148. For the base case structure with 17.8 ft of toe-fill (Case 17a), the final values of F_h = 49,008 lb (K_h = 0.45) and $(u_x)_{ave} = 11 \times 10^{-4}$ ft. The normalized intermediate values of F_h, $(u_x)_{ave}$, and height of fill during the nine stages of backfilling are shown in Figure 29.

149. Case 17a differs from Case 13a by the placement of 17.8 ft of toe-fill. During the first four stages of backfilling, 4.44-ft-thick lifts of fill were placed in front of as well as behind the wall, resulting in no

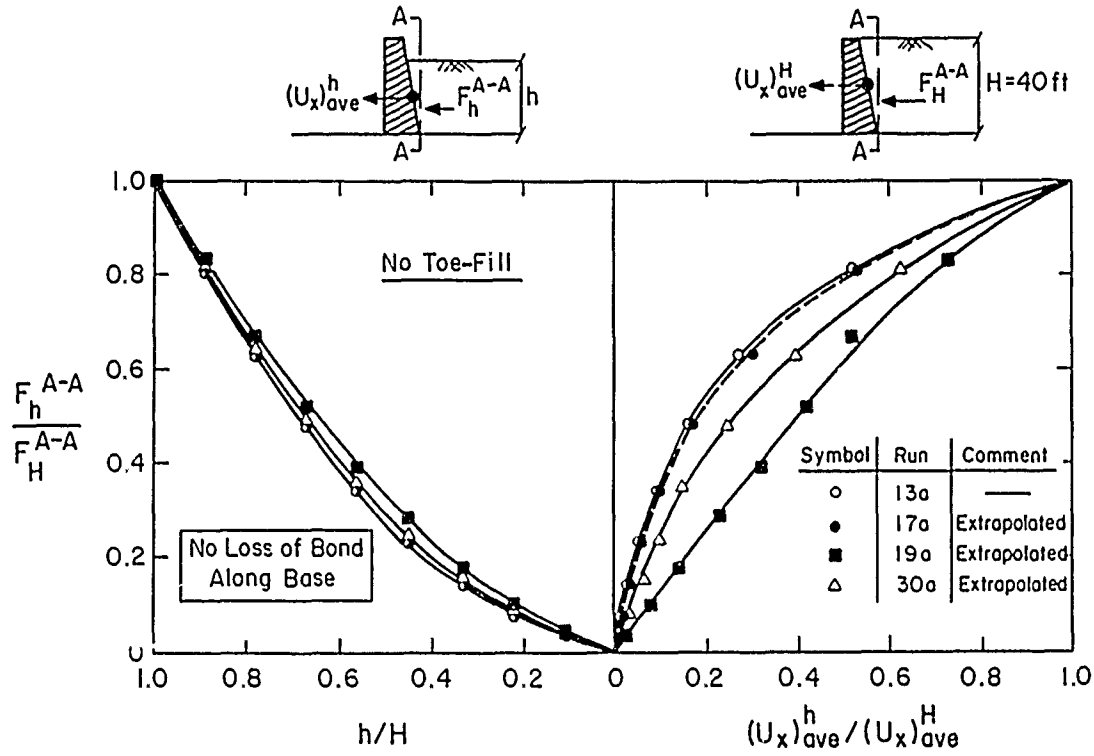

Figure 28. Variation of normalized lateral force acting on plane A-A with normalized height of backfill and wall displacements, without toe-fill

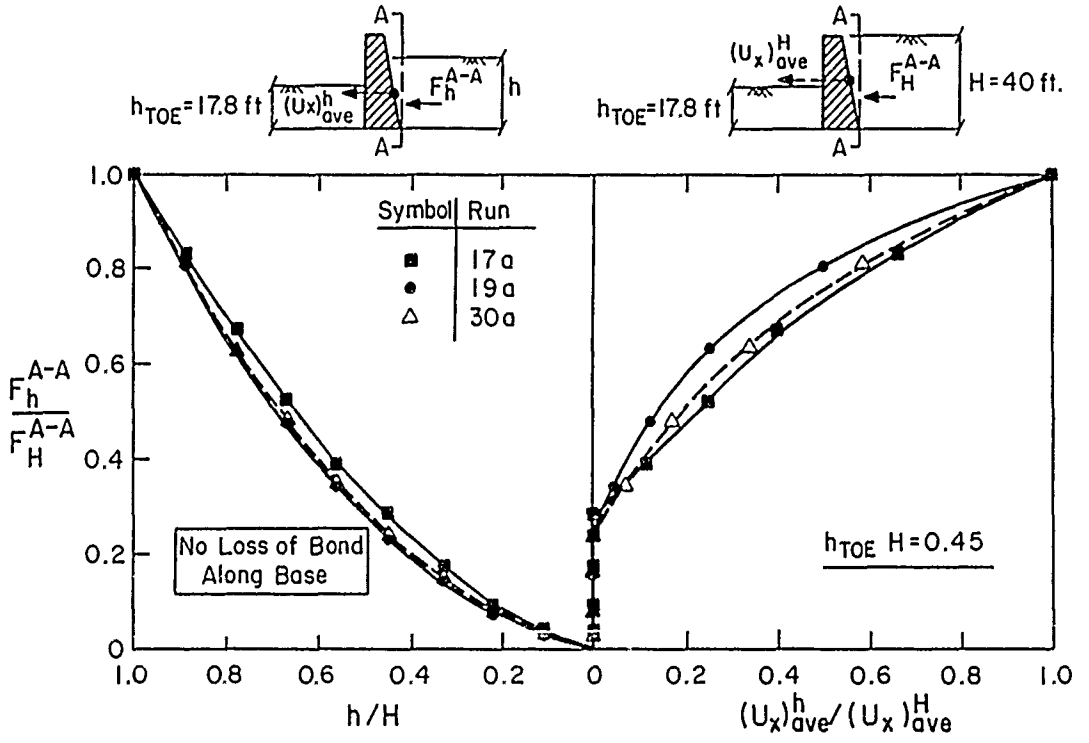

Figure 29. Variation of normalized lateral force acting on plane A-A with normalized height of backfill and wall displacements, toe-fill

lateral displacements until the height of backfill exceeded 17.8 ft. Due to the presence of the toe-fill, the final average lateral displacements were smaller by 22 percent.

150. The normalized results for the intermediate stages of backfilling for Cases 19a and 30a are shown in Figure 29. In Case 19a, a reduced shear stiffness was assigned to the concrete-to-rock interface for the base case wall. Compared to Case 17a, the backfill load on Section A-A was reduced and the wall movements were increased.

151. The rectangular wall of Case 30a retains backfill 40 ft in height and is buttressed by 17.8 ft of toe-fill. For this wall, both the lateral force on Section A-A and the average displacement were smaller than those of the base case. It can be seen in Figure 29 that there is good agreement between the normalized results for the three cases, which is quite interesting since the differences between the magnitudes of the final lateral forces and concrete-to-soil interface displacements were so large.

152. The normalized values of the lateral forces acting on Section A-A and average wall movements, are shown in Figure 30 for the four analyses. The lateral forces are characterized by the ratio K_h/K_o . The magnitude of the lateral force acting on Section A-A decreases with increasing wall movement and is lower when the back of the wall is vertical.

153. The results for Cases 17a, 19a, and 30a were used to estimate the increase in lateral displacements for walls without toe-fill by extrapolation of the computed results for walls with toe-fill, as shown in Figure 27 for Case 17a. The procedure resulted in a predicted increase in the total displacements of 7×10^{-5} ft. It can be seen in Figure 28 that the resulting normalized relationship for Case 17a is in good agreement with that of Case 13a, the base case wall without toe-fill. This is due in part to the smaller increments of wall movements occurring during the first stages of backfill placement, as compared to the latter stages. The extrapolation procedure was also applied to the results from Cases 19a and 30a, as shown in Figure 28. The variation in the results for the normalized forces (during backfilling) versus normalized displacements was larger than that of Figure 29, but the variation in normalized forces with height of backfill was about the same.

154. Using the normalized relationships of Figures 28 and 29, the relationships for the wall shown in Figure 22 ($h_{toe}/H = 0.175$) was developed, as shown in Figure 31. To use Figure 31, the values of F_h on Section A-A and

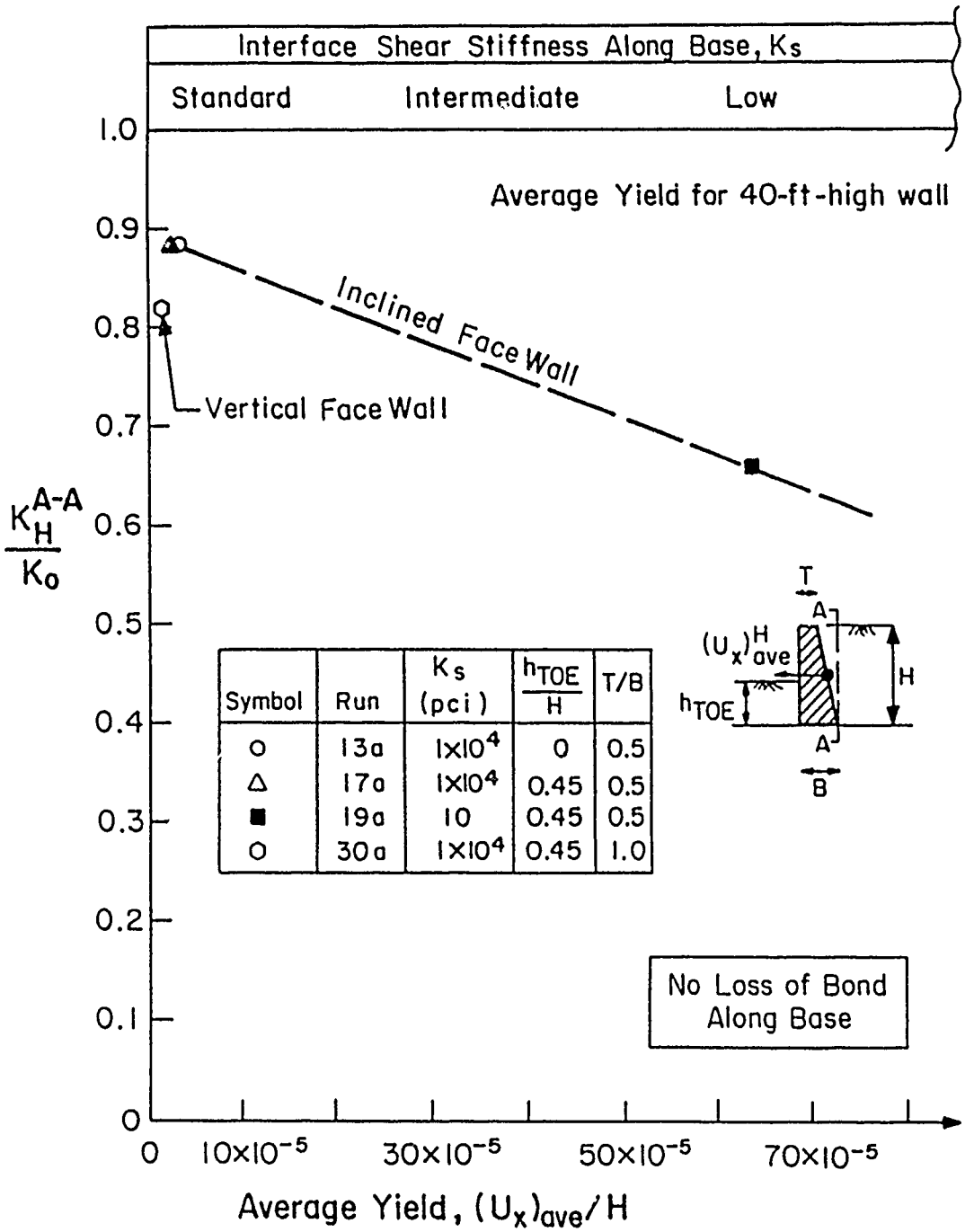

Figure 30. Normalized lateral earth pressure coefficient versus average yield of wall 40 ft in height

$(u_x)_{ave}$, after completion of backfilling, are required. These were determined using Figure 30. For a 40-ft-high wall with a vertical back and an intermediate concrete-to-rock interface shear stiffness, the average yield (after backfilling) was equal to 40×10^{-5} and K_h/K_o is equal to 0.66. In Part V of the first phase of study (Ebeling et al. in preparation), it was shown that the displacement of a wall varied with the square of its height.

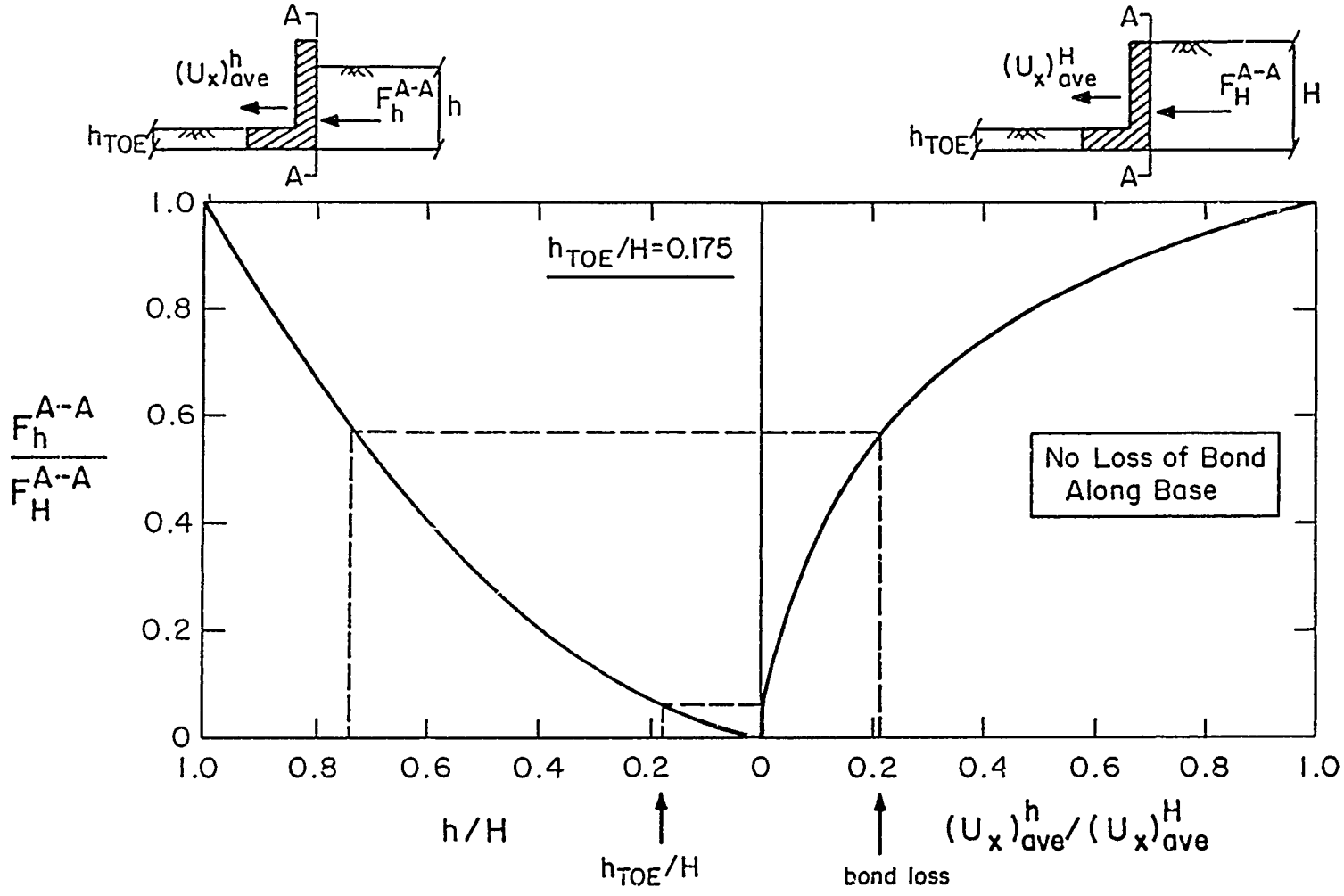

Figure 31. Variation of normalized lateral force acting on plane A-A with normalized height of backfill and wall displacements

The average yield would therefore be approximately 20×10^{-5} for a wall 20 ft in height, with the final $(u_x)_{ave}$ equal to 0.048 in.

155. The precise value of the factor between displacements for like structures of different heights is not known and thus needs to be evaluated in future studies. Since K_o was equal to 0.5 in the analyses, E_1 was equal to 8,950 lb after completion of 20 ft of backfilling. Intermediate values of E_1 and $(u_x)_{ave}$ during backfilling are determined using the normalized relationships shown in Figure 31.

Loss of bond along base of wall--equilibrium analyses

156. Three backfill placement analyses were performed for the retaining structure shown in Figure 23, considering possible deformations during backfilling exceeding 0.01 in., which would be sufficient to break the bond between the base of the wall and the rock foundation. The interdependence between the forces acting on the front and back of the wall (E_1 and E_2), the ultimate shear resistance along the base of the wall (T_b) and the resulting deformations can be demonstrated by these equilibrium analyses. The three analyses differed by the value of the angle of friction assigned to the interface (δ_{bp} and δ_{br}); the values of δ_{bp} and δ_{br} were equal to 30 deg for Case 1, 15 deg for Case 2, and 10 deg for Case 3.

Case 1 equilibrium analysis

157. The forces acting on the wall (Figure 23) at the end of backfilling and the subsequent lateral wall displacements are shown in Figure 32 for the Case 1 analysis ($\delta_{bp} = \delta_{br} = 30$ deg). E_1 is the earth load resulting from the placement of backfill, E_2 is the passive resistance from the toe-fill, and T_b is the shear load acting along the base of the wall.

158. The dashed relationship labeled $(E_1)_{complete\ backfill}$ describes the variation in E_1, after completion of backfilling with the average lateral wall displacements, as given in Figure 24. The earth load (E_1) must intersect this relationship at the completion of backfilling, which is labeled Stage 5 in the figures.

159. The ultimate resistance of the wall, labeled "shear and passive resistance" in Figure 32, is equal to the sum of the ultimate shear force developed along the base of the wall and E_2. This relationship is discontinuous at a lateral displacement equal to 0.01 in., the displacement that corresponds to the loss in bond between the wall and the foundation. For

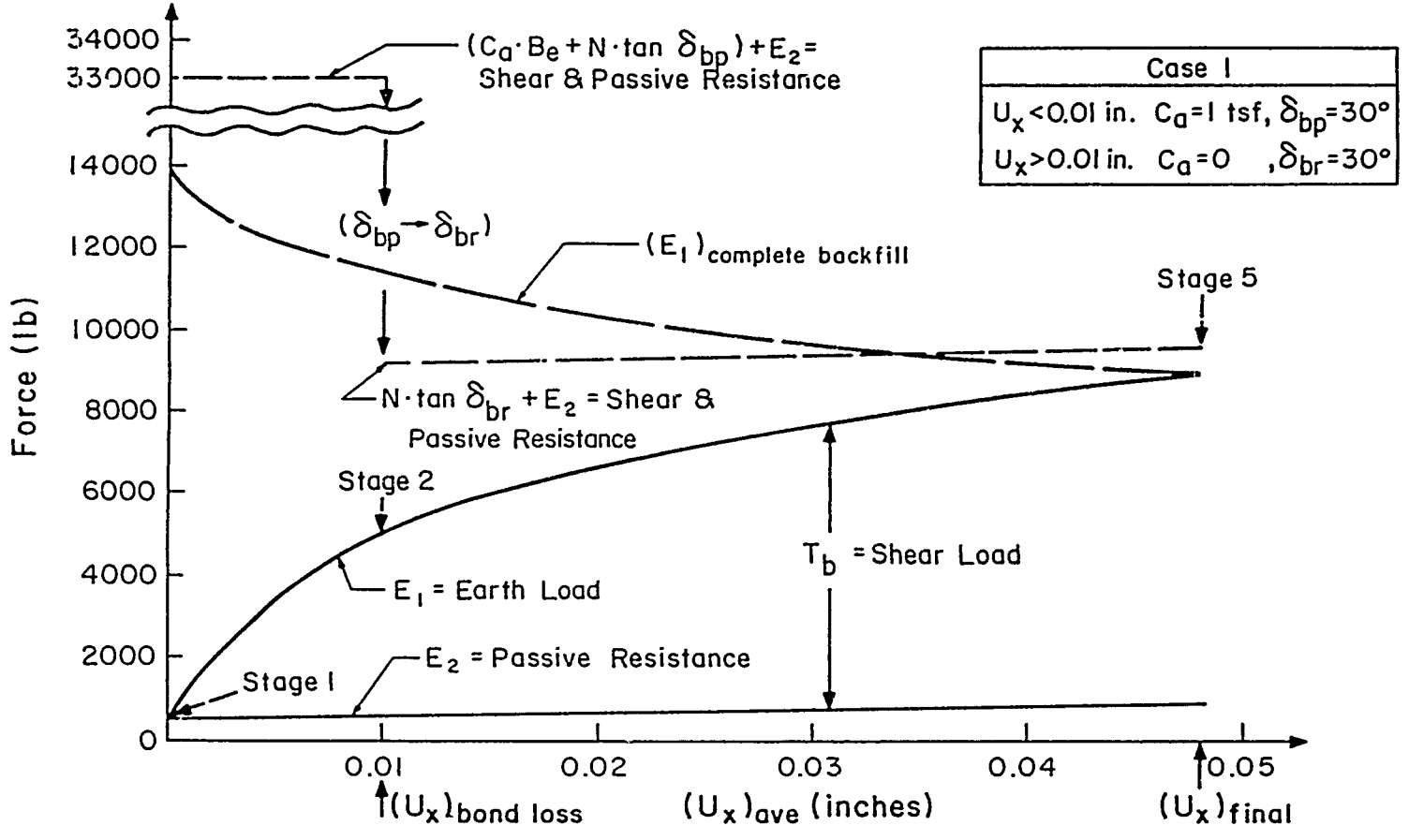

Figure 32. Variation of forces acting on the wall with deformation, Case 1

displacements less than 0.01 in., the ultimate shear resistance is given by Equation 11 with C_a = 2,000 psf (1 tsf) and δ_{bp} = 30 deg. At 0.01 in. of displacement, the adnesion was lost (C_a = 0), and the ultimate shear resistance is given by Equation 12 with δ_{br} = 30 deg.

160. For a bonded base, the value of E_1 for any level of backfill is determined using Figure 31, with E_1, after completion of backfilling, equal to 8,950 lb and the final $(u_x)_{ave}$ equal to 0.048 in. (corresponding to a final average yield equal to 20×10^{-5}). This relationship is valid until the loss of bond occurs ($(u_x)_{ave}$ = 0.01 in.) and under certain conditions, to be discussed subsequently, is valid after the displacements exceed 0.01 in.

161. The backfill placement equilibrium analyses involved as many as five stages. The first stage corresponded to the simultaneous placement of backfill and toe-fill to a height equal to h_{toe} (3.5 ft), with no lateral displacement. The value of E_1 was equal to 537 lb, using Figure 31, and E_2 was equal to 496 lb, using Figure 24. By equilibrium of forces in the horizontal direction, the shear load along the base of the wall is equal to the difference between E_1 and E_2, 41 lb. The ultimate shear and passive resistance (33,135 lb) was much larger than the required resistance ($T_b + E_2$ = 537 lb), and as expected, no shear failure occurred along the base of the wall at this stage of backfilling.

162. As backfilling behind the wall proceeded, the wall moved away from the backfill, displacing the toe-fill. The value of E_1 increased with increasing height of backfill (Figure 31), and the value of E_2 (Figure 24) increased with increasing wall displacements. With the increase in the magnitude of E_1 greater than that of E_2, an increase in the shear load on the base (T_b) resulted. When the height of backfill was equal to 14.8 ft (h/H = 0.74), the displacement of the wall was equal to 0.01 in. (Figure 31), resulting in the loss of bond along its base. At this stage of backfilling, labeled Stage 2 in the Figure 32, E_1 = 5,102 lb, E_2 = 580 lb, and T_b = 4,522 lb.

163. The transition in the ultimate shear resistance from the peak value to the residual value is shown in Figure 33 for an average normal stress equal to 1,250 psf along the base of the wall. The ultimate shear stress-deformation behavior of the interface was assumed to be brittle, as observed in the direct shear test results reported by Benson et al. (1987). The ultimate shear resistance was reduced from a value of 2,722 to 722 psf, due to the loss of the bond (C_a = 2,000 psf). This resulted in a decrease in the

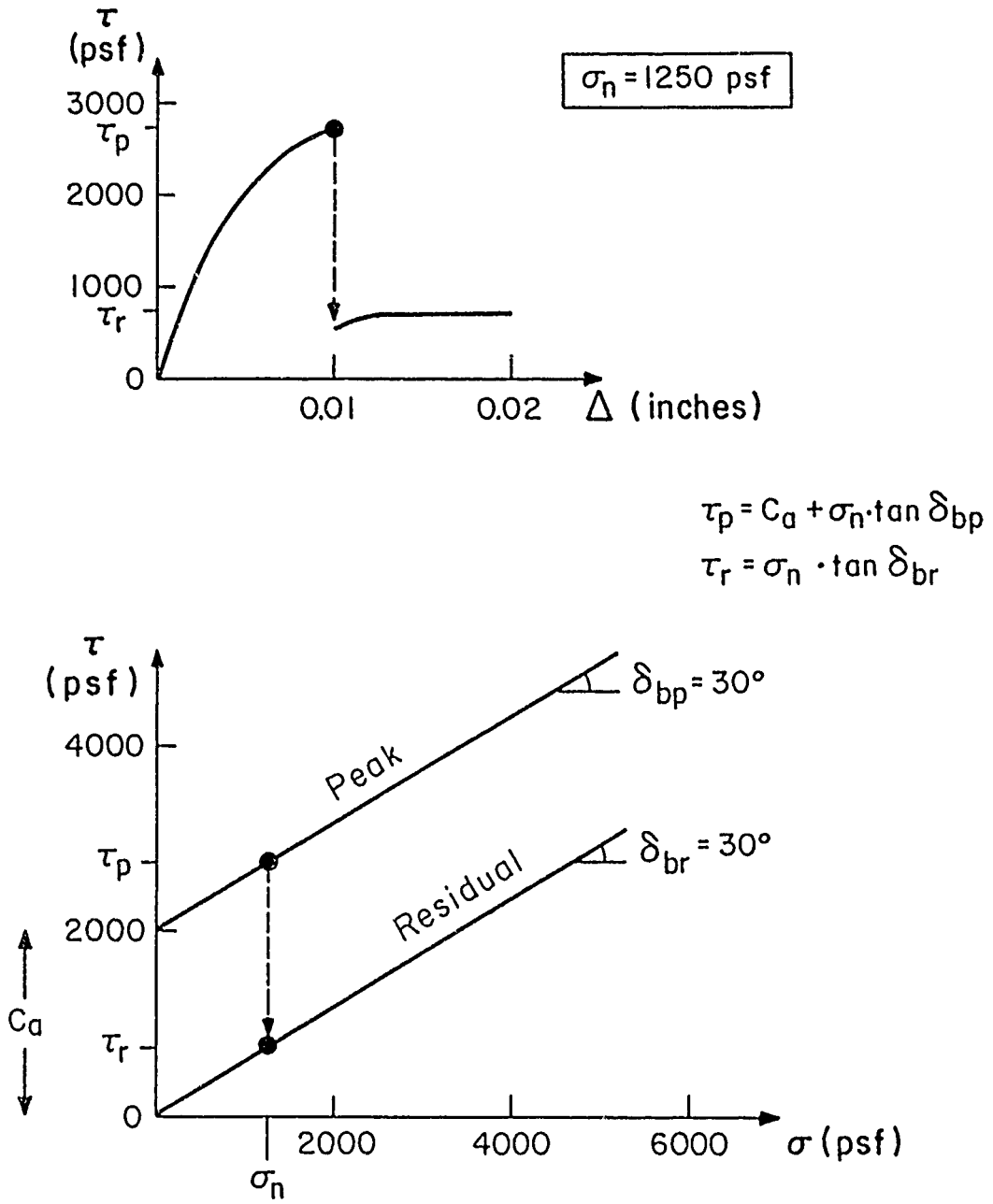

Figure 33. Available shear resistance during loss of bond between the wall and the foundation

ultimate shear and passive resistance from 33,219 to 9,219 lb, as shown in Figure 32. Since the ultimate shear and passive resistance (9,219 lb) is larger than the required resistance ($T_b + E_2$ = 5,102 lb), shear failure did not occur on the base of the wall.

164. After completion of backfilling (Stage 5), the final deformation of the wall was equal to 0.048 in., with E_1 = 8,950 lb, E_2 = 900 lb, and T_b = 8,050 lb. The ultimate shear and passive resistance (9,539 lb) was

larger than the required resistance ($T_b + E_2 = 8,950$ lb), thus no shear failure occurred along the base of the wall at any stage of backfilling. Since no shear failure occurred during the simulated placement of backfill, the relationships of Figure 31 remained valid throughout the analysis

Case 2 equilibrium analysis

165. In the second backfill placement analysis of the wall shown in Figure 23, all the material parameters were the same as those used in Case 1, with the exception that the values of the peak and residual base friction angles were equal to 15 deg. The relationships between the forces acting on the wall (E_1, E_2, and T_b) and the average lateral displacement of the wall are shown in Figure 34. The Figure 24 relationship between $(E_1)_{\text{complete backfill}}$ and $(u_x)_{ave}$, described in the Case 1 analysis, was also used in developing the relationships shown in Figure 34. The ultimate shear and passive resistance of the wall was computed using the same procedure as for Case 1, but with δ_{bp} and δ_{br} equal to 15 deg.

166. The forces acting on the wall and the displacements of the wall after Stage 1, the completion of filling in front of and behind the wall to $h = h_{toe}$ (3.5 ft), were the same as in the previous analysis; $E_1 = 537$ lb, $E_2 = 496$ lb, $T_b = 41$ lb, and $(u_x)_{ave} = 0$ The ultimate shear and passive resistance (28,505 lb) was much larger than the required resistance ($T_b + E_2 = 537$ lb), thus no shear failure occurred along the base of the wall at this stage of backfilling.

167. At Stage 2, when the height of backfill was equal to 14.8 ft (h/H = 0.7), $E_1 = 5,102$ lb, $E_2 = 580$ lb, $T_b = 4,522$ lb, and $(u_x)_{ave} = 0.01$ in. They are the same set of values as computed in the Case 1 analysis since the same relationships for E_1 (Figure 31) and for E_2 (Figure 24) were used in both analyses. At this value of lateral displacement, the base of the wall loses its bond with the foundation, resulting in a transition in the ultimate shear resistance from peak ($C_a = 2,000$ psf and $\delta_{bp} = 15$ deg) to residual values ($C_a = 0$ and $\delta_{br} = 15$ deg). A corresponding decrease in the ultimate shear and passive resistance from 28,589 to 4,589 lb occurred, as shown in Figure 34 (labeled $N \cdot \tan \delta_{br} + E_2$ in the figure with the expanded scale). Since the value for the ultimate shear and passive resistance (4,589 lb) was less than the required resistance (5,102 lb), a shear failure along the base of the wall resulted. Subsequently, the wall moved away from the backfill, displacing the toe-fill. The additional displacements resulted in a decrease in the value of E_1 and an increase in the value of E_2. The movement

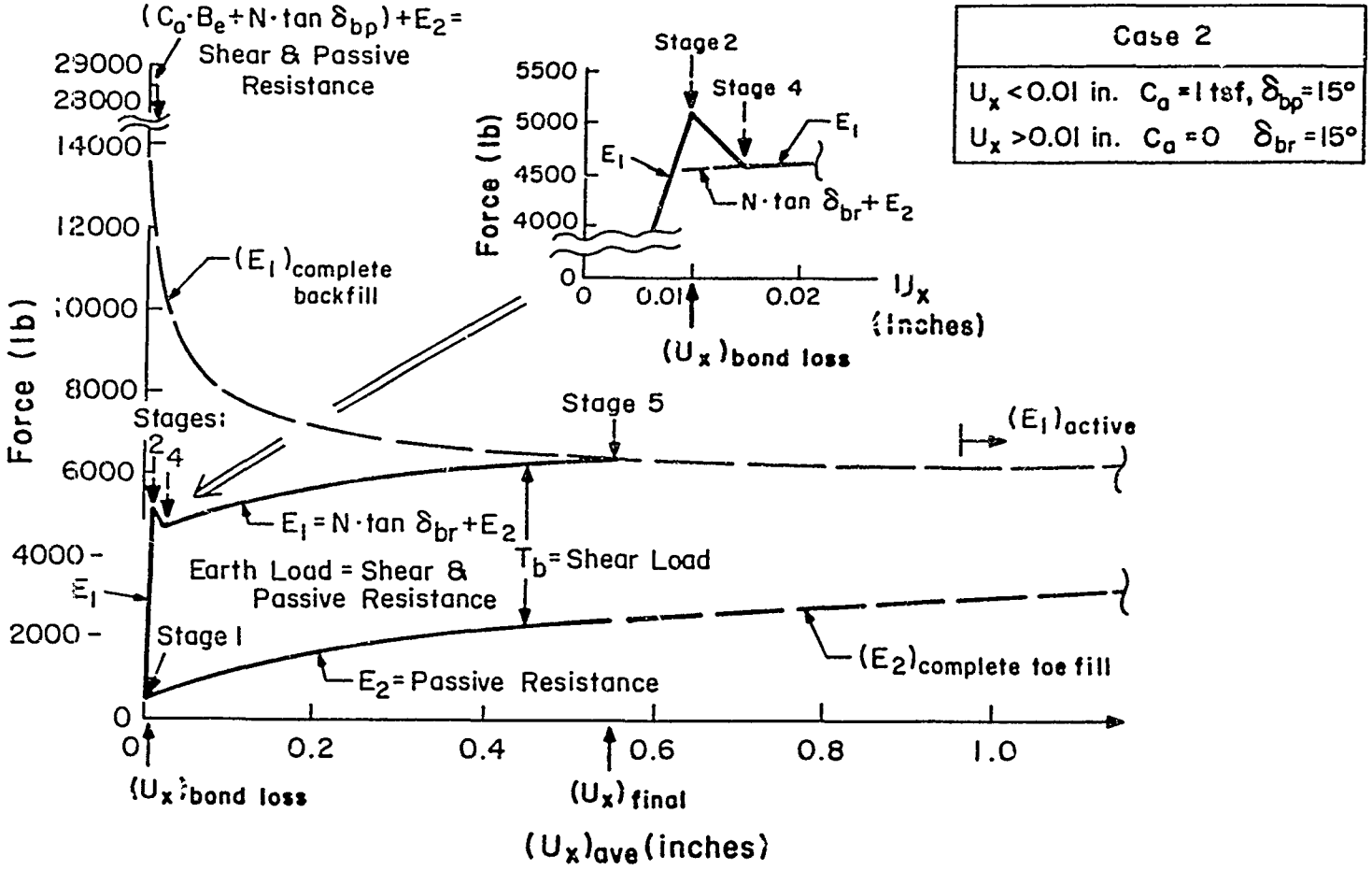

Figure 34. Variation of forces acting on the wall with deformation, Case 2

terminated when equilibrium was attained between the ultimate shear and passive resistance and the required resistance ($T_b + E_2$). Equilibrium was reestablished after a 45-percent increase in the lateral displacement of the wall, to 0.0145 in. At this stage, labeled Stage 4 in Figure 34, the value of E_1 was 4,602 lb. Thus, equilibrium among the forces acting on the wall was attained by reducing the earth load and increasing the passive resistance provided by the toe-fill, through the lateral translation of the wall.

168. Since the loss of bond along the base resulted in a shear failure and subsequent lateral wall movements to reestablish equilibrium among the forces, the relationships between the height of backfill, the lateral force, and the height of backfill and lateral displacements shown in Figure 31 were no longer valid. The increase in the value of E_2 with lateral displacements controlled the behavior of the wall when backfilling resumed, since the shear load (T_b) was equal to the ultimate shear resistance ($N \cdot \tan \delta_{br} = 4{,}009$ lb) along the base of the wall. During this phase of backfilling, the earth load (E_1) was equal to the shear and passive resistance. The final lateral displacement of the wall was determined by the intersection of the shear and passive resistance relationship with the relationship for $(E_1)_{\text{complete backfill}}$. The value of $(u_x)_{\text{final}}$ was equal to 0.55 in. (Stage 5), $E_1 = 6{,}409$ lb and $E_2 = 2{,}400$ lb.

169. In this case, where a reduced angle of internal friction ($\delta = 15$ deg) was assigned to the base, a loss in bond along the concrete-to-rock interface resulted in shear failure during backfilling, with a lateral translation of the wall required to reestablish equilibrium among the loading and resisting forces. The behavior of the wall at subsequent stages of backfilling was controlled by the residual shear strength along the base and passive force provided by the toe-fill. The final displacement of the wall in this case was 11 times as large as that for Case 1.

Case 3 equilibrium analysis

170. The results of the third backfill placement analysis of the wall (Figure 23) are shown in Figure 35. This equilibrium analysis differed from the previous Case 1 and Case 2 analyses by the value of δ_{bp} and δ_{br}, each equal to 10 deg. From Figure 24, the relationship for $(E_1)_{\text{complete backfill}}$ was obtained, and the ultimate shear and passive resistance was computed as described in the previous two analyses.

171. At Stage 1, after backfilling to 3.5 ft ($h = h_{toe}$), $E_1 = 537$ lb, $E_2 = 496$ lb, $T_b = 41$ lb, and $(u_x)_{ave} = 0$. The ultimate shear and passive

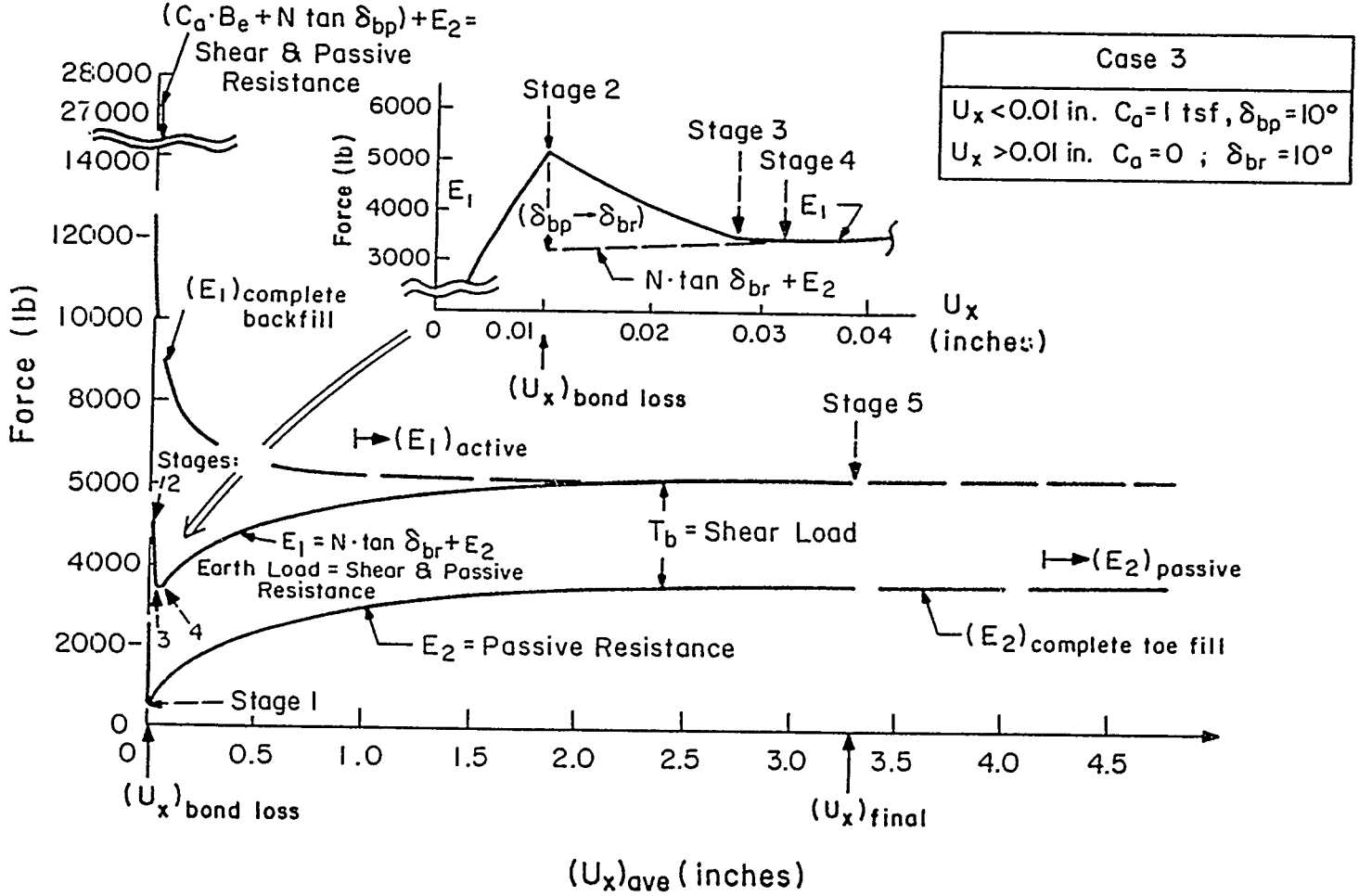

Figure 35. Variation of forces acting on the wall with deformation, Case 3

resistance was equal to 27,134 lb, while the required resistance ($T_b + E_2$) was equal to 537 lb.

172. After 14.8 ft of backfilling was completed and the lateral displacement of the wall was equal to 0.01 in. (Stage 2), E_1 = 5,102 lb, E_2 = 580 lb, T_b = 4,522 lb, as in Cases 1 and 2. The ultimate shear and passive resistance decreased from 27,218 to 3,218 lb, with the loss of the bond along the base of the wall. Since the value of the required resistance, equal in value to E_1, was larger than the sum of $N \cdot \tan \delta_{br}$ and E_2, as shown in the upper figure with the expanded scale, a shear failure along the base of the wall resulted. As in Case 2, the wall moved away from the backfill, displacing the toe-fill; thereby decreasing the value of E_1 and increasing the value of E_2.

173. When $(u_x)_{ave}$ = 0.028 in., the earth pressures were equal to their active values (K_a = 0.23), and E_1 attained a minimum value of 3,401 lb (Stage 3). The wall continued to move laterally because the required resistance, equal to 3,401 lb (same value as E_1), was less than the ultimate shear and passive resistance, equal to 3,370 lb. Since equilibrium was not achieved, the wall continued to move, resulting in a further increase in the value of E_2, while the values of E_1 (3,401 lb) and T_b (= $N \cdot \tan \delta_{br}$ = 2,638 lb) were constant. Equilibrium was reestablished at $(u_x)_{ave}$ = 0.032 in. (Stage 4), when the required resistance (= E_1) was the same magnitude as the ultimate shear and passive resistance, a value of 3,401 lb. Thus equilibrium was attained through the translation of the wall in two stages: first, a reduction in the earth load to active pressures, accompanied by an increase in the value of the resistance provided by the toe-fill, and secondly, a continued increase in the value of the toe-fill resistance, with a constant earth load. During the wall movements, the shear load acting along the base of the wall was equal to the ultimate residual shear resistance.

174. The relationships between height of backfill, wall load, and wall displacement of Figure 31 were no longer valid since a shear failure occurred along the base of the wall, as in the Case 2 analysis. The increase in the value of the toe-fill resistance (E_2) with displacements controlled the subsequent behavior of the wall when backfilling was resumed. During the final stages of backfilling, the shear load along the base of the wall (T_b) was equal to the ultimate shear resistance (2,638 lb), and E_1 was equal to the sum of T_b and E_2, as shown in Figure 35. The final lateral wall

displacement was equal to 3.3 in. (Stage 5). It is observed that at $(u_x)_{ave}$ = 0.96 in. $[(u_x)_{ave}/H = 0.004]$, the earth load attained its minimum value of 6,210 lb, which corresponds to the active earth pressures (K_a = 0.23). During placement of the last 5.2 ft of backfill, from Stage 4 to Stage 5, the backfill was in a state of active failure, and the base shear load was equal to the ultimate residual shear resistance.

175. A reduced ultimate shear resistance along the base (δ_{bp} and δ_{br} = 10 deg) resulted in larger lateral wall translations than the previous analyses. In fact, the displacement was 69 times larger than that of Case 1 (δ_{bp} and δ_{br} = 30 deg). The larger lateral displacements for Case 3 were required to reestablish equilibrium among the forces acting on the wall during backfilling when a loss of bond and subsequent shear failure occurred along the base. Like Case 2, the subsequent behavior of the wall was controlled by the residual shear strength along the base and the passive force provided by the toe-fill. The final displacement of the wall was larger by a factor of about 6.0 than that of Case 2 (δ_{bp} and δ_{br} = 15 deg), because the displacements during backfilling were of a sufficient magnitude so as to achieve a minimum value for the earth load, corresponding to active earth pressures (K_a = 0.23), when the height of backfill exceeded 14.8 ft.

PART IV: SUMMARY, CONCLUSIONS, AND RECOMMENDATIONS

Summary

176. The results discussed in this second phase describe the continued evaluations of the accuracy and reliability of CEA of earth-retaining structures founded on rock.

177. As a result of several simplifying assumptions, CEA of gravity earth-retaining structures neglect the true process of soil-structure interaction and tend to produce highly conservative results. It is believed that improvements based on soil-structure interaction studies like those described in this report are likely to lead to more realistic and less conservative predictions of response. This assertion is supported by the fact that some existing gravity walls under Corps of Engineers' jurisdiction, e.g. navigation lock walls, do not satisfy current stability criteria based on CEA, while at the same time they do not exhibit signs of distress or substandard performance.

178. The studies performed under this research contract are divided into first and second phases. The first phase report (Ebeling et al. in preparation) defined the analytical requirements for this category of structure and resulted in the development of new finite element procedures, while this report explored a number of variables on the stability of the wall. The results of the initial phase were discussed by Ebeling et al. (in preparation) while the results of this study, the second phase, are included in both reports.

179. The gravity earth-retaining structures evaluated in this study were consistent with the characteristics of Corps of Engineers retaining structures as described in the initial report. In addition, an "L" shaped earth-retaining structure was used in the studies of the loss of bond and possible slippage along the base of the wall during backfilling.

180. The results from FEA and equilibrium analyses utilizing the results from select FEA were used in the evaluations. These studies were performed using "backfill placement" analysis procedures in which the placement of backfill behind the walls was simulated, layer by layer. The finite element program used in this series of analyses has the capability to model the development of a gap between the base of the wall and its rock foundation,

and this phenomenon was analyzed in Case 4 as described in the initial phase study.

181. In the parametric studies discussed in this volume, it was observed that increases in stiffness of the backfill or a reduction in the values of soil-to-concrete interface shear stiffnesses resulted in a slight increase in the lateral earth pressures acting on the wall. Variations in the magnitudes of the stiffness of the backfill or the interface shear stiffnesses resulted in larger variations in the magnitude of the shear force acting on a vertical plane passing through the heel of the wall (Section A-A). In the initial analyses, it was observed that vertical shear stress coefficient (K_v) was within the narrow range of 0.13 to 0.14 for variations in the magnitudes of Poisson's ratio, the unit weight of the backfill, and base interface shear stiffness. Studies discussed in this report indicated that:

a. The value of K_v increased from 0.12 to 0.15 as the stiffness of the backfill was reduced over the range of values of stiffness representative of clean granular backfills.

b. K_v decreased in value from 0.14 to 0.09 as the values of the concrete-to-soil and rock-to-soil interface shear stiffnesses were reduced.

182. A reduction in the magnitude of the stabilizing shear force acting on the wall results in a reduction of the actual margin of wall safety.

183. As the slope of the back of the wall increased, the magnitude of K_v increased from a value equal to 0.09 to a value equal to 0.21 for a wall with a vertical back face. As expected, it was found that the margin of wall stability increased with increasing wall mass. In an additional set of analyses, it was observed that a stepped face wall has a greater margin of stability than a smooth face wall due to a larger value of K_v and slightly smaller earth pressure loads.

184. In the evaluation of the base case structure with water in front of and behind the wall, it was observed that the water in front of the wall provides a stabilizing influence , decrease in the pool elevation results in the loss of a corresponding contribution to the resisting force, which is then provided by shear on the base of the wall and the toe-fill. The exact proportion of the redistribution of the resisting force between the wall and the toe-fill depends upon the movements of the wall. The greater the wall movements, the larger the contribution of the toe-fill to the redistributed resisting force.

185. Results from the CEA and the FEA were used to show the interdependency between the factors of safety for the structure and the backfill. The factor of safety against a shear failure within the backfill was referred to as a shear factor. It was observed that the factor of safety against sliding for the structure and the shear factor of the backfill are not necessarily equal in magnitude.

186. The interdependence between wall deformations and the loading and resisting forces was examined in a series of equilibrium analyses in which the deformation of the wall during backfilling was hypothesized to be sufficient to break the bond between the base of the wall and the rock foundation. It was demonstrated that a backfill placement analysis can be conducted using equilibrium methods, and that the magnitude of the ultimate base shear resistance and the resistance provided by the toe-fill controls the displacement of the wall. When a loss of bond along the base of the wall occurs during backfilling, the wall must slide along its base to reestablish equilibrium. Two actions occur during sliding: the earth load is reduced as a result of the wall movement away from the backfill, while the passive force acting on the toe of the wall is increased with the wall movement toward the toe-fill. During sliding, the strength of the interface along the base is at its residual value. In general, the lower the available resistance along the interface between the wall and its foundation, the greater the resulting wall displacements.

187. Finally, this study has shown that the displacements of the wall have a significant influence on the distribution of both stabilizing and destabilizing forces exerted on the wall by the fill, and on the base of the wall. In general, as the wall moves away from the backfill, the lateral forces behind the wall decrease and the lateral forces in front of the wall increase. Calculations indicate that the magnitude of the wall displacements required to develop significant changes in the magnitude of the shear forces acting on the base of the wall are less than those required to develop active pressures behind the wall and much less than those required to develop passive pressures in front of the wall.

Conclusions

188. The results from these studies indicate that the traditional assumptions used in the CEA of earth-retaining structures founded on rock are

conservative. One of the assumptions in the CEA is that the shear force acting on the plane through the heel of the wall is equal to zero. In the finite element studies for a select set of hypothetical walls, with characteristics similar to those of Corps of Engineers structures, it was found that the shear force acting on a vertical plane within the backfill, passing through the heel of the wall, was not zero. These studies showed that the values of K_v for the walls studied varied from 0.09 to 0.21, depending on the geometrical and material parameters of the wall and backfill.

Recommendations

189. Because of the potential importance of these findings with regard to evaluations of the stability of gravity retaining structures, it is recommended that the studies be continued to investigate two important questions which remain unanswered:

a. Will similar analytical results be found for walls founded on soil?

b. Can the existence of shear forces on the backs of gravity walls be confirmed experimentally?

REFERENCES

Benson, C. P., Brandon, T. L., Clough, G. W., and Duncan, J. M. 1987. "Literature Review of Rock Properties for Analysis of Navigation Structures Founded on Rock," Interim report prepared for US Army Corps of Engineers, Virginia Polytechnic Institute and State University, Blacksburg, VA.

Clough, G. W., and Duncan, J. M. 1971 (Dec). "Finite Element Analyses of Retaining Wall Behavior," Journal of the Soil Mechanics and Foundation Division, American Society of Civil Engineers, Vol 97, No. SM12, pp 1657-1673.

Department of the Navy. 1982. "Foundations and Earth Structures," NAVFAC DM7.2. Available from: Department of the Navy, Naval Facilities Engineering Command, 200 Stovall St., Alexandria, VA.

Ebeling, R. M., Clough, G. W., Duncan, J. M., and Brandon, T. L. "Methods of Evaluating the Stability and Safety of Gravity Earth Retaining Structures Founded on Rock" (in preparation), prepared for US Army Engineers Waterways Experiment Station, Vicksburg, MS.

Johnson, E. G. 1953 (Apr). The Effects of Restraining Boundaries on the Passive Resistance of Sand (Results of a Series of Tests With a Medium-Scale Testing Apparatus), MS thesis in Engineering from Princeton University, Princeton, NJ.

Kezdi, A. 1975. "Lateral Earth Pressure," Foundation Engineering Handbook, Van Nostrand Reinhold, pp 197-220.

Terzaghi, K. 1934 (Feb). "Large Retaining Wall Tests. I. Pressure of Dry Sand," Engineering News Record, Vol III, pp 136-140.

Terzaghi, K. 1936 (Apr). "A Fundamental Fallacy in Earth Pressure Calculations," Journal of the Boston Society of Civil Engineers, pp 71-88.

APPENDIX A: INTERPRETATION OF THE FINITE ELEMENT RESULTS

1. In the traditional finite element method of analysis the primary unknowns are the nodal point displacements, and the secondary unknowns are the stresses within the elements. For each of the two-dimensional elements used by the program SOILSTRUCT, stresses are computed only at the centers of the elements, although the stress varies across the element. This variation may be nonlinear, depending upon the distortion of the element. However, the variation in stress across an interface element is linear, due to the mathematical formulation of this element.

2. The results of the finite element analyses discussed in this and the initial study (Ebeling et al. in preparation)* are summarized using the resultant forces acting along the interfaces between the wall and the backfill, the wall and the rock foundation, and along vertical planes within the backfill. For the planes passing through the two-dimensional elements, such as vertical Section A-A within the backfill, the resultant forces were computed using the stresses calculated at the center of each of the soil elements, as shown in Figure A1 (Method 1). These computations were made by first graphically constructing shear and lateral stress distributions along Section A-A, connecting the stresses between element centers as shown in the figure. The set of resultant forces (F_v and F_h) and point of action (h_{Fh}) were then computed from the plotted stress distributions.

3. Along the base of the wall and vertical Section E-E, the resulting stress distributions are known since the values of stresses are computed at the nodal points and their variation across the element is linear. Thus, the computed magnitudes and point of action of the resulting interface forces are exact.

4. An alternative procedure for computing the magnitude of the resultant forces and their point of action on Section A-A (Method 2) is shown in Figure A1. In this procedure the unknown values of F_v, F_h, and h_{Fh} are determined using the three equations of equilibrium (vertical, horizontal, and moment), since the remaining forces of the weight and resultant interface forces along the base and Section E-E are known both in magnitude and point of action.

---

* References cited in this Appendix are included in the References following the main text.

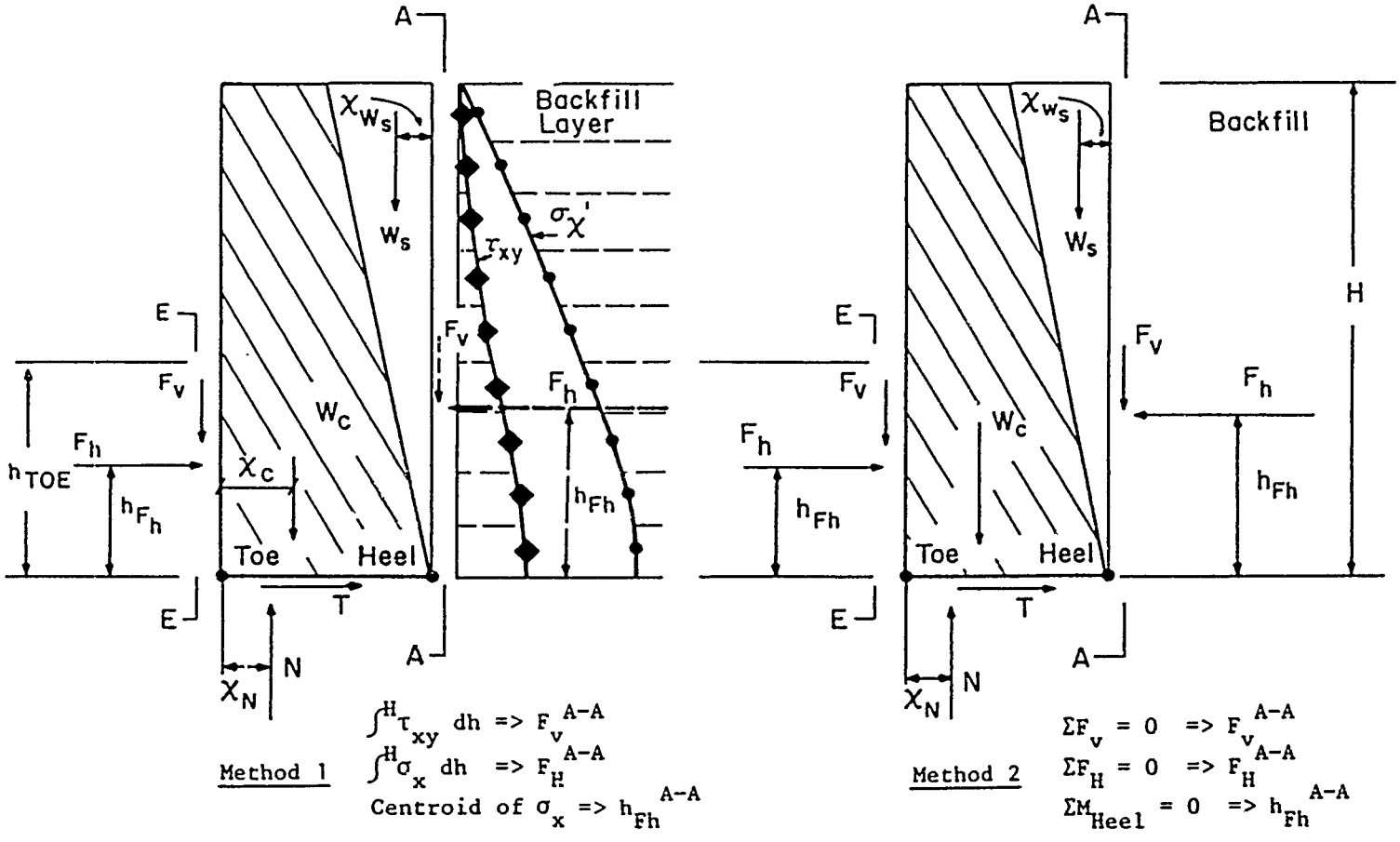

Figure A1. Two methods for computing the magnitude and point of action of the resultant forces along plane A-A

5. The resultant forces acting on Section A-A were computed using both methods for all of the backfill placement analyses discussed herein and in the initial study (Ebeling et al. in preparation), and the results are summarized in Table A1. It is observed that the values of lateral resultant forces (F_h) and their points of action along Section A-A (h_{Fh}) are in agreement for the two methods in all cases. The values of the resultant shear forces (F_v) computed by the two methods differ by less than 8 percent for all except Cases 24a and 32a. This corresponds to a difference in values of vertical earth pressure coefficients (K_v) of less than 0.01.

6. Case 24a is a parametric evaluation with stiffness parameters that do not reflect those characteristic of typical backfills. In Case 32a, the difference between the values of F_v reflect an involved stress field, due to both the presence of irregular geometry adjacent to the backfill (i.e. stepped interface) and an analytical boundary condition specified along this interface. For this analysis, the nodal points along the stepped interface were shared by both the wall and the backfill. This introduced a kinematic constraint since the predominant direction of backfill displacements are downward, while those of the wall are lateral and directed away from the backfill.

7. It was concluded that the accuracy of the results are dependent not only upon the interpretation of the resulting stress field but also the size of the mesh. For Case 32a, it is concluded that the true value of vertical earth pressure coerficient is within the range from 0.12 to 0.17.

Table A1

Summary of Results for Backfill Placement Analyses

Case	Section A-A, Method 1, Vertical Section Through Heel							Section A-A, Method 2, Vertical Section Through Heel						
	F_v lb	F_h lb	K_v	K_h	h_{Fh} ft	δ_m deg	EPI	F_v lb	F_h lb	K_v	K_h	h_{Fh} ft	δ_m deg	EPI
13a	14,888	48,992	0.138	0.453	14.7	16.9	0.21	13,808	48,922	0.128	0.453	14.7	15.8	0.21
14a	14,278	59,108	0.132	0.547	14.3	13.6	0.20	13,496	59,108	0.125	0.547	14.5	12.9	0.20
15a	14,053	67,074	0.130	0.621	14.3	11.8	0.22	13,782	67,074	0.128	0.621	14.3	11.6	0.22
16a	13,242	43,460	0.144	0.452	14.6	16.9	0.21	12,293	43,460	0.134	0.452	14.8	15.8	0.21
17a	14,795	49,008	0.137	0.454	14.7	16.8	0.21	13,728	49,008	0.127	0.454	14.7	15.7	0.21
18a	14,670	49,542	0.136	0.459	14.9	16.5	0.18	13,640	49,542	0.126	0.459	14.7	15.4	0.18
19a	14,863	36,405	0.138	0.337	16.8	22.2	0.61	15,157	36,405	0.140	0.337	18.3	22.6	0.61
20a	15,453	48,558	0.143	0.450	14.7	17.6	0.22	14,455	48,553	0.134	0.450	14.8	16.6	0.22
21a	12,718	50,145	0.118	0.464	14.5	14.2	0.17	11,620	50,147	0.108	0.464	14.5	13.0	0.17
22a	8,932	51,117	0.083	0.473	14.5	9.9	0.14	7,855	51,122	0.073	0.473	14.5	8.7	0.14
23a	5,892	51,573	0.055	0.478	14.3	6.5	0.11	4,895	51,582	0.045	0.478	14.4	5.4	0.11
24a	3,252	51,567	0.030	0.478	14.2	3.6	0.11	2,287	51,663	0.021	0.478	14.2	2.5	0.11
25a	10,185	52,166	0.094	0.483	14.2	11.1	0.10	9,431	52,166	0.087	0.483	14.2	10.3	0.10
26a	14,986	48,784	0.139	0.452	14.7	17.1	0.21	13,970	48,784	0.129	0.452	14.8	16.0	0.21
27b*	11,742	38,843	0.137	0.453	16.0	16.8	0.21	11,022	38,843	0.128	0.453	16.0	15.8	0.21
28b*	12,036	38,332	0.140	0.447	16.0	17.4	0.23	11,364	38,332	0.133	0.447	16.0	16.5	0.23
29b*	12,369	39,393	0.144	0.436	15.8	18.3	0.27	11,703	37,393	0.136	0.436	16.0	17.4	0.27
30a	22,389	45,316	0.207	0.420	13.9	26.3	0.32	22,389	45,316	0.207	0.420	13.9	26.3	0.32
31a	9,849	51,270	0.091	0.475	14.9	10.9	0.13	9,090	51,270	0.084	0.475	14.9	10.1	0.13
32a	12,622	48,053	0.117	0.445	15.1	14.7	0.24	18,371	49,622	0.170	0.459	15.0	20.3	0.19

* $F_h = F'_h$ for Cases 27b, 28b, and 29b.

APPENDIX B: SOILSTRUCT (ISOTROPIC) USER'S MANUAL WITH BASE SEPARATION MODEL USING THE ALPHA METHOD

1. IDENTIFICATION CARD FORMAT (20A4)

Column	Variable	Explanation
1-80	HED	Analysis identification.

2. DATA CONTROL CARD FORMAT (13I5, D5.1, D10.1)

(a) MESH PARAMETERS

All nodes and two-dimensional and interface elements to be used in the analysis must initially be included in the mesh; additions or deletions are not allowed, but the material parameters can be changed to make them inactive. One-dimensional bar elements usually are added in subsequent construction steps, but may initially be included in the mesh.

Column	Variable	Explanation
1-5	NUMNP	Number of nodal points (500 maximum).
6-10	NUMEL	Number of elements initially in the mesh, excluding bar and beam elements, but including interface elements. NUMEL, then, includes NUMJT (450 maximum). Interface elements should be numbered first.
11-15	NUMJT	Number of interface elements (50 maximum).
16-20	NUMBAR	Number of bar elements initially in the mesh (15, including elements added in subsequent construction steps).

(b) ANALYSIS PARAMETERS

Column	Variable	Explanation
21-25	NC	Number of loading and construction steps (60 maximum).
26-30	NMOD	Modulus specification code = 0 if modulus calculation codes input with Loading Information Card. = 1 if modulus calculation codes input with Modulus Calculation Card.

Column	Variable	Explanation
31-35	INIT	Initial stress input code = 0 if external input from cards or tape included in input sequence. = 1 if internally generated from gravity turn-on analysis. = 2 if the initial stresses are to be set equal to zero internally. (If INIT is not equal to 0, 1, or 2, initial stresses are generated assuming a horizontal ground surface with the water table at the ground surface, both soil and interface elements are included in the mesh. In this case, initial stresses are generated by the direct gravity ($\sigma_x = K_o \sigma_y$) for a horizontal ground and water table. The unit weight of the soil is that of the first soil for which properties are given.)
36-40	KI	Equal to zero (interface is automatically activated). KI is used when INIT is not equal to 0. If INIT = 0, then KI can be left blank.
41-45	IHORIZ	Ground surface inclination code - = 0 horizontal ground surface. Vertical stresses computed from gravity turn-on. Horizontal stresses are computed assuming $K_o = \nu/(1 - \nu)$. Unless K_o is specified. = 1 sloping ground surface. Vertical and horizontal stresses are calculated from gravity turn-on analysis linear elastic response soil, i.e., $K_o = \nu/(1 - \nu)$.

(c) OUTPUT PARAMETERS

Column	Variable	Explanation
46-50	ITRD	Analysis printout code = 0 if initial stresses are to be printed. = 2 if initial stresses are <u>not</u> to be printed.
51-55	ILIST	Element and nodal point card data printout code = 0 if not printed. = 1 if printed.
56-60	IPUNCH	Idle.

Column	Variable	Explanation
61-65	ITAPE	Initial disc storage code = 0 if no disc storage. = 1 if storage of analysis continuation data and displacements from final iterations is required. The continuation data and displacements are stored in separate files that are set up on the IBM job control cards (tape 9).

(d) BASIC PARAMETERS

The unit weight of water and the atmospheric pressure are included as basic parameters. Either English or SI units can be used, but must, of course, be compatible with input coordinate, pressure, and material property parameters.

Column	Variable	Explanation
66-70	GAMW	Unit weight of water.
71-80	PATM	Atmospheric pressure.

3. MATERIAL ALLOCATION CARD FORMAT (6I5)

All two-dimensional material types are assigned numbers first, followed by the interface material types. (Note that bar elements are not assigned a material type number, but are identified solely by their element number.) If a number for NATYP, for example, is not required, assign a value of zero or leave blank.

Column	Variable	Explanation
1-5	NUMMAT	Total number of material types, including two-dimensional soil or construction material types and interface material types (40 maximum).
6-10	NUMSOL	Total number of material types excluding the interface material types. Thus the different between NUMMAT and NUMSOL must equal the number of interface material types.
11-15	NATYP	Material type number assigned to two-dimensional elements having the properties of air. Usually, elements that will be built are initially identified as air elements.
16-20	NA2TYP	Material type number assigned to interface elements having the properties of air. Usually, elements that will be built are initially identified as air elements.

Column	Variable	Explanation
21-25	NCTYP	Structural material type, such as concrete or sheetpiling.
26-30	NB1TYP	Backfill material type 1. (Refer to section 14b, Fill or Concrete Placement.)
31-35	NB2TYP	Backfill material type 2. (Refer to section 14b, Fill or Concrete Placement.)

4. BASE SEPARATION--ALPHA METHOD

The following set of variables control the model of the loss of contact between a structure and its foundation using the alpha method. Note that only horizontal interface elements may be used along the base of the structure. If this base separation routine is not required, assign a value of zero to NLOOP and proceed to Loading Information Card (section 5).

(a) FIRST CARD FORMAT (2I5, 20x, 3I5)

Column	Variable	Explanation
1-5	NLOOP	Maximum number of iterations using alpha method for each loading step.
6-10	KEYFRC	Linear stress increment applied to interface elements during transfer of shear stress to adjacent element. = 0
31-35	NOELF1	First horizontal interface element checked for tension.
36-40	NOELF2	Last horizontal interface element checked for tension.
41-45	NGROUP	Number of groups of interface elements for which resultant forces are to be computed.

(b) SECOND CARD FORMAT (2I5)

Column	Variable	Explanation
1-5	NELGRP(I,1)	First interface element in group I.
6-10	NELGRP(I,2)	Last interface element in group I.
		Repeat until I is equal to NGROUP sets of interface elements.

5. LOADING INFORMATION CARD FORMAT (6I3, 2x, 15A4)

One card is supplied for each loading step. One to three loading/construction modes can be included in each loading step. The loading or construction mode codes include:

KCS(NC,I)	DESCRIPTION
1	Excavation (equivalent nodal loads can be applied in equal increments).
2	Fill placement (subroutine SUBSTP cannot be used in conjunction with the fill placement procedures of subroutine BUILD).
3	Seepage loading (equivalent nodal loads can be applied in equal increments).
4	Deletion of bar element (force in the element can be applied in equal increments).
5	Installation of bar element (prestress force can be applied in equal increments).
6	Boundary pressure loading (equivalent nodal loads can be applied in equal increments).
7	Temperature loading (the total temperature change can be applied in equal increments).
8	Support displacement (the total displacement can be applied in equal increments).
9	Concentrated nodal loads (can be applied in equal increments).
10	Element material type change.

As indicated in the listing, input loads, displacements, or temperature changes can be analyzed in equal increments or substeps. Subroutine SUBSTP generates the increments, then MAIN analyzes all increments prior to analyzing the next load step. With one exception, all loading/construction modes that can be applied in increments, or substeps, can also be applied in any combination in any loading step. The number of substeps, however, will be the same for all loading or construction modes included in the loading step. The exception is temperature loading; if a temperature change is specified, and a given number of substeps is specified, then only temperature loading can be specified in the loading step--i.e., KCS(N,2) and KCS(N,3) must be set equal to zero or left blank. If the number of substeps, NSBSP, is equal to zero, then temperature loading can be included with other loading/construction modes in a load step.

Since the same input format is used and similar operations are performed for loading or construction modes 8 and 9, the following rules in the usage of these two codes apply. If only concentrated nodal loads are specified, use mode 9. If only support displacements are specified, use mode 8. If both loads and displacements are specified, use mode 8.

Column	Variable	Explanation
1-3	KCS(NC,1)	First loading/construction mode code.
4-6	KCS(NC,2)	Second loading/construction mode code.
7-9	KCS(NC,3)	Third loading/construction mode code.

KCS(NC,1), KCS(NC,2), and KCS(NC,3) can be input in any numerical order, but the modes are processed in ascending numerical order: If second and/or third loading construction nodes are not required, then KCS(NC,2) and KCS(NC,3) should be set equal to zero or left blank.

10-12	NUMIT(NC)	Number of iterations for the loading step. NUMIT(NC) applies to each substep if substeps are specified. A maximum of 10 iterations can be specified. NUMIT(NC) = 0 is the same as NUMIT(NC) = 1.
13-15	NUMSS(NC)	Number of substeps. A maximum of 10 substeps can be specified. NUMSS(NC) cannot be zero.
16-18	MOD(1,NC)	Modulus calculation code = 1 if a loading modulus is to be calculated. = 2 if an unload-reload modulus is to be calculated. = 0 if the computer is to decide the type of modulus to be calculated. In this case, if the most recently calculated maximum shear stress for an element is less than all previous values of maximum shear stress, an unload-reload modulus is calculated. Otherwise, a loading modulus is calculated.

Input is required here only if NMOD = 0. All material types, other than interface or bar elements, are given one of the above codes. If NMOD = 0 and NC = 0, as might be the case for an analysis of initial stresses, MOD(I,1) is set equal to zero, or the computer decides.

Column	Variable	Explanation
19	IPRT(1,NC)	Print code = 0 print displacements and stresses for final iteration only. = 1 print interface stresses for each iteration, stresses for all elements, and displacements for final iteration only. = 2 print stresses for all elements for each iteration, stresses and displacements for final iteration only. = 3 print stresses and displacements for each iteration.
20	IPUN(1,NC)	Disc storage code (tape 9) = 0 if no disc storage. = 1 if storage of analysis continuation data prior to implementation of base separation by alpha method. = 2 if storage of analysis continuation data after completion of base separation by alpha method.
21-80	HEDCS(NC)	Description of loading step.

6. MODULUS SPECIFICATION CARD FORMAT (40I2)

This card is required only if NMOD = 1 and NC = 0. A card is required for each loading step, 1 to NC. In this option, values of the modulus specification code are specified for each material type (and thus each element, excluding bar and interface elements), regardless of the change in maximum shear strain that may have occurred.

Column	Variable	Explanation
2,4,6,...	MOD(I,NC)	Modulus calculation code for each material type (1 to NUMSOL) for the first load step. Separate cards are required for each load step. Columns not used can be left blank.

7. MATERIAL PROPERTY CARDS

These cards are used only for two-dimensional elements; the first and second cards must be supplied for each material type, excluding bar and interface material types. The first and second cards, as a pair, are supplied in order of material type number N = 1 to NUMSOL. Information or properties not required for a material type can be left blank.

(a) FIRST CARD FORMAT (7D10.5, I10)

Column	Variable	Explanation
1-10	GUI(N)	Poisson's ratio before failure.
11-20	GUF(N)	Poisson's ratio at failure (no greater than 0.49).
21-30	GAM(N)	Total unit weight (always specified, regardless of drained or undrained material behavior).
31-40	FR(N)	Correlation factor: ratio of measured strength at failure to ultimate hyperbolic strength.
41-50	AO(N)	Coefficient of lateral earth pressure at rest, K_o, pertaining to effective stresses.
51-60	PHI(N)	Friction angle in degrees.
61-70	XXP(N)	Exponent n in the initial tangent and unload-reload modulus expressions. Its value is assumed to be independent of loading mode. For a linear elastic material, n must be 0. For saturated soils when PHI(N) = 0, n should normally be 0.0001.
71-80	IDRAIN(N)	Material behavior code = 0 if undrained. = 1 if drained.

(b) SECOND CARD FORMAT (3D10.3, D20.5, 3D10.0)

Column	Variable	Explanation
1-10	HCOEF(N)	Coefficient K_m in the initial tangent modulus expression $$E_i = P_a K_m (\sigma_3/P_a)^n$$
11-20	ULCOEF(N)	Coefficient K_{ur} in the unload-reload modulus expression $$E_{ur} = P_a K_{ur} (\sigma_3/P_a)^n$$
21-30	COHE(N)	Undrained strength or cohesion.

Column	Variable	Explanation
31-50	E(N)	Tangent modulus at failure for isotropic anisotropic nonlinear (nonelastic) materials. Young's modulus for elastic materials.
51-60	ALPHA(N)	Coefficient of linear thermal expansion for structural element; zero or blank, otherwise.
61-70	EIMN(N)	Minimum initial tangent modulus for isotropic nonlinear (nonelastic) materials. Zero or left blank for elastic materials.
71-80	TENS(N)	Minimum allowable value of the minor principal stress for isotropic nonlinear (nonelastic) materials. If tensile, input as a negative value. Zero or blank for elastic materials.

8. INTERFACE PROPERTY CARDS

One pair of cards are supplied for each interface material type, N = 1 to NUMJT. If no interface materials, no cards are required.

(a) FIRST CARD FORMAT (6D10.5, I5)

Column	Variable	Explanation
1-10	PHJ(N)	Interface friction angle in degrees.
11-20	RKS(N)	Shear stiffness before failure.
21-30	RKN(N)	Normal stiffness before failure.
31-40	COJ(N)	Interface cohesion.
41-50	FRJ(N)	Correlation coefficent for shear displacement relationship, FRJ = 0.0 for bilinear.
51-60	TENSJ(N)	Tensile strength of interface material.
61-65	IADJMT(N)	Material number of two-dimensional soil element next to the interface.

(b) SECOND CARD FORMAT (2D10.5)

Column	Variable	Explanation
1-10	STFSMN(N)	Shear stiffness after failure.
11-20	STFNMN(N)	Normal stiffness after failure.

9. NODAL POINT CARDS FORMAT (I10, 4D10.2)

One card is supplied for each node. The numbering of nodal points must be sequential and some of the nodes can be omitted. Those nodes omitted are automatically generated by the program at equal spacings between those specified. The first and last nodes must always be specified. Note that DP(N) and PP(N) are automatically generated in equal increments for those nodes omitted.

Column	Variable	Explanation
1-10	N	Nodal point number.
11-20	X(N)	X coordinate, positive to right.
21-30	Y(N)	Y coordinate, positive upward.
31-40	PP(N)	Pore pressure in head of water; zero or blank, if not specified. Pore pressure must not be specified for undrained materials but must be specified for drained materials.
41-50	DP(N)	Change in pore pressure in head of water for soil elements; change in temperature for linear elastic structural material; zero or blank, otherwise.

10. BOUNDARY CONDITION CARDS

Cards 1 through 8 are supplied as required to specify restraints of boundary nodes. If there are no nodes restrained in the mode specified for cards 2, 3, or 4, then the card is not required. For a given card, specified nodes N = 1 to NOY, NOX, or NOXY must be in sequential order.

(a) FIRST CARD FORMAT (3I5)

Column	Variable	Explanation
1-5	NOY	Number of nodal points fixed against Y-movement only.
6-10	NOX	Number of nodal points fixed against X-movement only
11-15	NOXY	Number of nodal points fixed against both X- and Y-movement.

(b) SECOND CARD FORMAT (16I5)

Column	Variable	Explanation
1-5	IC(N)	Nodal point number of the first nodal point fixed against Y-movement.
		Additional nodal points fixed against Y-movement, N = 2 to NOY, are specified in the next 15 five-column fields and on additional cards as required.

(c) THIRD CARD FORMAT (16I5)

Column	Variable	Explanation
1-5	IC(N)	Nodal point number of the first nodal point fixed against X-movement.
		Additional nodal points fixed against X-movement, N = 2 to NOX, are specified in the next 15 five-column fields and on additional cards as required.

(d) FOURTH CARD FORMAT (16I5)

Column	Variable	Explanation
1-5	IC(N)	Nodal point number of the first nodal point fixed against both X- and Y-movement.
		Additional nodal points fixed against both X- and Y-movement, N = 2 to NOXY, are specified in the next 15 five-column fields and on additional cards as required.

11. ELEMENT CARD FORMAT (6I5)

One card is supplied for each interface or two-dimensional element; bar elements are not included in this series of cards. All interface elements are supplied in sequential order first, followed by two-dimensional elements, also in sequential order. (If 'Build' is used; place interface elements which will be built up at the end of joint list, i.e., start numbering these elements with N = NUMJT - NJTFIL.) Thus, interface elements must be numbered from N = 1 to NUMJT, and two-dimensional elements from N = (NUMJT + 1) to NUMEL.

Nodal point numbers must be specified consecutively, processing counterclockwise around the element. The first and last nodal point numbers specified for interface elements must have the same coordinates. Triangular two-dimensional elements having four different nodal point numbers may not be used; the first and last point numbers of a triangular element must be identical.

Element numbers in a row may be omitted, in which case the omitted elements will be generated by incrementing the element number N and the nodal point numbers I, J, K, and L by one and by assigning the same material type number as specified for the last element. The first and last elements in the row must be specified. If no elements are omitted, the element numbering may be done in any order, provided all interface elements are numbered first.

Column	Variable	Explanation
1-5	N	Element number.
6-10	IL(N,1)	Number of nodal point I.
11-15	IL(N,2)	Number of nodal point J.
16-20	IL(N,3)	Number of nodal point K.
21-25	IL(N,4)	Number of nodal point L.
26-30	IL(N,5)	Material type number.

12. BAR ELEMENT CARD FORMAT (4I5, 2D10.7, 2D10.1, D10.5)

One card is supplied for each bar element initially in the mesh or, if a continuation analysis, added in an incremental loading step of the previous analysis. Note that for a continuation analysis this card is not automatically generated. Elements are numbered sequentially from N = 1 to NMBAR.

Column	Variable	Explanation
1-5	N	Element number.
6-10	IB(N,1)	Number of nodal point I.
11-15	IB(N,2)	Number of nodal point J.
16-20	IB(N,3)	Spring response type code = 1 if both compression and tension of bar allowed. = 2 if only compression allowed. = 3 if only tension allowed.
21-30	BAR(N,1)	cos α
31-40	BAR(N,2)	sin α The sign of angle α is determined as shown in Figure 6 of the Isotropic SOILSTRUCT manual. Angle α is measured counterclockwise from a line drawn in the positive x-direction at the I node to the line of action connecting the I node to the J node. (See comments that follow.)
41-50	BAR(N,3)	Prestress force in the bar element. This only inputs the force; the force must be applied as loads at nodes I and J using loading/ construction mode 9 in a loading step.
51-60	BAR(N,4)	Stiffness of bar element. This usually computed as AE/L, but the mesh length (distance from node I to node J) need not, and usually does not, correspond to the actual length.
61-70	BAR(N,5)	Displacement of bar element at activation. This allows for a specified degree of slack at the strut connection; the bar will deform BAR(N,5) prior to its stiffness being activated.

Bar elements can function as either anchors or strut (spring) supports. The required parameters are dependent on the type of bar element specified.

If a strut support is specified, nodal point J is a node fixed against x- or y-movement, depending on the orientation of the strut being modeled. For program storage efficiency, the number of node J should be as close as possible to the number of node I. Nodal point I represents the point of connection between the wall and the actual strut. Nodal points I and J, then, are not necessarily physically connected, since the element stiffness is input independently. Nodal point J allows the force at the J node to be carried into the system as a reaction at a fixed node. This is consistent with the typical mesh representation of one-half of a symmetric excavation. The values are input to represent the line of action of the strut support and do not need to correspond to the relative positions of the I and J nodes.

If an anchor is specified, nodal points I and J physically represent two ends of the anchor and must be restrained appropriately. The values of $\sin \alpha$ and $\cos \alpha$ must correspond to the relative positions of the I and J nodes representing the ends of the anchor. Stiffness is computed as AE/L, with L being the distance between nodes I and J, and either A or E altered to give the correct stiffness. Stiffness for an anchor or a strut support is input as force per length per length of wall.

For either element type, specifying the prestress force does not apply the force. The concentrated force loading/construction mode must be used for this purpose. Thus, bar elements initially in the mesh cannot carry a prestress force, since it is not applied by a gravity turn-on analysis.

13. CONTINUATION OR INITIALIZATION CARDS

This input is supplied only if INIT = 0; it can be supplied from external disc storage or punched cards input from a preceding analysis. Input format is the same for both input modes. This option is provided so that a required sequence of loading steps can be stopped at an intermediate step, then restarted from that step without redoing the complete analysis. However, these cards may also be used to specify values of particular variables in an initial analysis without using the gravity turn-on procedure followed with INIT = 1 or the special procedure followed with INIT = 2. Similarly, particular parameter values can be changed, if the sequence of loading is stopped, prior to a restart analysis.

(a) FIRST CARD (ELEMENT INFORMATION) FORMAT (5I5)

Column	Variable	Explanation
1-5	NUMEL	Number of elements in the mesh, excluding bar elements, but including interface elements.
6-10	NUMJT	Number of interface elements.
11-15	NUMBAR	Number of bar elements, including those initially in the mesh and those added in previous loading steps (if a restart analysis).
16-20	NUMNP	Number of nodes.

Column	Variable	Explanation
21-25	NSTART	Interface element code = 0 if all interface elements are active (i.e. no shear or tension failures). IFLOLD and IFAIL keys are set equal to zero for all interface elements within the program. See card groups g and h. = 1 if IFLOLD and IFAIL keys are to be read for all interface elements. When NSTART = 1, the keys IFLOLD and IFAIL have usually been determined in a previous analysis and are included as standard output to tape 9 when the disc storage option (see LOADING INFORMATION CARD) was activated.

(b) SECOND CARD (STRESS INFORMATION)
INTERFACE ELEMENTS FORMAT (2(1P,1D13.6,2x))
2-DIM ELEMENTS FORMAT (4(1P,1D13.6,2x))

Three cards are supplied for each interface element, in numerical sequence N = 1 to NUMJT. For each interface element, the pair of normal and shear stresses at node I [SIGI], the center [SIG], and node J [SIGJ] are supplied.

Column	Variable	Explanation
1-13	SIG(N,1)	Normal stress for an interface element.
16-28	SIG(N,2)	Shear stress for an interface element.

One card is supplied for each two-dimensional element, in numerical sequence N = (NUMJT + 1) to NUMEL.

Column	Variable	Explanation
1-13	SIG(N,1)	Stress in the x-direction for a two-dimensional element, σ_x , normal stress for an interface element.
16-28	SIG(N,2)	Stress in the y-direction for a two-dimensional element, σ_y , shear stress for an interface element.

Column	Variable	Explanation
31-43	SIG(N,3)	x-y shear stress for a two-dimensional element τ_{xy}, zero or blank for interface element.
46-58	SIG(N,4)	Maximum previous value of x-y shear stress for a two-dimensional element, zero or blank for interface element.

(c) THIRD CARD (NODAL POINT INFORMATION) FORMAT (3(1P1D14.7,1x))

Information for three nodal points is supplied on each card. Nodal points are specified in numerical order, N = 1 to NUMNP.

Column	Variable	Explanation
1-14	DISPX(N)	Displacement in x-direction
16-29	DISPY(N)	Displacement in y-direction
31-44	PP(N)	Pore pressure in head of water.

(d) FOURTH CARD (MATERIAL TYPE DESIGNATION) FORMAT (15I5)

Materials type numbers for 15 interface or two-dimensional elements are specified on each card. Material type numbers for elements in numerical sequence, N = 1 to NUMEL, are specified.

Column	Variable	Explanation
1-5	IL(N,5)	Material type number. Material type numbers for the next 14 elements are supplied in the next fourteen 5-column fields.

Note that material type numbers supplied on these cards supersedes the material type numbers specified on the element card (section 9). Thus, material type changes can be made as part of a restart analysis rather than including such changes in a loading step of an analysis.

(e) FIFTH CARD (BAR ELEMENT INFORMATION) FORMAT (4(D10.2, D10.0))

This card is supplied only if bar elements are included (NUMBAR > 0).

Information for four bar elements is specified on each card. Information is supplied for bar elements in numerical sequence, N = 1 to NUMBAR.

Column	Variable	Explanation
1-10	BAR(N,3)	Force in bar element.
11-20	BAR(N,4)	Stiffness of bar element.
		Information for the next three bar elements is supplied in the next six 10-column fields.

Note that these parameters, if changed for a restart analysis, supersede those specified on the Bar Element Card (section 12). Also, if bar elements are initially included in the mesh, and an initialization procedure is used, then this card must be included, duplicating the information specified in the Bar Element Card.

(f) SIXTH CARD (INTERFACE INFORMATION) FORMAT (8D10.4)

This card is supplied only if interface elements are included (NUMJT > 0). Information for four interface elements is specified on each card. Information is supplied for interface elements in numerical sequence, N = 1 to NUMJT. If no interface elements are present, proceed to group 12 input data.

Column	Variable	Explanation
1-10	STFS(N)	Shear stiffness of first interface element.
11-20	STFN(N)	Normal stiffness of first interface element.
		Information for the next three interface elements is supplied in the next six 10-column fields.

Note that the value of the shear stiffness, if changed for a restart analysis, supersedes the value specified on the Interface Property Card (section 8). Thus, the interface stiffness can be changed as part of a restart analysis.

(g) SEVENTH CARD (INTERFACE KEY) FORMAT (15I5)

This card is supplied if interface elements are included (NUMJT > 0) and NSTART = 1. Information for 15 interface elements is specified on each card. Information is supplied for interface elements in numerical sequence, N = 1 to NUMJT. If no interface elements are present or NSTART = 0, proceed to group 12 input data.

Column	Variable	Explanation
1-5	IFLOLD(N)	Modulus assignment key = 0 if interface element N is active. = 1 if tension failure occurred. = 2 if shear failure occurred.

(h) EIGHTH CARD (INTERFACE KEY) FORMAT (15I5)

This card is supplied only if NSTART = 1 and for only those interface elements along the horizontal base of the structure used to model the base separation, with element numbers from NOELF1 to NOELF2. Information for 15 interface elements is specified on each card.

Column	Variable	Explanation
1-5	IFAIL(N)	Stress transfer key = 0 if interface element number N is active. = 1 if transfer of normal and shear stress in failed interface element number N has been completed.

14. LOADING STEP CARDS

These cards are required only if NC is not equal to 0. Cards are assembled in the order specified on the Loading Information Card (section 5): cards for the first loading/construction mode specified for the first loading step are followed by the cards for the second loading/construction mode specified for the first loading step, and so on to the cards for the last loading/construction mode specified for the last construction step.

For a given loading step, the lowest numbered loading/construction mode is processed first, but the analysis of the loading step is made for the combined effect of all loading/construction modes included in the loading step. Care must therefore be exercised in specifying some loading/construction modes, such as material type changes or concentrated forces representing prestress forces, in the same loading step with other loading/construction modes.

(a) EXCAVATION

These cards are supplied only if KCS(N,1), KCS(N,2), or KCS(N,3) = 1. Input is handled by subroutine EXCAV. Free excavated elements and common excavated element are input separately. A free excavated element is an element specified to be excavated that has no boundary in common with an element not specified to be excavated in the loading step. A common excavated element, therefore, has at least one boundary in common with an unexcavated element.

Interface elements can only be included as free excavated elements, even if they have a boundary in common with an unexcavated element. Interface elements cannot be used as interpolation elements. Free excavated elements (other than interpolation elements) can be used as interpolation elements, though common excavated elements are more commonly used.

If possible, adjacent common excavated elements should be input sequentially as this procedure avoids repetitive computation; nodal loads for a nodal point common to the two sequential elements will only be calculated once.

(1) FIRST CARD (CONTROL DATA) FORMAT (2I5)

Column	Variable	Explanation
1-5	NFXEL	Number of free excavated elements.
6-10	NXELCB	Number of common excavated elements.

(2) SECOND CARD (FREE EXCAVATED ELEMENT DATA) FORMAT (16I5)

Element numbers of 16 free excavated elements can be supplied on one card. A maximum of 50 can be specified in one loading step. Element numbers of all free excavated elements, N = 1 to NFXEL are to be specified.

Column	Variable	Explanation
1-5	LNXEL(N)	Element number of first free excavated element. Information for the next 15 free excavated elements is supplied in the next fifteen 5-column fields.

(3) THIRD CARD (COMMON EXCAVATED ELEMENT DATA) FORMAT (8I5)

One card is supplied for each common excavated element, N = 1 to NXELCB. A maximum of 50 common excavated elements can be specified in one loading step. Loading codes include:

0 - The node is not loaded by excavation forces and <u>is not</u> common to both an excavated and an unexcavated element.

1 - The node is loaded by excavation forces and <u>is</u> common to both an excavated and an unexcavated element.

Note: I, J, K, and L refer to the same nodes I, J, K, and L specified on the Element Card (section 11).

Interpolation elements should be specified in a crisscross fashion. Further, x- and y-coordinates of diagonal elements must not be the same. If these rules are not adhered to, the interpolation routine will detect a singularity and processing will stop.

Column	Variable	Explanation
1-5	LUL(N,1)	Element number of the first common excavated element. This element is also the first interpolation element.
6-10	LUL(N,2)	Element number of second interpolation element.
11-15	LUL(N,3)	Element number of third interpolation element.
16-20	LUL(N,4)	Element number of fourth interpolation element.
21-25	LUL(N,5)	Loading code for node I.
26-30	LUL(N,6)	Loading code for node J.
31-35	LUL(N,7)	Loading code for node K.
36-40	LUL(N,8)	Loading code for node L.
		Loading codes are specified for the nodes of the element to be excavated specified in columns 1 through 5.

(b) FILL OR CONCRETE PLACEMENT

These cards are supplied only if KCS(N,1), KCS(N,2), or KCS(N,3) = 2. Input is handled by subroutine BUILD. The types of elements that can be placed include structural, soil, and interface elements. Subroutine SUBSTP cannot be used in conjunction with subroutine BUILD.

(1) FIRST CARD (CONTROL DATA) FORMAT (5I5, D10.2)

Column	Variable	Explanation
1-5	NLEL	Total number of elements to be placed, including interface and structural elements.
6-10	NJ	Total number of elements to be placed less the number of inactive interface elements to be placed.
11-15	NONP	Number of nodal points within the placed layers to be assigned zero displacements. This includes all nodal points of the elements to be placed except those nodal points in common with an already existing element.
16-20	NCE	Number of structural elements to be placed.

Column	Variable	Explanation
21-25	NB1E	Number of backfill type 1 elements to be placed. (The number of NB2TYP elements is determined internally.)
26-35	HTB	New y-coordinate of the top of the placed backfill.

(2) SECOND CARD (ELEMENT NUMBERS) FORMAT (16I5)

Element numbers of 16 placed elements can be supplied on one card. A maximum of 100 can be specified in one loading step. Element numbers of all placed elements, N = 1 to NLEL, are to be supplied. The elements must be read in by material type according to the following sequence:

1. structural elements
2. backfill type 1 elements
3. backfill type 2 elements
4. interface elements to be activated
5. interface elements to be left inactive but to be placed between elements of like materials

Column	Variable	Explanation
1-5	LEL(N,1)	Element number of first element to be placed.
6-10	LEL(N,2)	Material number of the element.
		Information for the next seven placed elements is supplied in the next fourteen 5-column fields.

(3) THIRD CARD (NODE NUMBERS) FORMAT (16I5)

Nodal point numbers of 16 nodes to be assigned zero displacement can be supplied on one card. A maximum of 50 can be specified in one loading step. Nodal point numbers, N = 1 to NONP, are to be specified in sequential order.

Column	Variable	Explanation
1-5	NP(N)	Nodal point number of first node assigned zero displacement.
		Information for the next 15 nodal points is supplied in the next fifteen 5-column fields.

(c) SEEPAGE

These cards are supplied only if KCS(N,1), KCS(N,2), or KCS(N,3) = 3. Input is handled by subroutine SEEP. Seepage loads are determined from changes in pore pressure specified as DP(N) on Nodal Point Cards or from the specified phreatic level changes.

(1) FIRST CARD (CONTROL DATA) FORMAT (I5)

Column	Variable	Explanation
1-5	NCODE	Option code specifying how seepage is input = 0 if specified as DP(N) on Nodal Point Cards (Section 9). = 1 if to be calculated using the new phreatic surface input on the following cards.

(2) SECOND CARD (NUMBER OF PHREATIC SEGMENTS) FORMAT (I5)

This card is required only if NCODE = 1.

Column	Variable	Explanation
1-5	NWAT	Number of phreatic surface segment end points used to specify the new phreatic surface. NWAT must be greater than or equal to 2. The number of phreatic surface segments is equal to NWAT. The maximum value of NWAT is 30.

(3) THIRD CARD (PHREATIC LEVEL DATA) FORMAT (6D10.2)

This card is required only if NCODE = 1.

The end points of the phreatic surface segments delineating the new and old phreatic surfaces are specified as x-coordinates that must be the same as the x-coordinates of a nodal point. Both the present and new phreatic surfaces are assumed to be linear between the bounding x-coordinates. The left-hand side of the mesh is always the first bounding x-coordinate specified. A bounding x-coordinate on the old phreatic surface will require, usually, specification of the same x-coordinate on the new phreatic surface.

Two end points (x-coordinates), with associated new and old phreatic levels (y-coordiantes), are supplied on each card. All end points, N = 1 to NWAT, must be specified.

Column	Variable	Explanation
1-10	XW(N)	X-coordinate bounding the levels PREL(N) and FUEL(N) on the right-hand side. (Must be the same as the x-coordinate of a nodal point.)
11-20	PREL(N)	Present level (y-coordinate) of the phreatic surface at XW(N).
21-30	FUEL(N)	New level (y-coordinate) of the phreatic surface at XW(N). Information for the next end point is supplied in the next three 10-column fields.

(d) DELETION OF BAR ELEMENTS

These cards are supplied only if KCS(N,1), KCS(N,2), or KCS(N,3) = 4. Input is handled by the main program.

The deleted bar elements remain in the mesh but with zero stiffness. The force the bar element carried is applied to the free node or nodes at its ends.

This loading/construction mode cannot be specified in the same loading step as fill or concrete placement.

(1) FIRST CARD (CONTROL DATA) FORMAT (I5)

Column	Variable	Explanation
1-5	NCARDS	Number of deleted bar elements. There is no limit other than the number of bar elements presently in the mesh.

(2) SECOND CARD (ELEMENT NUMBERS) FORMAT (16I5)

The element numbers of 16 deleted bar elements can be specified on one card. A total of N = 1 to NCARDS cards must be supplied.

Column	Variable	Explanation
1-5	N	Element number of bar element to be deleted. Element numbers for the next 15 elements are supplied in the next fifteen 5-column fields.

(e) ADDITION OF BAR ELEMENTS

These cards are supplied only if KCS(N,1), KCS(N,2), or KCS(N,3) = 5. Input is handled by the main program.

Information on the second card is the same as that explained for the Bar Element Card (Section 12). The added bar elements are numbered sequentially from NUMBAR + 1, where NUMBAR is the number of bar elements in the mesh before the present loading step.

(1) FIRST CARD (CONTROL DATA) FORMAT (I5)

Column	Variable	Explanation
1-5	NCARDS	Number of bar elements to be added. Any number can be added in a loading step, however, the maximum number of bar elements that can be in the mesh (including inactive or deleted elements) is 15.

(2) SECOND CARD
(ADDED BAR ELEMENT DATA) FORMAT (4I5, 2D10.7, 2D10.1, D10.5)

Column	Variable	Explanation
1-5	N	Element number of added bar element.
6-10	IB(N,1)	Number of nodal point I.
11-15	IB(N,2)	Number of nodal point J.
16-20	IB(N,3)	Spring response type code.
21-30	BAR(N,1)	cos α
31-40	BAR(N,2)	sin α

Column	Variable	Explanation
41-50	BAR(N,3)	Prestress force in the bar element.
51-60	BAR(N,4)	Stiffness of bar element.
61-70	BAR(N,5)	Displacement of bar element at activation.

(f) BOUNDARY PRESSURE LOADING

These cards are supplied only if KCS(N,1), KCS(N,2), or KCS(N,3) = 6. Input is handled by subroutine SURFLD. Linear pressure distributions are assumed, based on the pressures specified for the nodal points. The right (positive x-direction) and positive up (positive y-direction).

(1) FIRST CARD (CONTROL DATA) FORMAT (2I5)

Column	Variable	Explanation
1-5	NLDS	Number of loaded boundaries. There is no limit to the number of loaded boundaries that can be specified.
6-10	NPRTB	Print code = 1 if equivalent nodal point forces are to be printed.

(2) SECOND CARD (LOADED BOUNDARY DATA) FORMAT (2I5, 4D10.2)

Information for one loaded boundary is specified on each card. Nodes I and J are interchangeable; there is no convention regarding their assignment. A total of N = 1 to NLDS loaded boundaries must be specified.

Column	Variable	Explanation
1-5	I	Nodal point number of the first node of the loaded boundary.
6-10	J	Nodal point number of the second node of the loaded boundary.
11-20	WS1	Value of the pressure acting in the x-direction at node I.
21-30	WS2	Value of the pressure acting in the x-direction at node J.
31-40	WS3	Value of the pressure acting in the y-direction at node I.
41-50	WS4	Value of the pressure acting in the y-direction at node J.

(g) TEMPERATURE LOADING

No cards are required for this loading/construction mode. Temperature Card (section 9). If KCS(N,1), KCS(N,2), or KCS(N,3) = 7, then the values of DP(N) are acknowledged by the main program and processed as temperature changes. Note that DP(N) can also be used to input phreatic level changes for the seepage loading/construction mode. Thus, if seepage is specified as being input through values of DP(N), seepage and temperature loading cannot be included in the same loading step. Generally, temperature loading requires a restart analysis, with the DP(N) values being changed to reflect the temperature changes prior to the analysis.

The temperature scale used (°C or °F) must correspond to the coefficient of thermal expansion designated on the Material Property Cards (section 7). Temperature changes are typically designated for structural materials only.

(h) CONCENTRATED FORCE OR DISPLACEMENT LOADING

These cards are supplied only if KCS(N,1), KCS(N,2), or KCS(N,3) = 8 or 9. Input is handled by the main program. Refer to the Loading Information Card (section 5) for instructions on using loading/construction modes 8 and 9.

(1) FIRST CARD (CONTROL DATA) FORMAT (I5)

Column	Variable	Explanation
1-5	NUMNDE	Number of loaded or displaced nodes. There is no limit to the number of loaded or displaced nodes that can be specified.

(2) SECOND CARD

DISPLACEMENT DATA FORMAT (2(I5,2(1x,1D14.7)))
[LOAD DATA] FORMAT (2(I10,2D10.2))

Information for two loaded or displaced nodal points is supplied on each card. A total of N = 1 to NUMNDE nodes must be specified. Sign convention is positive to the right (positive x-direction) and positive up (positive y-direction). Nodal points specified as being loaded or displaced do not have to be in numerical order.

Column	Variable	Explanation
1-5 [1-10]	I	Node number of the first loaded or displaced node.
7-20 [11-20]	X1	Component of force or displacement in the x-direction at node I.
22-35 [21-30]	Y1	Component of force or displacement in the y-direction at node I.
36-40 [31-40]	J	Node number of the second loaded or displaced node.
42-55 [41-50]	X2	Component of force or displacement in the x-direction at node J.
57-70 [51-60]	Y2	Component of force or displacement in the y-direction at node J.

If there is not a second, or J, node to be specified on the last card, then leave the second set of columns blank.

(i) ELEMENT MATERIAL TYPE CHANGE

These cards are supplied only if KCS(N,1), KCS(N,2), or KCS(N,3) = 10. Input is handled by the main program.

The material type of the specified element is changed before the analysis of the loading step which specifies the change. The material type change includes modifying the values of modulus, E, and Poisson's ratio, GUI, and zeroing the stresses, SIG(N,1). Thus, if a material type change is specified in conjunction with boundary loading in the same loading step, the elements with changed material type will respond to the loading with new material properties.

As included, this loading/construction mode is intended to physically represent the grouting of an anchor. At a given step in the analysis, the material types of soil elements can be changed to represent the assumed linear elastic grout zone. If there is a need to change material types for any other reason, this can be done by stopping the analysis after the appropriate load step, modifying the material types on the Material Type Designation Card (section 13d), then restarting the analysis.

(1) FIRST CARD (CONTROL CARD) FORMAT (I5)

The maximum number of elements with material type number that can be changed in a load step is 120. The excavation and material type change loading/construction modes cannot be specified in the same loading step since the same variable, LUL(N,1) and LUL(N,2), are used to input data for both.

Column	Variable	Explanation
1-5	NELCH	Number of elements with material type number being changed.

(2) SECOND CARD (ELEMENT DATA) FORMAT (16I5)

The element numbers and new material type numbers of eight elements can be supplied on one card. A total of N = 1 to NELCH elements must be specified.

Column	Variable	Explanation
1-5	LUL(N,1)	Element number of first element with a specified new material type number.
6-10	LUL(N,2)	New material type number of the specified element.

Information for the next seven elements is supplied in the next seven pairs of five-column fields.